Supplementary Information

for

Taming the Captodative Glycyl Radical for Nickel-Photocatalytic Cross-Coupling with Alkyl Chlorides

Rani Kumari, Ning Wei and Sebastian B. Beil

Max-Planck-Institute for Chemical Energy Conversion, Department of Electrosynthesis, Stiftstr. 34-36, 45470 Mülheim an der Ruhr, Germany.

Stratingh Institute for Chemistry, University of Groningen, 9747 AG Groningen, The Netherlands

sebastian.beil@cec.mpg.de

Table of Contents

1. General Remarks

All chemicals and solvents were purchased from commercial suppliers and used without further purification unless specified. Photocatalysts were previously synthesized according to literature.[1]

Flash Chromatography

Preparative column chromatography was performed on prepacked puriFlash™ silica columns (15 µm or 30 µm, PF-15SIHP-F0012, PF-15SIHP-F0025, PF-25SIHC-F0025, PF-15SIHP-F0040, PF-25SIHC-F0120 Interchim, Montlucon Cedex, France) using a puriFlash™-System (puriFlash™ XS520Plus, Interchim, Montlucon Cedex, France) with an integrated UV detector.

High Resolution Mass Spectrometry

High resolution mass spectra were recorded using a Q Exactive Plus (Thermo Fischer Scientific, San Jose, CA, USA), or Q Exactive GC Orbitrap with Trace 1310 GC (Thermo Fischer Scientific, San Jose, CA, USA) spectrometer.

Nuclear Magnetic Resonance (NMR) Spectroscopy

NMR spectra were recorded at 25 °C on a Bruker AVANCE III HD 500 or a Bruker Ascend Evo 400 NMR spectrometer, respectively with a Bruker Prodigy probe 80 K or a Bruker iProbe BBFO (Bruker BioSpin GmbH, Rheinstetten, Germany) using $CDCl_3$, CD_3CN, acetone-d_6 or DMSO-d6 as deuterated solvent. All chemical shifts are reported in δ-scale as parts per million [ppm] (multiplicity, coupling constant J, number of protons), relative to the solvent residual peaks as the internal standard. Coupling constants *J* are given in Hertz [Hz]. Besides ^{1}H, ^{13}C and ^{19}F experiments, the 2D techniques $^{1}H,^{1}H$-COSY, $^{1}H,^{13}C$-HSQC and $^{1}H,^{13}C$-HMBC were used assisting to assign the signals. The following abbreviations were used to describe the signals: s (singlet), d (doublet), t (triplet), q (quartet), pent (pentet), sext (sextet), hept (heptet), m (multiplet), br (broad signal). The spectra obtained were evaluated with MestReNova 14 (Mestrelab Research S.L., Spain).

Gas Chromatography

Analysis of crude reaction mixtures and purified products were performed using a GC-2030 (Shimadzu, Kyoto, Japan) equipped with a flame ionization detector (FID) and a quartz capillary column HI-5 MS (Avantor VWR, Radnor, USA) with following specification: length of 30 m, inner diameter of 0.25 mm and a stationary phase ((5%-phenyl)dimethylsiloxane) of 0.25 µm thickness. Hydrogen was used as carrier gas with a constant velocity of 40 cm/s. Measurements were performed at an injector temperature of 270 °C and a detector temperature of 320 °C, starting at 50 °C (holding for 1 min) and heating to 300 °C (holding for 4.71 min) with a temperature ramp of 17.5 °C/min (method: 2_medium, total program time: 20.0 min). GC-MS analysis was performed on a GCMS-QP2010SE (Shimadzu, Kyoto, Japan) equipped with an electron ionisation (EI) source and a quadrupole mass analyser. HI-5MS quartz capillary column (Avantor VWR, Radnor, USA) with a length of 30 m, 0.25 mm inner diameter and a stationary phase ((5% phenyl)dimethylsiloxane) of 0.25 µm thickness was used. Helium is the carrier gas at a constant velocity of 30 cm/s. The temperature started at 50 °C (held for 1 min) and was heated to 300 °C (held for 4.71 min) with a temperature rise of 17.5 °C/min.

Ultra-performance liquid chromatography – mass spectrometry (UPLC-MS)

Ultra-performance liquid chromatography – mass spectrometry (UPLC-MS) was performed on a Waters™ ACQUITY™ UPLC™ H-Class PLUS System (Waters Corporation, Milford, USA) using a quaternary solvent manager (ACQ H-CLASS QSM PLUS), a sample manager with flow-through needle (ACQ H-Class FTN-H PLUS) design, a column heater (ACQUITY UPLC CM-A) and an ACQUITY UPLC® BEH C18 1.7 µm 2.1 x 50 mm column. Mass spectra were measured using a single quadrupole mass detection (ACQUITY QDa Detector) employing ESI+. Acetonitrile (HPLC-MS grade) and water (Milli-Q®) were used as eluents, eluent with 0.1% (v/v) formic acid was added directly before mass detection using a second isocratic solvent manager (Waters™ ACQ Isoc Solvent Mgr).

Photochemical Setup

All photochemical reactions were performed in an integrated photoreactor PennPhD M2 from Sigma Aldrich or Acceled. As light source 450 nm LED plates was used at 100% intensity. Stirring was kept at 1000 rpm with maximum fan speed of 6800 rpm.

CV data and DFT (ORCA) input and output files, as well as NMR spectra and HRMS data are available at the Edmond repository, DOI: https://doi.org/10.17617/3.DPOBYI

2. Reaction Optimization

The investigation began with the synthesis of the desired substrate from commercially available diethyl aminomalonate hydrochloride (**S1**), following the procedure reported from literature (Scheme S1).[2] Full conversion of **S1** to the intermediate product **S2a** was confirmed by ^{1}H NMR, with an almost quantitative yield and no further purification was needed. However, the subsequent hydrolysis of **S2a** to produce final product **2a** proved challenging. Ultimately, the addition of a catalytic amount of 4-dimethylaminopyridine (DMAP) was critical.

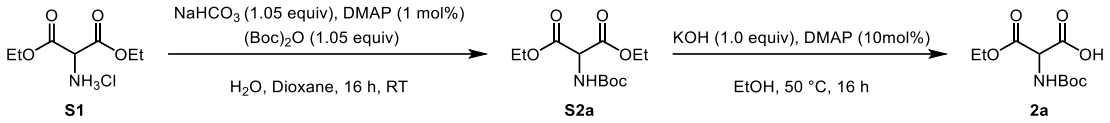

Scheme S1: Synthesis of *N*-Boc amino malonate mono-ethyl ester (**2a**).

We performed screening experiments to understand the trend of proto-decarboxylation of **2a**. We screened a range of bases ranging from organic bases to inorganic ones. In case of inorganic bases, we found that carbonates (Na_2CO_3 and K_2CO_3) in DMSO show no proto-decarboxylation (Scheme S2).[3]

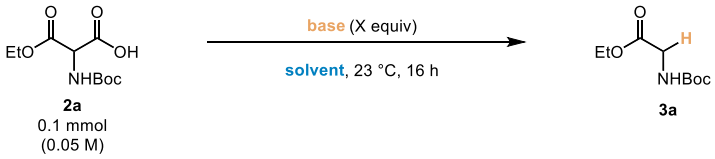

	base	$NaHCO_3$	Na_2CO_3	NaOAc	K_2CO_3	KOAc	K_2HPO_4	K_3PO_4	Cs_2CO_3	CsF
DMF	1.5 equiv	32%	9%	36%	24%	40%	29%	38%	36%	32%
DMSO	1.5 equiv	3%	0%	24%	0%	21%	3%	6%	10%	27%

		Lutidine	BTMG	DBU	DBN	DBA	TMG
DMSO	1.0 equiv	0%	54%	28%	32%	24%	54%

	H_2O:PhMe	0.2 : 1.8	0.4 : 1.6	0.6 : 1.4	0.8 : 1.2
Na_2CO_3	1.0 equiv	0%	0%	0%	0%

	DMF:PhMe	0.2 : 1.8	0.4 : 1.6	0.6 : 1.4	0.8 : 1.2
Na_2CO_3	1.0 equiv	8%	19%	36%	36%

Scheme S2: Inorganic and organic base screening in DMSO and DMF to quantify background proto-decarboxylation of **2a** to **3a**. ^{1}H NMR yield vs. 1,3,5-trimethoxybenzene (TMB) as internal standard in DMSO-d_6.

We performed further screening by changing the fan speed and observed that with 4800 rpm fan speed the reaction gave nearly 6% yield of the desired cross-coupling product **5a** (Scheme S3).[3]

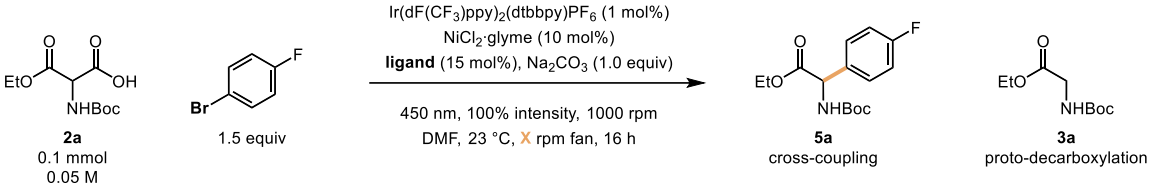

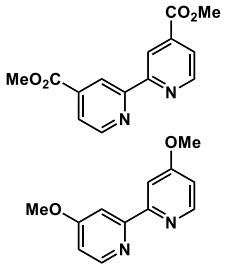

X	ArBr	ArH	cross-coupling	proto-decarboxylation
6800	76%	12%	0%	90%
4800	64%	13%	0%	90%
6800	0%	6%	1%	50%
4800	0%	13%	6%	75%
6800*	28%	22%	6%	47%

Scheme S3: Screening of ligands with varying fan speed under cross-coupling conditions toward desired product **5a**. ^{1}H NMR yield vs. TMB as internal standard in $CDCl_3$. ***** DMSO was used instead.

Subsequently, the equivalence of the aryl halide was screened. Increasing the loading from 1.0 to 3.0 equivalents led to similar yields of 18–19% under the above conditions (Scheme S4).

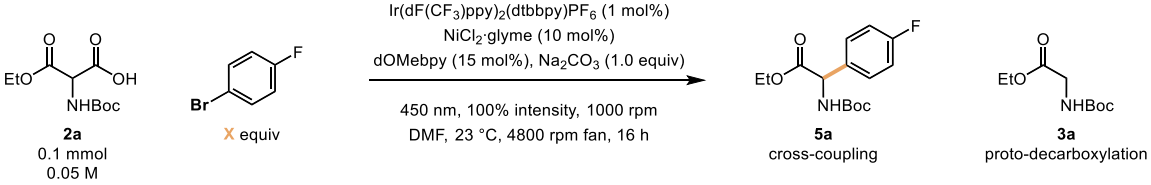

X	ArBr	cross-coupling	proto-decarboxylation
1.0	0%	11%	75%
1.5	0%	9%	73%
2.0	18%	18%	63%
2.5	63%	18%	56%
3.0	100%	19%	56%

Scheme S4: Screening of aryl bromide equivalents under cross-coupling conditions toward desired product **5a**. ^{1}H NMR yield vs. TMB as internal standard in DMSO-d_6.

As we observed that carbonate and phosphate bases were yielding less proto-decarboxylation, we tested to form the desired product in acetonitrile (Scheme S5).

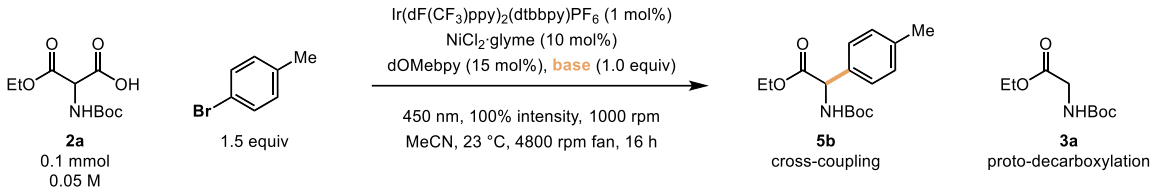

base	ArBr	cross-coupling	proto-decarboxylation
K_2CO_3	67%	7%	139%
KH_2PO_4	110%	0%	75%
K_2HPO_4	100%	0%	88%
Cs_2CO_3	112%	0%	140%

Scheme S5: Screening of bases under cross-coupling conditions toward desired product **5b**. ^{1}H NMR yield vs. TMB as internal standard in DMSO-d_6.

Screenings with different solvent were performed this time with 4-CF_3 substituted benzamide protection group (see DFT-guided optimization below), in case of MeCN and DCM nearly 10% of desired product **5c** was observed along with proto-decarboxylation. Though the reaction with MeCN seem to be cleaner as compare to DCM making it the best solvent choice for further screenings (Scheme S6).

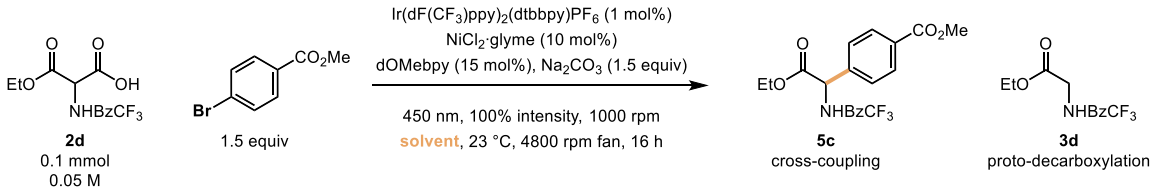

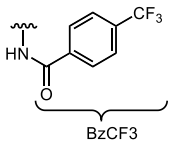

solvent	cross-coupling	proto-decarboxylation
DMSO	0%	70%
THF	0%	70%
DCM	**10%**	**50%**
MeCN	**10%**	**60%**

Scheme S6: Photochemical decarboxylative arylation screening for solvents. ^{1}H NMR yield vs. TMB as internal standard in DMSO-d_6.

Our next approach was to try benzyl halides for photoredox decarboxylative alkylation. We observe a significantly higher yield of **6b** along with proto-decarboxylation. It is worth noticing that benzyl chloride gave higher yield than benzyl bromide. Screening was continued to optimize the equivalence of Na_2CO_3.

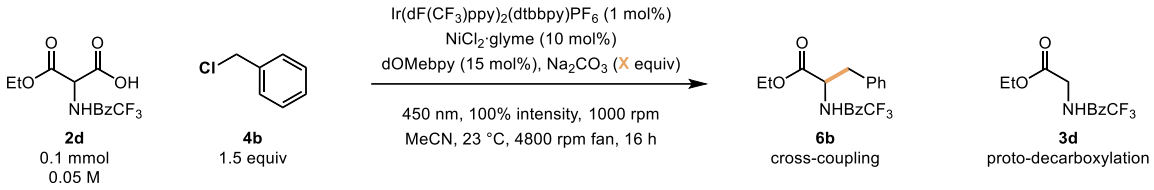

2d
0.1 mmol
0.05 M

4b
1.5 equiv

6b
cross-coupling

3d
proto-decarboxylation

X	cross-coupling	proto-decarboxylation
0.5	27%	50%
1.0	30%	40%
2.0	33%	39%
2.5	**34%**	**39%**
4.0	10%	48%
5.0	25%	38%

Scheme S7. Photochemical decarboxylative alkylation screening for base equivalent. ^{1}H NMR yield vs. TMB as internal standard in DMSO-d_6.

Next, we screened for nickel pre-catalyst and its loading together with ligand loading and the equivalents of benzyl chloride needed.

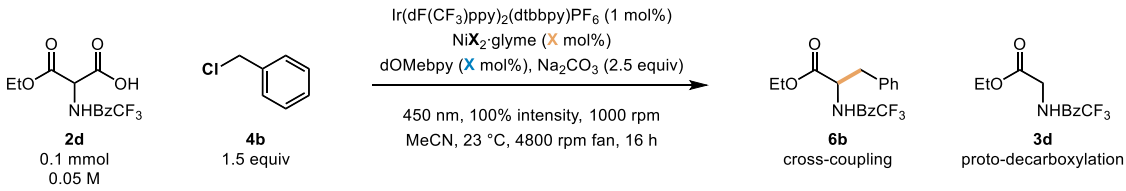

2d
0.1 mmol
0.05 M

4b
1.5 equiv

6b
cross-coupling

3d
proto-decarboxylation

	X	X	cross-coupling	proto-decarboxylation
Cl	5	7.5	16%	54%
	10	15	30%	40%
	15	**20**	**35%**	**49%**
	50	75	15%	50%
Br	5	7.5	17%	35%
	10	15	19%	45%

Scheme S8: Photochemical decarboxylative alkylation screening to optimize Ni source and ligand equivalence. ^{1}H NMR yield vs. TMB as internal standard in DMSO-d_6.

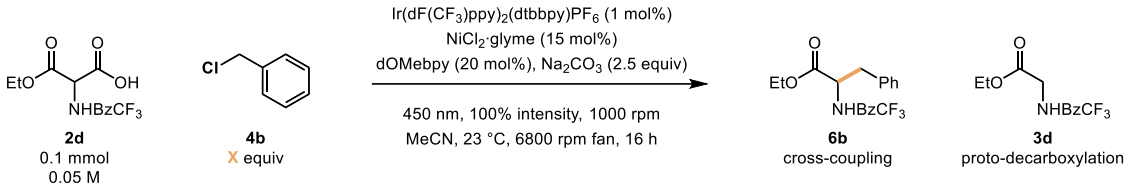

X	cross-coupling	proto-decarboxylation
1.0	32%	35%
1.5	19%	50%
2.5	**49%**	**75%**
4.0	20%	50%
5.0	36%	25%

Scheme S9. Photochemical decarboxylative alkylation screening to optimize the benzyl chloride equivalence. ^{1}H NMR yield vs. TMB as internal standard in DMSO-d_6.

We reevaluated the conditions for the new substrate **2d** for solvent of choice and irradiation time and observed that MeCN outcompetes all other polar aprotic solvents and reaction times of 16 h are needed.

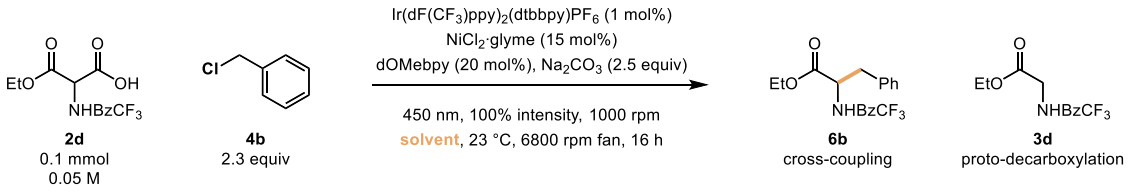

solvent	cross-coupling	proto-decarboxylation
EtOAc	6%	50%
DCM	6%	21%
DMF	0%	80%
THF	7%	68%
DMSO	0%	80%
MeCN	**35%**	**40%**
DME	5%	82%
Et_2O	0%	16%
MTBE	0%	42%

Scheme S10. Photochemical decarboxylative alkylation screening to optimize solvents again. ^{1}H NMR yield vs. mesitylene as internal standard in DMSO-d_6.

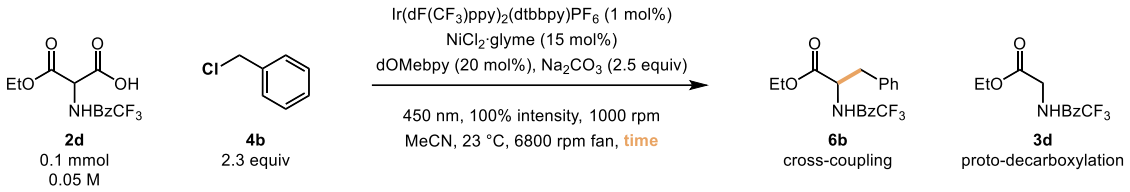

time (h)	cross-coupling	proto-decarboxylation
2	2%	22%
4	13%	48%
6	14%	40%
10	24%	40%
16	**35%**	**39%**
24	9%	60%

Scheme S11. Photochemical decarboxylative alkylation screening to optimize reaction time. ^{1}H NMR yield vs. mesitylene as internal standard in DMSO-d_6.

We confirmed that inorganic bases are superior to organic ones. Most likely, high solubility enhances proto-decarboxylation kinetics outcompeting any radical reactions.

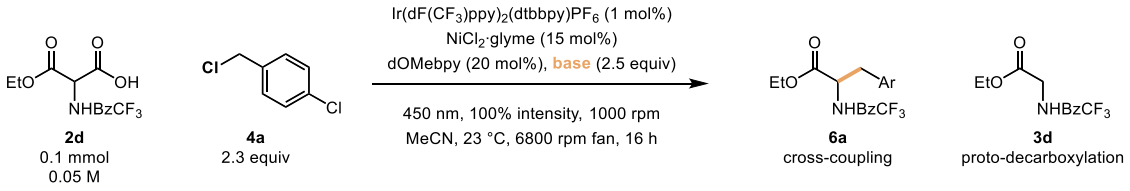

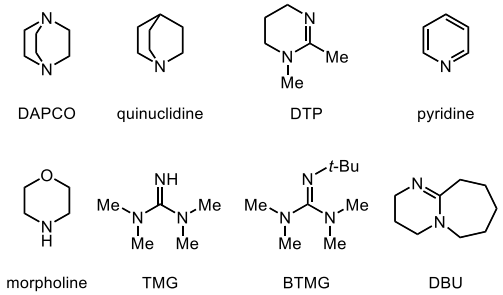

base	cross-coupling	proto-decarboxylation
pyridine	16%	56%
quinuclidine	0%	>95%
DABCO	0%	>95%
morpholine	0%	80%
TMG	0%	80%
BTMG	0%	>95%
DBU	0%	>95%
DTP	35%	62%

Scheme S12. Photochemical decarboxylative alkylation screening for organic bases. ^{1}H NMR yield vs. mesitylene as internal standard in DMSO-d_6. DTP: 1,2-dimethyl-1,4,5,6-tetrahydropyrimidine.

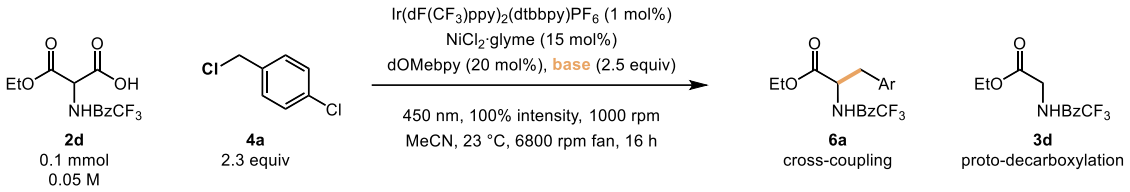

base	cross-coupling	proto-decarboxylation
KH_2PO_4	0%	70%
K_2HPO_4	10%	60%
Na_2CO_3	**35%**	**50%**
K_2CO_3	21%	50%
Cs_2CO_3	2%	50%
NaOH	26%	46%
KOH	5%	50%

Scheme S13. Photochemical decarboxylative alkylation screening for inorganic bases. ^{1}H NMR yield vs. mesitylene as internal standard in DMSO-d_6.

Bipyridine ligands were crucial for nickel-catalyzed reactions compared to phosphines.

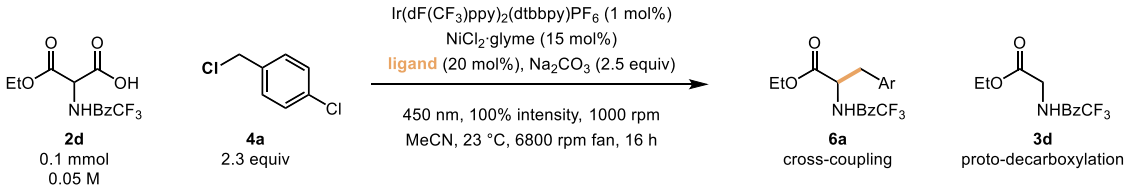

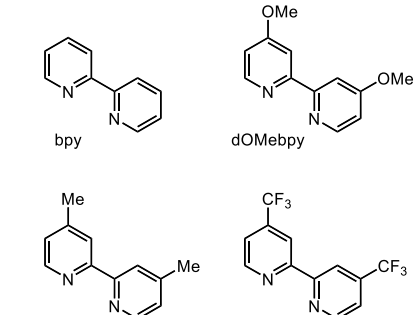

ligand	cross-coupling	proto-decarboxylation
bpy	47%	34%
dOMebpy	50%	42%
dMebpy	33%	25%
dCF_3bpy	35%	55%
dMephen	10%	80%
$Ni(dppe)Cl_2$	0%	67%
dppb	0%	83%
Me-DuPhos	0%	64%
BINAP	0%	93%
xantphos	0%	83%
DavePhos	0%	92%

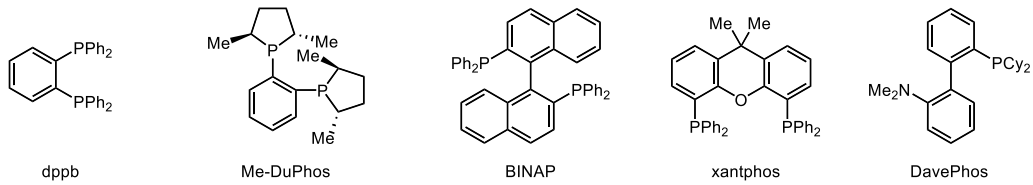

Scheme S14. Photochemical decarboxylative alkylation screening for bpy and phosphine ligands. ^{1}H NMR yield vs. mesitylene as internal standard in DMSO-d_6.

A final photocatalyst screening showed that $Ir(dFppy)_2(bpy)PF_6$ performed best and organic sensitizers were insufficient in this transformation.

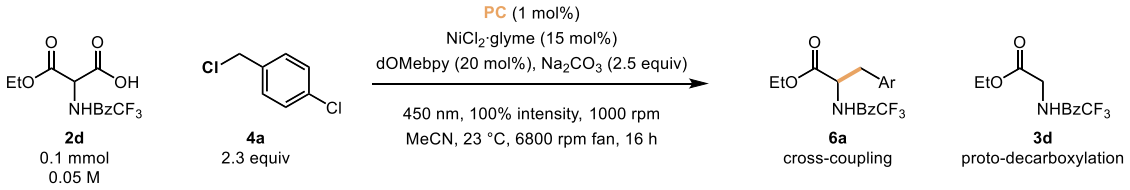

PC	cross-coupling	proto-decarboxylation
$Ir(dF(CF_3)ppy)_2(bpy)PF_6$	46%	73%
$Ir(ppy)_2(bpy)PF_6$	29%	58%
$Ir((CF_3)ppy)_2(bpy)PF_6$	29%	78%
$Ir(dFppy)_2(bpy)PF_6$	**59%**	**38%**
$Ir(Fppy)_3$	17%	64%
$Ir(ppy)_3$	10%	83%
4CzIPN	53%	58%
Eosin Y	0%	>95%
4DPAPN	27%	80%
$CzBr_2IPN$	25%	77%
DZP	0%	91%

Scheme S15. Photochemical decarboxylative arylation screening for iridium and organic photocatalysts. ^{1}H NMR yield vs. mesitylene as internal standard in DMSO-d_6.

We finally assessed the optimized conditions for both Boc and benzamide protected monomalonates with varies electrophiles. Cross-coupling was most effective with benzyl chlorides and 4-CF_3 benzamide as protection group.

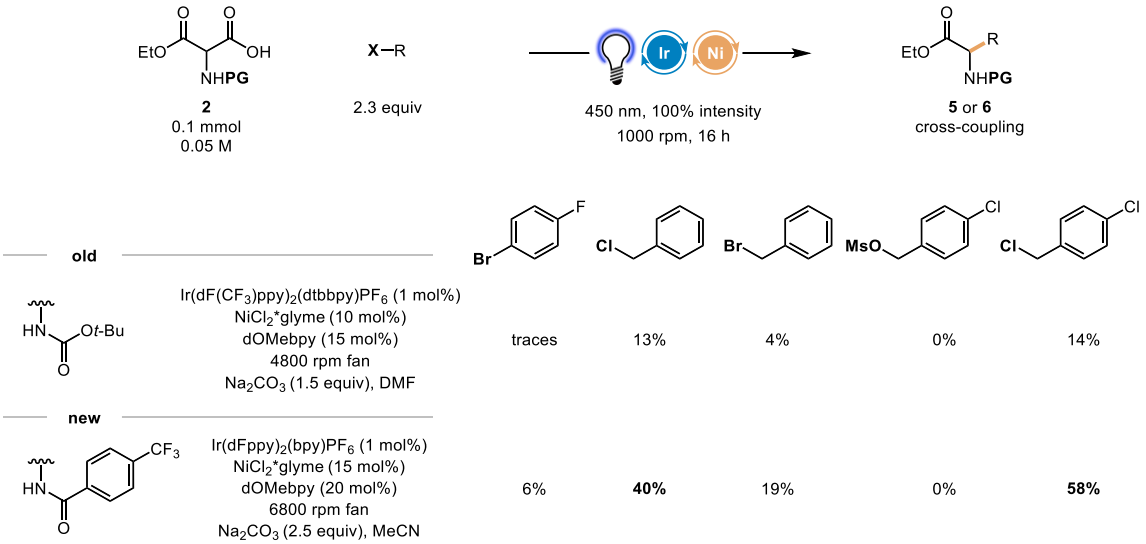

Scheme S16. Compression between reactivity of Boc protected and benzoyl protected acid substrates. ^{1}H NMR yield vs. mesitylene as internal standard in DMSO-d_6.

3. Optimization by DFT

To access a more electrophilic radical species, we conducted DFT calculations to evaluate the SOMO and LUMO energies and their respective SOMO–LUMO energy gaps of a series of structurally related radical models. All initial calculations were performed at the B3LYP/def2-TZVP level of theory.

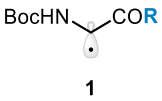

1

R	E_{SOMO} (eV)	E_{LUMO} (eV)	$\Delta E_{SOMO-LUMO}$ (eV)
OEt	-5.18	+0.75	5.93
NHEt	-4.86	+1.03	5.89
NEt_2	-4.85	+0.97	5.82
NHPh	-5.14	-0.55	4.60

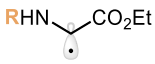

1

R	E_{SOMO} (eV)	E_{LUMO} (eV)	$\Delta E_{SOMO-LUMO}$ (eV)
Boc	-5.18	+0.75	5.93
Ac	-5.33	+0.07	5.40
Bz	**-5.29**	**-1.44**	**3.85**
AcF	-5.98	-1.00	4.99
Ts	-5.30	-1.48	3.83
Phth	-5.78	-2.57	3.21
Ph	-4.56	-0.42	4.14
PMP	-4.31	-0.48	3.83

Figure S1: Initial DFT calculations to assess the SOMO-LUMO gap of protected glycyl radicals.

Drawing on the framework proposed by Nagib and co-workers,[4] which showed that electrophilicity and nucleophilicity indices together offer a quantitative measure of radical polarity, we calculated the global electrophilicity index (ω) for each radical in our series (Figure S2).

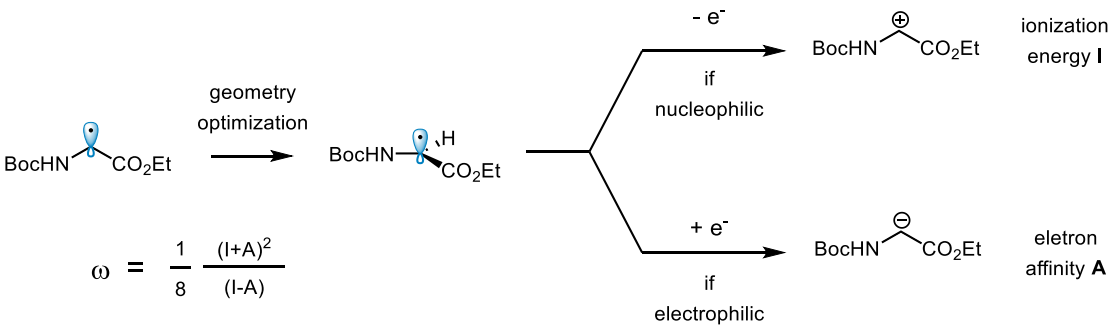

Figure S2: Workflow for determining electrophilicity and nucleophilicity and the equation to calculate electrophilicity (ω) index calculation.

All calculations were performed at the BP86-D3/def2-TZVP level of theory, which has been shown to provide reliable geometries and qualitatively accurate frontier orbital energy trends for radical

species at a balanced computational cost.[5] we examined how changes in frontier orbital properties relate to global electrophilicity. The obtained values were compared to the corresponding SOMO–LUMO gaps (Figure S3). As expected, radicals with smaller SOMO–LUMO gaps generally exhibited higher ω values, consistent with their lower SOMO energies and increased capacity to accept electron density. This trend supports the idea that electronically softened radicals are more electrophilic and potentially better suited for interaction with electron-rich Ni(II) intermediates.

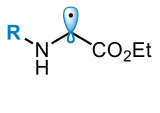

1

R	E_{SOMO} (eV)	E_{LUMO} (eV)	$\Delta E_{SOMO-LUMO}$ (eV)	ω (eV)	Exp yield[a]
Boc	-4.61	-0.58	4.026	1.35	14%[b]
Ac	-4.86	-1.28	3.581	1.50	-
Bz	-4.82	-2.54	2.274	1.65	34%

increased electrophilicity

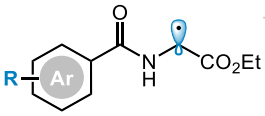

1

Ar	R	E_{SOMO}(eV)	E_{LUMO}(eV)	$\Delta E_{SOMO-LUMO}$ (eV)	ω (eV)	Yield[a]
Ph	***p*-CF_3**	**-5.03**	**-2.96**	**2.07**	**1.78**	37%
Ph	*m*-CF_3	-5.02	-2.86	2.16	1.76	-
Ph	*o*-CF_3	-4.89	-2.51	2.38	1.59	-
Ph	*dimeta*-CF_3	-5.20	-3.2	2.00	1.94	45%
Ph	*p*-OMe	-4.64	-2.20	2.44	1.75	-
Ph	*m*-OMe	-4.71	-2.32	2.38	1.52	-
Ph	*o*-OMe	-4.63	-2.14	2.49	1.43	0%
2-py	-	-4.69	-2.86	2.09	1.52	0%
2-py	4-CF_3	-4.92	-3.30	1.62	1.75	-
3-py	6-CF_3	-5.20	-3.30	1.90	1.81	-
4-py	-	-5.05	-2.93	2.12	1.92	-

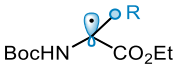

R	ΔE_{SOMO}(eV)	ΔE_{LUMO}(eV)	$\Delta E_{SOMO-LUMO}$ (eV)	ω (eV)
H	-4.61	-0.58	4.03	1.35
Me	-4.54	-0.79	3.75	1.38
Ph	-4.35	-1.17	3.18	1.35

Figure S3: Computational analysis of SOMO, LUMO and SOMO–LUMO gap in glycyl radical and its electrophilicity index calculations. (a= Isolated experimental yields, b= NMR yield with Int. St. 1,3,5-trimethylbenzene)

Overall, these results further highlight how protecting group modification provides a viable strategy for tuning radical polarity through orbital energy control. In this direction, we synthesized a series of acid substrates bearing benzoyl protecting groups to modulate the captodative stabilization of the radical.

We then turned our attention to the orbital interaction between the glycyl radicals and nickel(II) oxidative addition complexes. Following the established protocol,[6] we determined ΔE(SOMO-LUMO) and ΔE(SOMO-HOMO), depending on the interaction of the SOMO of the organic radical

and the HOMO or LUMO or the closed-shell reaction partner. We determined the energies for both glycyl radicals **1a** and **1d**, the oxidative addition complexes **I**-**IV** with the four different electrophiles (ArBr, BnCl, BnBr, BnOMs), and the respective eight combinations.

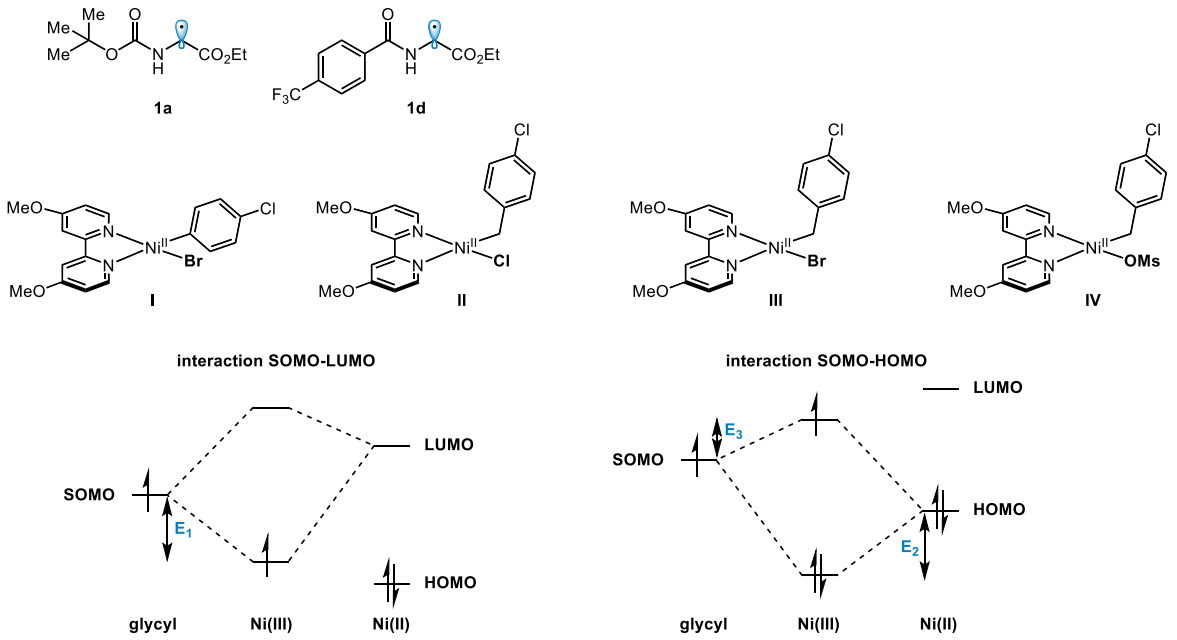

Figure S4: Glycyl radicals and nickel (II) complexes used for frontier orbital interactions ($\Delta E_{SOMO\text{-}LUMO}$ and $\Delta E_{SOMO\text{-}HOMO}$).

Table S1: Summary of HOMO, SOMO, and LUMO energies (in eV) for glycyl radicals, nickel(II) complexes, and their nickel(III) complexes as combinations.

	HOMO (eV)	SOMO (eV)	LUMO (eV)
1a		-4.61	-0.58
1d		-5.03	-2.96
I	-4.381		-3.197
II	-4.128		-3.134
III	-4.119		-3.152
IV	-4.427		-3.383
I-1a	-4.942	-4.636	-3.131
I-1d	-5.213	-4.941	-3.282
II-1a	-4.970	-4.064	-3.046
II-1d	-5.186	-4.806	-3.256
III-1a	-5.117	-4.483	-3.107
III-1d	-5.122	-4.809	-3.267
IV-1a	-5.210	-4.128	-3.090
IV-1d	-5.641	-5.101	-3.241

with $\Delta \mathbf{E_{SOMO-LUMO}} = \mathbf{E_1}$ and

$\Delta \mathbf{E_{SOMO-HOMO}} = \mathbf{2} \cdot \mathbf{E_2} - \boldsymbol{E_3}$ we obtain:

Table S2: Analysis of orbital interactions (in eV).

	E1 (eV)	**$\Delta E_{SOMO-LUMO}$ (eV)**	**(kcal mol^{-1})**	**E2 (eV)**	**E3 (eV)**	**$\Delta E_{SOMO-HOMO}$ (eV)**	**(kcal mol^{-1})**
I-1a	0.026	0.026	0.6	0.561	-0.026	1.148	26.5
I-1d	-0.089	0.089	21	0.832	0.089	1.575	36.3
II-1a	-0.546	0.546	**12.6**	0.842	0.546	1.138	26.2
II-1d	-0.224	0.224	**5.2**	1.058	0.224	1.892	43.6
III-1a	-0.127	0.127	2.9	0.998	0.127	1.869	43.1
III-1d	-0.221	0.221	5.1	1.003	0.221	1.785	41.2
IV-1a	-0.482	0.482	11.1	0.783	0.482	1.084	25.0
IV-1d	0.071	0.071	1.6	1.214	-0.071	2.499	57.6

4. Investigating Tertiary Glycyl Radicals for Quaternary Amino Acids

Based on DFT calculations (Figure S3) we aimed to compare the reactivity of secondary and tertiary glycyl radicals. Therefore, we performed methylation of amino malonates to study tertiary radical reactivity later on.

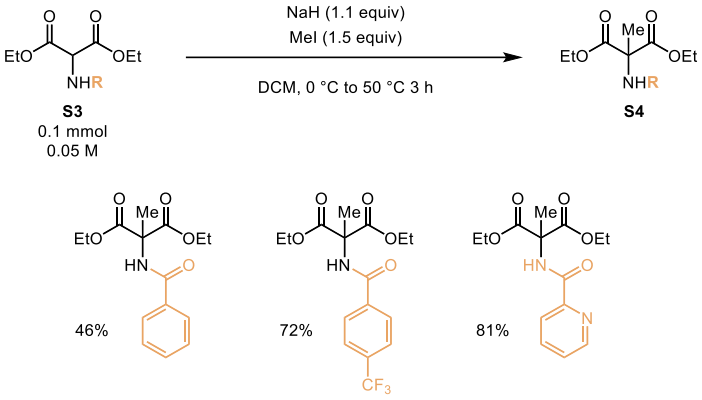

Scheme S17. Methylation of the benzamide protected malonate esters.

The respective methylated protected amino monomalonates were subjected to the optimized conditions. However, only low yields of cross-coupling products were observed.

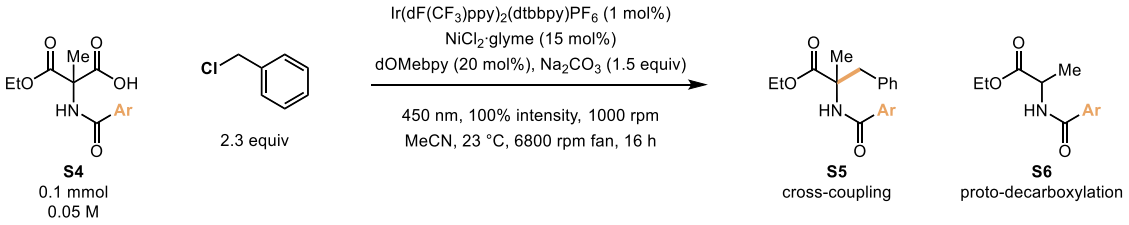

Ar	cross-coupling	proto-decarboxylation
4-CF_3 Ph	10%	50%
Ph	10%	30%
2-py	10%	22%
2-py*	5%	45%

Scheme S18. Photochemical decarboxylative cross-coupling screening with methylated substrates. * Cs_2CO_3 instead of Na_2CO_3. ^{1}H NMR yield vs. mesitylene as internal standard in DMSO-d_6.

5. Limitations

We have evaluated various alkyl and benzyl chlorides and bromides. However, many did not provide the desired product. Based on high proto-decarboxylation yields, fundamental reactivity challenges can be deduced. Due to the fairly nucleophilic nickel catalyst, oxidative addition to electron-rich electrophiles may be hampered. Likewise, radical dehalogenation and benzylic dimerization was observed and may cause low cross-coupling yields. Stronger alkyl or secondary chlorides might be unreactive for this nickel catalyst to undergo oxidative addition.

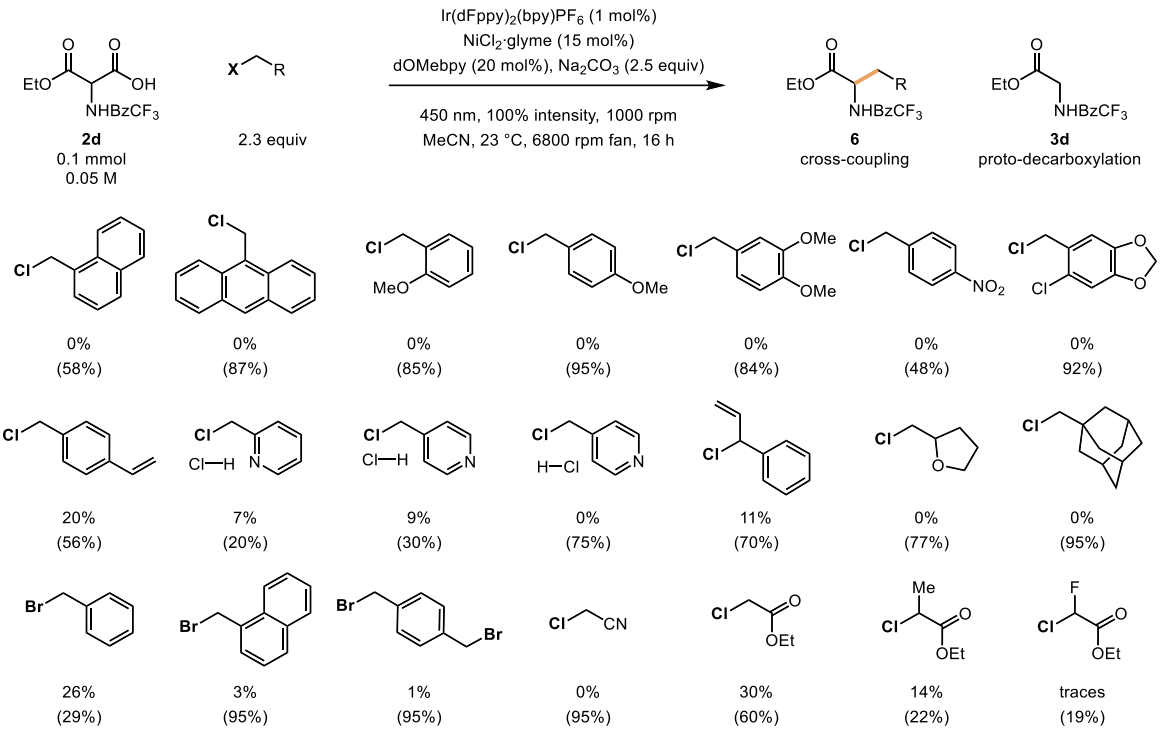

Scheme S19. Photochemical decarboxylative cross-coupling with poorly performing alkyl halides. Yield of proto-decarboxylation in parentheses. ^{1}H NMR yield vs. mesitylene as internal standard in DMSO-d_6.

6. Mechanistic Analysis

Control experiments show that when reaction components are omitted, the cross-coupling behavior is fully inhibited. The background proto-decarboxylation was still observed in all cases.

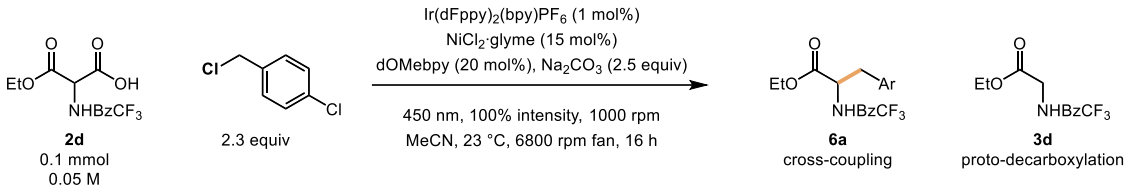

variation	cross-coupling	proto-decarboxylation	
no Ni	0%	47%	
no ligand	0%	50%	
no PC	0%	>95%	
no light	0%	45%	
no base	0%	30%	(60%)

Scheme S20: Photochemical decarboxylative cross-coupling control reactions. Yield of unreacted starting material **2d** in parentheses. ^{1}H NMR yield vs. mesitylene as internal standard in DMSO-d_6.

At this point we were wondering whether the reaction proceeds *via* a radical polar crossover mechanism, where the stable radical is reduced by the same photocatalyst resulting in a carbanion, which is protonated to the proto-decarboxylation product **3**.[7]

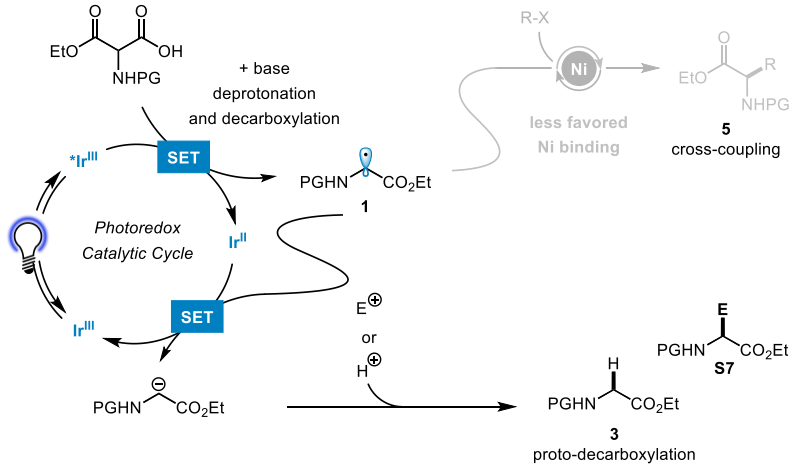

Scheme S21: Proposed mechanism of the decarboxylation of amino malonate. E^+ = electrophile.

To probe whether the reaction proceeds via a radical pathway or an anionic substitution mechanism, we performed trapping experiments with several additives. The addition of 2,2,6,6-tetramethylpiperidine 1-oxyl (TEMPO) as a conventional radical scavenger.[8] Addition of methyl acrylate and 3,4-dihydro-2*H*-pyran to test for polarity-based radical addition reactions. Benzaldehyde, glyoxal, and imine were employed as a trap for carbanions, despite benzaldehyde is also known to trap radical intermediates.[9]

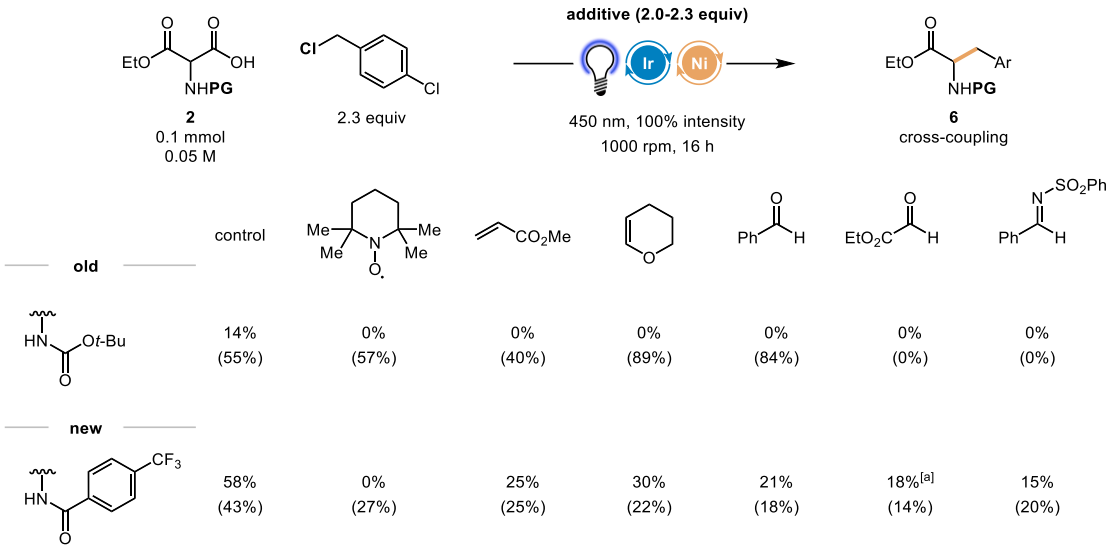

Scheme S22: Radical trapping and radical polar crossover reaction. For reaction conditions see Scheme S16. Yield of proto-decarboxylation in parentheses. ^{1}H NMR yield vs. mesitylene as internal standard in DMSO-d_6. [a] A potential adduct was observed by GCMS analysis.

Analysis of the reaction mixtures of the optimized conditions gave no indication for adduct formation (see below GCMS for benzamide **2d** as substrate shown). Addition of additives resulted mostly in product inhibition as can be seen above. Significant amounts of the dimer from benzyl chloride were observed (Bn2), most likely originating from benzyl radical dimerization. TEMPO led to full inhibition. Addition of electron-poor methyl acrylate, electron-rich 3,4-dihydropyran, or nucleophilic benzaldehyde led to diminished reaction kinetics. For dihydropyran additional amounts of radical addition products were observed. Benzyl radicals are known to form readily in nickel photocatalytic reactions.[10] Only in the case of ethyl glyoxylate a potential adduct was observed by GCMS analysis, but only in the case of the more reactive benzoate protection group.

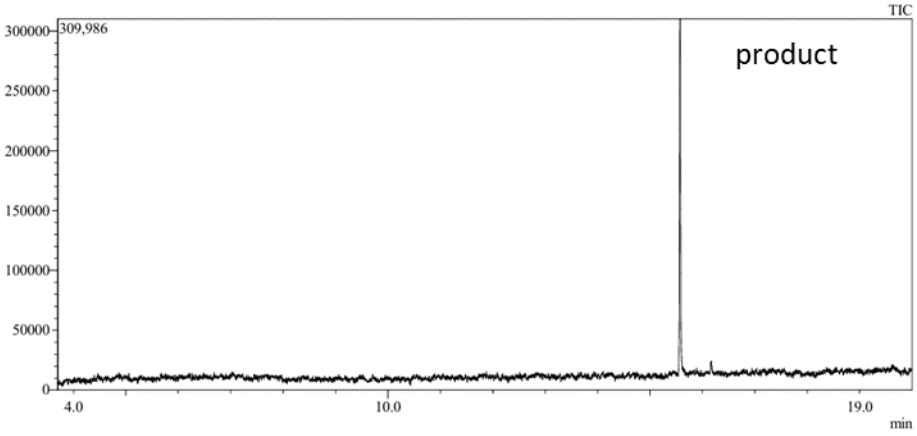

Figure S5: GCMS of the parent control reaction.

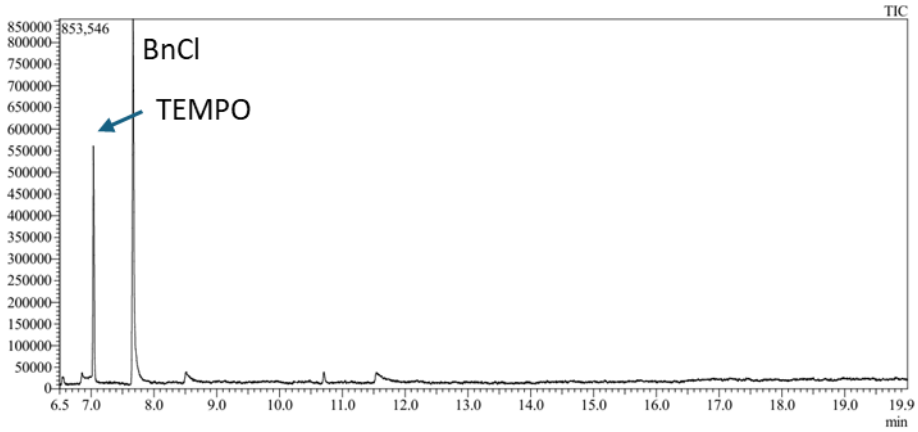

Figure S6: GCMS of the reaction mixture upon addition of TEMPO.

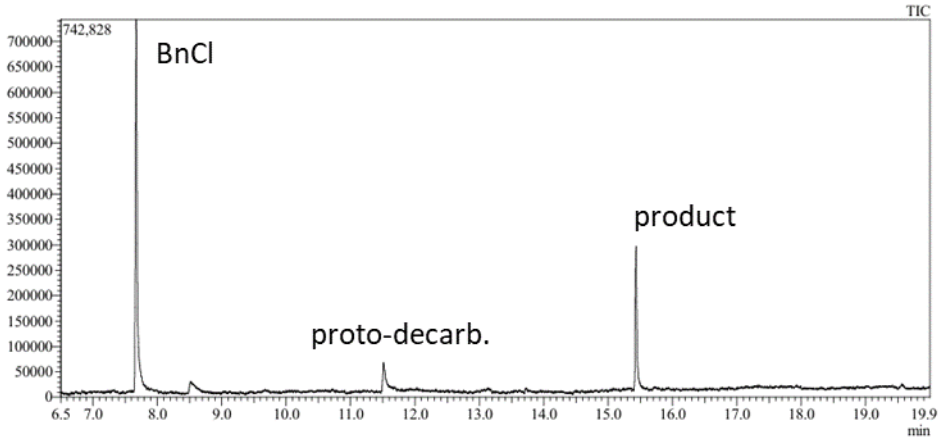

Figure S7: GCMS of the reaction mixture upon addition of methyl acrylate.

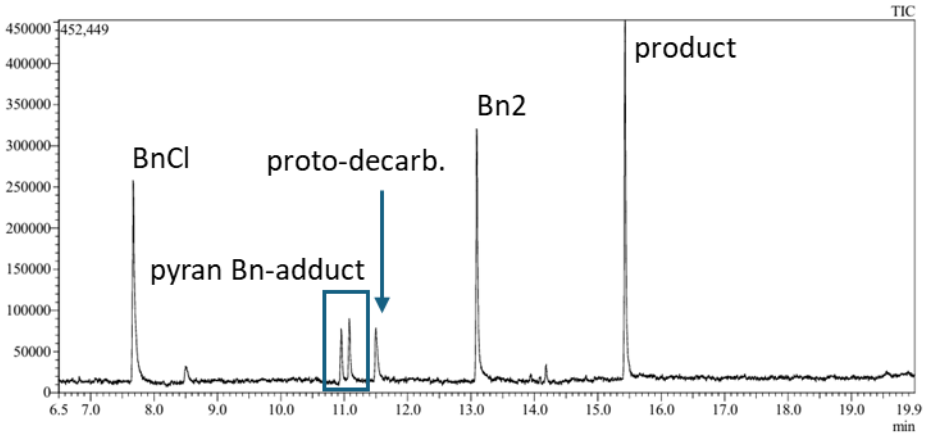

Figure S8: GCMS of the reaction mixture upon addition of 3,4-dihydropyran.

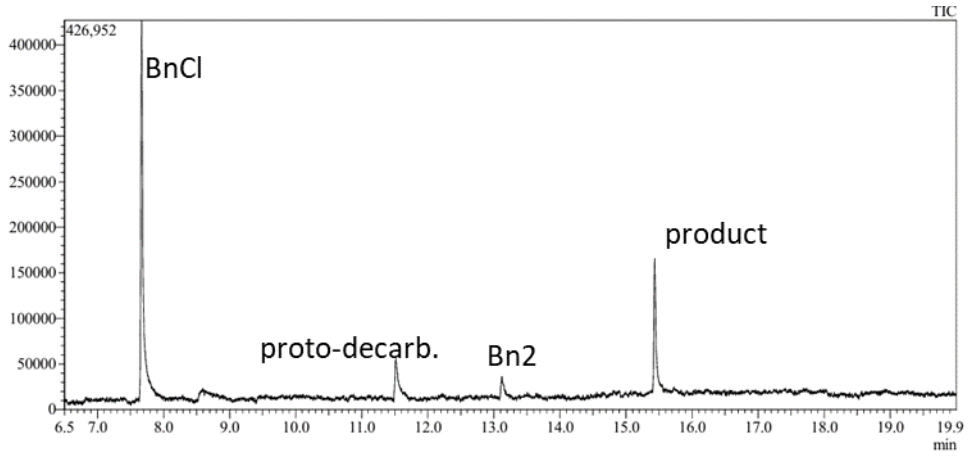

Figure S9: GCMS of the reaction mixture upon addition of benzaldehyde.

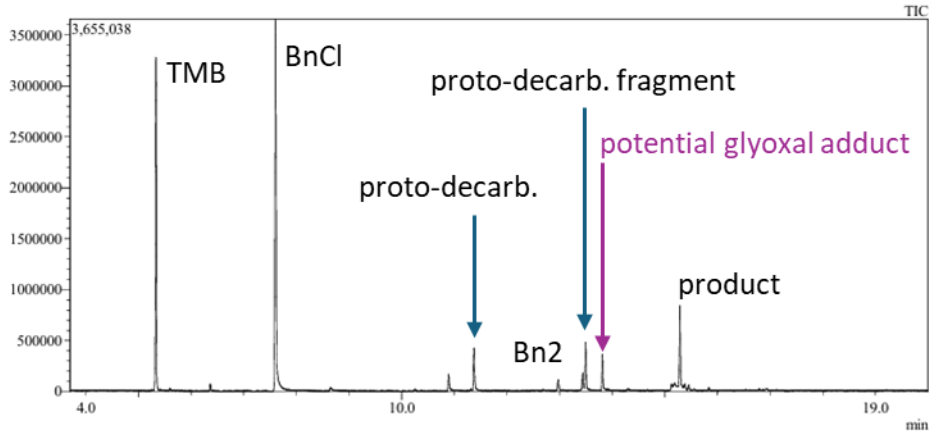

Figure S10: GCMS of the reaction mixture upon addition of ethyl glyoxylate.

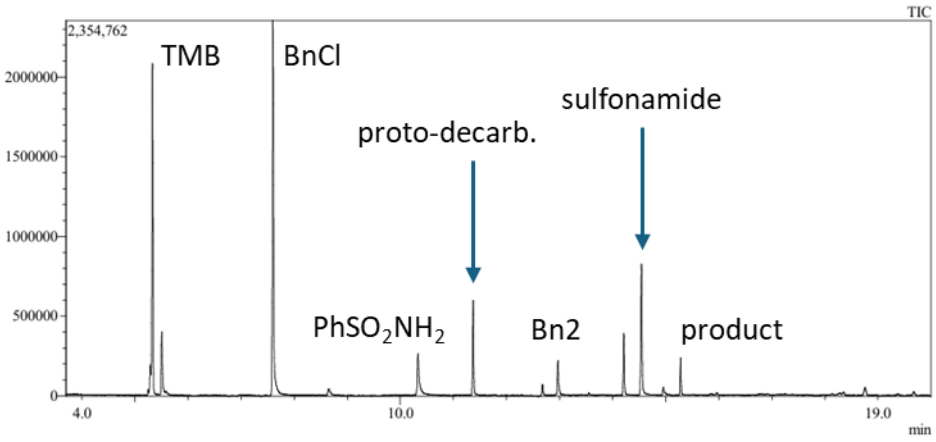

Figure S11: GCMS of the reaction mixture upon addition of *N*-benzylidenbenzolsulfonamid.

Since no other addition products were observed, we conclude that free radicals are preferentially formed during the reaction and are inhibited by TEMPO. The respective radicals are too amphiphilic to react with either electron-rich or electron-poor olefins and a predominant radical-

polar cross-over mechanism is unlikely, since addition was only observed for glyoxylate together with the desired product.

7. CV analysis

Based on the literature, a direct dehalogenation by outer-sphere reduction and mesolytic cleavage could be operational to activate benzyl chlorides, in a halogen-atom transfer (XAT) mechanism.[11, 12] We probed four different nickel complexes. From the cyclic voltammetry (CV) measurements of pure nickel complexes (yellow) and their mixtures (red) with 5 equivalents of 4-chloro benzyl chloride (4-Cl BnCl, pure in blue). All three bpy ligand complexes show a significant increase in current prior to the major redox feature of Ni(II)/Ni(I) or Ni(I)/Ni(0), most likely associated to oxidative addition into the benzyl chloride ($C(sp^3)$–Cl) bond. Only in the case of Ni(salen) an increase of catalytic current at the respective reduction potential indicates the respective outer-sphere behavior. Respectively, in the decarboxylative cross-coupling reaction toward **6a**, only the salen complex gave no yield, while all bpy-based ligands gave productive cross-coupling with benzyl chlorides. A radical-radical recombination of benzyl radical with glycyl radical can thus be ruled out.

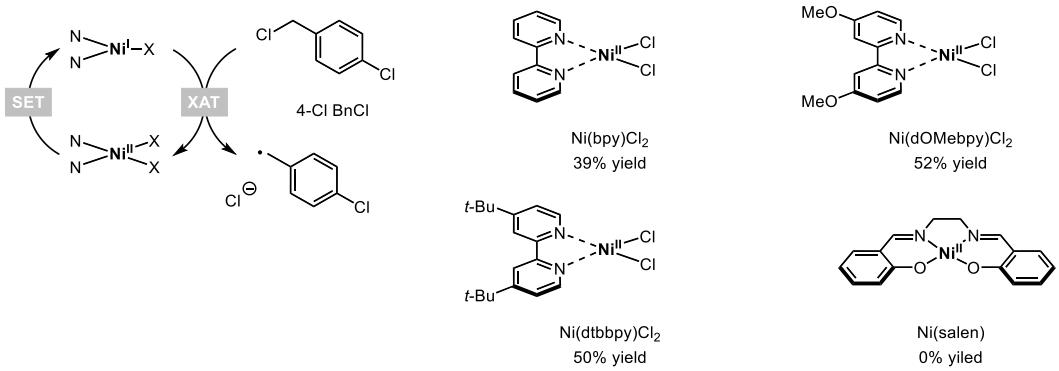

Figure S12: Simplified mechanism and applied nickel catalysts. ^{1}H NMR yields in DMSO-d_6 vs. Mes as internal standard for the parent cross-coupling reaction (*e.g.*, see Scheme S22). XAT: halogen-atom transfer.

For the CV measurement, the samples were prepared as follows: 100 mM tetrabutylammonium hexafluorophosphate ($TBAPF_6$) as supporting electrolyte was dissolve in anhydrous acetonitrile (MeCN). Then, nickel catalyst or 4-Cl BnCl was added to the mixture to obtain a 1 mM solution. Prior to conducting the CV measurements, the mixture was degassed with Argon (Ar). For mixtures, a 1:5 ratio of nickel to benzyl chloride was used. CVs were performed with glassy carbon (GC) as working electrode, glassy carbon (GC) as counter electrode, and potentials are reported against Platinum (Pt) as reference electrode. Reversible or peak potentials are summarized.

Table S3: Summary of the CV analysis.

Entry	Ni complex	$E_{1/2}$ (V)	E_{max} (V)	
1	$Ni(bpy)Cl_2$	- 1.706	- 1.610	- 1.395
2	$Ni(dOMebpy)Cl_2$	- 1.791	N/A	
3	$Ni(dtbbpy)Cl_2$	- 1.819	- 1.884	- 1.527
4	Ni(salen)	- 1.642	- 1.901	

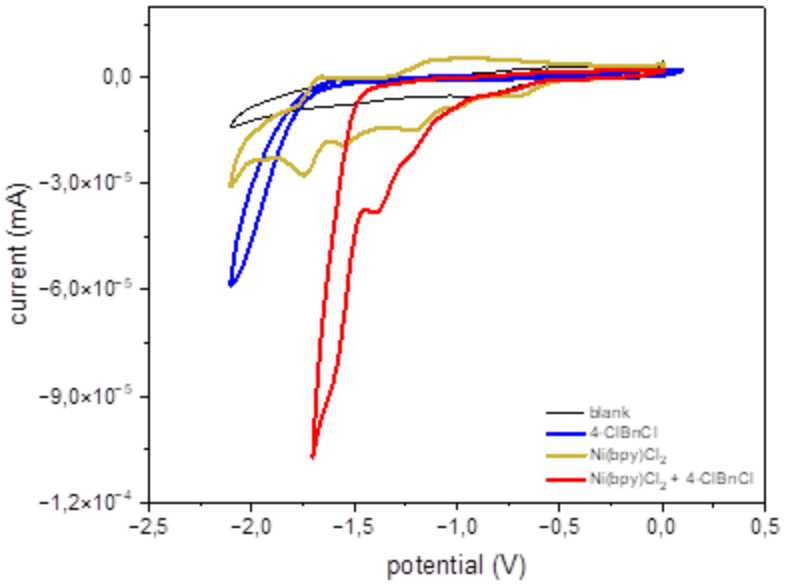

Figure S-13: CV analysis of Ni(bpy)Cl_2 and 4-Cl BnCl.

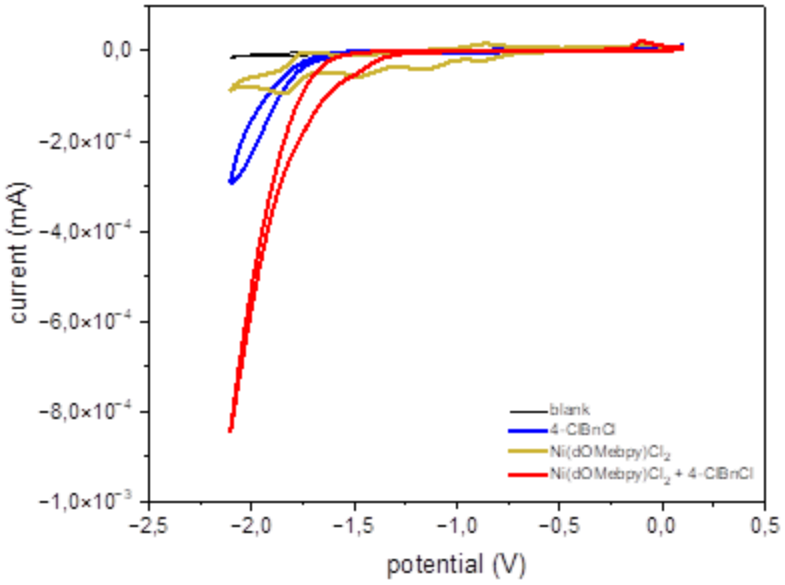

Figure S-14: CV analysis of Ni(dOMebpy)Cl_2 and 4-Cl BnCl.

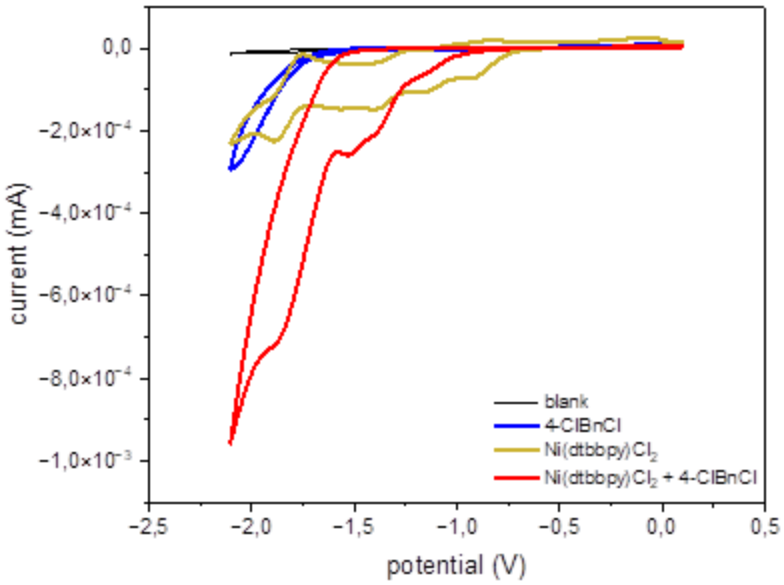

Figure S-15: CV analysis of Ni(dtbbpy)Cl_2 and 4-Cl BnCl.

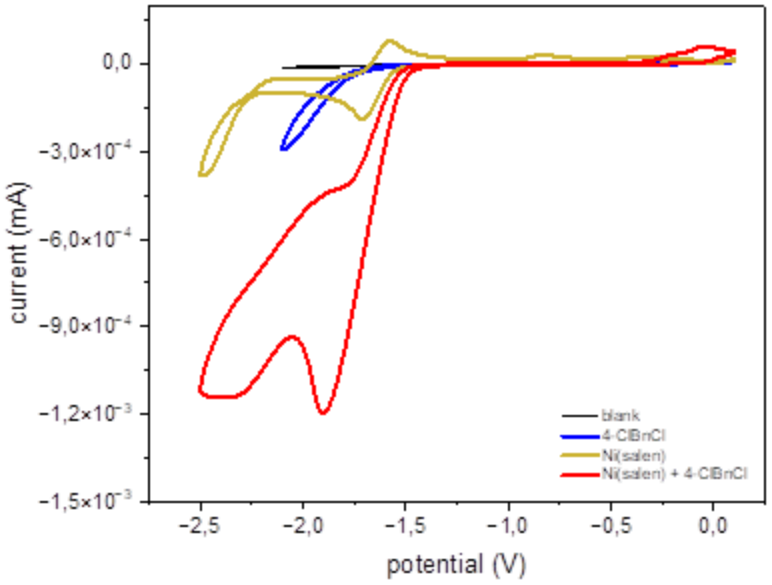

Figure S-16: CV analysis of Ni(salen) and 4-Cl BnCl.

8. Synthesis

Diethyl 2-((*tert*-butoxycarbonyl)amino)malonate

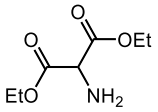

To suspended diethyl aminomalonate hydrochloride (6.0 g, 28.35 mmol, 1 equiv) in a mixture of water (30 mL) and dioxane (15 mL) in a round bottom flask with magnetic bar, $NaHCO_3$ (2.5 g, 29.77 mmol, 1.05 equiv) was slowly added while stirring at room temperature. When the solution became clear after 15 min, a catalyst amount of DMAP (1 mol%, 30 mg) was added followed with a dropwise addition of a solution of $(Boc)_2O$ (6.50 g, 29.77 mmol, 1.05 equiv) in dioxane (45 mL). After the reaction was complete after 16h, the solvents were evaporated in vacuo. The residue was dissolved in EtOAc. The organic phase was washed with solutions of 5% $KHSO_4$, satd. $NaHCO_3$, water, and brine, and dried over anhydrous $MgSO_4$, then filtered and evaporated *in vacuo* to give the product as the white solid (7.71 g, 28.0 mmol, 99% yield). Analytical data in accordance with the literature.[2]

^{1}H NMR (400 MHz, $CDCl_3$): δ = 5.55 (d, *J* = 7.8 Hz, 1H), 4.93 (d, *J* = 7.7 Hz, 1H), 4.26 (qq, *J* = 10.8, 7.1 Hz, 4H), 1.44 (s, 9H), 1.29 (t, *J* = 7.1 Hz, 6H) ppm.

^{13}C NMR (101 MHz, $CDCl_3$): δ = 166.8, 154.9, 80.7, 62.5, 57.7, 28.3, 27.5, 14.1 ppm.

R_f = 0.4 (cyclohexane:ethyl acetate, 7:3).

UPLC-MS t_R = 2.356 min, m/z = 276 $[(M+H)\text{-Boc}]^+$.

2-((*tert*-Butoxycarbonyl)amino)-3-ethoxy-3-oxopropanoic acid

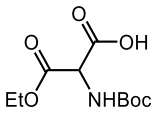

To a solution of diethyl 2-((tert-butoxycarbonyl)amino)malonate (6.37 g, 23.14 mmol, 1 equiv) in dry EtOH (130 mL) in a round bottom flask, a solution of KOH (1.430 g, 25 mmol, 1 equiv) in EtOH (15 mL) was added dropwise, then a catalyst amount of DMAP (10 mol%, 300 mg) while stirring at room temperature. The reaction mixture was kept stirring for overnight at 50 °C. After the reaction was completed, 90% of solvent was removed by evaporated in vacuo. The residue was dissolved in solution of 1 M $NaHCO_3$ (20 mL) and extracted with EtOAc. The aqueous phase was then acidified by $KHSO_4$ (powder) at 0 °C and extracted with EtOAc. The organic phase was dried over anhydrous $MgSO_4$, then filtered and evaporated in vacuo to give the product as the white solid (3.3 g, 13.0 mmol, 57.7% yield). Analytical data in accordance with the literature.[2]

^{1}H NMR (400 MHz, DMSO-*d_6*): δ = 13.37 (s, 1H), 7.49 (d, J = 8.1 Hz, 1H), 4.71 (d, J = 8.1 Hz, 1H), 4.14 (qd, J = 7.1, 3.4 Hz, 2H), 1.41 – 1.36 (m, 17H), 1.19 (t, J = 7.1 Hz, 3H) ppm.

^{13}C NMR (101 MHz, DMSO-*d_6*): δ = 167.7, 167.2, 155.0, 78.8, 61.2, 57.5, 28.0, 13.9 ppm.

R_f = 0.2 (DCM:MeOH, 8:2).

UPLC-MS t_R = 0.65-0.75 min, m/z = 248 $[(M+H) -Boc]^+$.

6.1 General Procedures

General procedure 1 (GP1)

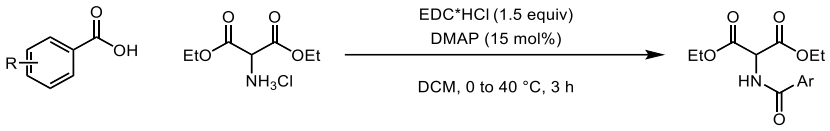

A 100 ml round bottom flask was charged with ***benzoic acid*** (1 equiv), diethyl aminomalonate hydrochloride (5 g, 23.7 mmol, 1 equiv) and DCM (25 mL) under nitrogen at 0 °C and allowed to stir for 5 min. A solution of 1-(3-dimethylaminopropyl)-3-ethylcarbodiimide hydrochloride (EDC, 6.8 g, 35.5 mmol, 1.5 equiv), *N,N*-dimethylpyridin-4-amine (DMAP, 434 mg, 3.5 mmol, 0.15 equiv) dissolved in DCM (25 mL) was added dropwise to the reaction mixture and allowed to stir at 40 °C for 3 h. The reaction was monitored by TLC (cyclohexane: ethyl acetate) until substrate was fully consumed. The reaction mixture was quenched with water and extracted with DCM (3 x 15 mL). The organic phase was then dried over anhydrous magnesium sulfate and concentrated to obtain crude product as colorless oil which was purified by silica flash column chromatography in system (40 g column) (70:30; cyclohexane: ethyl acetate) to afford pure compound as colorless solid.

General procedure 2 (GP2)

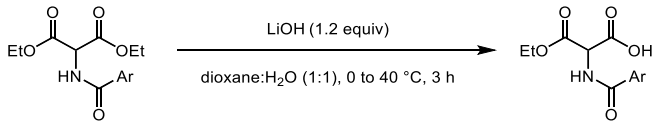

A 100 mL round bottom flask was charged with diethyl 2-[[***aryloxy***] amino] propanedioate (1 equiv) in 1,4-dioxane (25 mL) followed by addition of LiOH (273 mg, 11.4 mmol, 1.2 equiv), dissolved in water (25 mL), which was added dropwise to the reaction mixture at 0 °C and allowed to stir at 40 °C for next 1.5 h. The reaction was monitored by TLC (20% MeOH in DCM). The reaction was quenched with water (25 mL) and acidified with 1 N HCl up to pH of 1-2. A white precipitate formed and was filtered to obtain colorless solid. The obtained solid was purified by silica flash column chromatography (25 g column, DCM: MeOH, 5→10%) for 30 min, to afford the product as a colorless solid.

General procedure 3 (GP3)

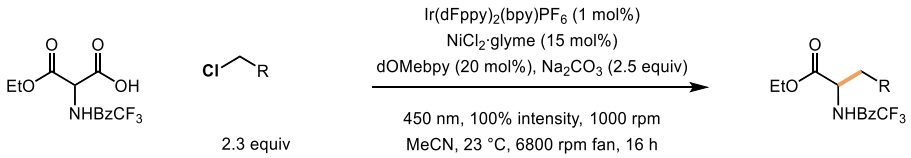

A 20 mL vial was charged with 3-ethoxy-3-oxo-2-(4-(trifluoromethyl)benzamido)propanoic acid (**2d**, 96 mg, 0.3 mmol, 1 equiv), ***alkyl chloride*** (2.3 equiv), dOMebpy (13 mg, 0.06 mmol, 20 mol%), Na_2CO_3 (80 mg, 0.75 mmol, 2.5 equiv), $NiCl_2$ • glyme (10 mg, 0.05 mmol, 15 mol%), $Ir(dFppy)_2(dtbbpy)PF_6$ (1.05 mg, 1 mol%) and MeCN (3 mL). The reaction mixture was degassed by bubbling nitrogen for 5 min. The reaction mixture was then stirred and irradiated in the IPR (450 nm, 100% intensity, 1000 rpm stirring, 6800 rpm fan) for 16 h. The reaction was diluted with water (4 mL) and extracted with ethyl acetate (2 x 5 mL). The organic phase was then dried over anhydrous magnesium sulfate and concentrated to obtain an orangish brown crude product. The crude product was purified by silica flash column chromatography (12 g column, cyclohexane: ethyl acetate) to obtain the pure product as a solid.

6.2 Substrate Synthesis

Diethyl 2-[[4-(trifluoromethyl)benzoyl] amino] propanedioate

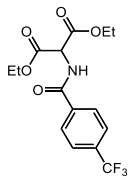

Following **GP1**, 4-(trifluoromethyl) benzoic acid (4.5 g, 23.7 mmol), was used and the reaction mixture and allowed to stir at 40 °C for 3 h. The pure product was obtained as a colorless solid (6.45 g, 18.5 mmol, 78%).

^{1}H NMR (400 MHz, DMSO-*d*$_6$): δ = 9.60 (d, *J* = 7.6 Hz, 1H), 8.13 – 8.06 (m, 2H), 7.91 – 7.87 (m, 2H), 5.33 (d, *J* = 7.5 Hz, 1H), 4.30 – 4.13 (m, 4H), 1.23 (t, *J* = 7.1 Hz, 6H) ppm.

^{13}C NMR (101 MHz, DMSO-*d*$_6$): δ = 166.3, 165.4, 136.7, 128.6, 125.5 (d, *J* = 3.8 Hz), 61.8, 56.6, 13.9 ppm.

^{19}F NMR (376 MHz, DMSO-*d*$_6$): δ = -61.4 ppm.

R_f = 0.6 (cyclohexane:ethyl acetate, 7:3).

HRMS (ESI+) calculated for $C_{15}H_{16}F_3NO_5$ ([M+Na]$^+$) 370.0878, found 370.0875.

Diethyl 2-benzamidomalonate

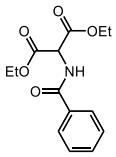

Following **GP1**, benzoic acid (1.15 g, 9.4 mmol), was used and the reaction mixture and allowed to stir at 40 °C for 3 h. The pure product was obtained as a colorless solid (2.1 g, 7.5 mmol, 79%).[13, 14]

^{1}H NMR (400 MHz, DMSO-*d*$_6$): δ = 13.54 (s, 1H), 9.12 (d, *J* = 7.5 Hz, 1H), 7.96 – 7.89 (m, 2H), 7.60 – 7.53 (m, 1H), 7.49 (dd, *J* = 8.2, 6.7 Hz, 2H), 5.19 (d, *J* = 7.5 Hz, 1H), 4.23 – 4.14 (m, 2H), 1.22 (t, *J* = 7.1 Hz, 3H) ppm.

^{13}C NMR (101 MHz, DMSO-*d*$_6$): δ = 169.8, 166.4 (d, J = 37.6 Hz), 131.7, 131.50, 128.3 (d, J = 1.7 Hz), 127.2, 60.4, 41.3, 14.1 ppm.

R_f = 0.2 (DCM:MeOH, 8:2).

UPLC-MS t_R = 2.67 min, m/z = 280.04 [M+H]$^+$.

Diethyl 2-(3,5-bis(trifluoromethyl)benzamido)malonate

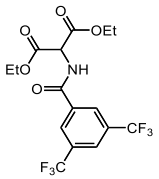

Following **GP1**, 3,5-bis(trifluoromethyl)benzoic acid (1.3 g, 5.2 mmol), was used and the reaction mixture and allowed to stir at 40 °C for 3 h. The pure product was obtained as a colorless solid (0.63 g, 1.5 mmol, 45%).

^{1}H NMR (400 MHz, DMSO-d_6): δ = 9.96 (d, *J* = 7.6 Hz, 1H), 8.56 (d, *J* = 1.8 Hz, 2H), 8.41 – 8.36 (m, 1H), 5.40 (d, *J* = 7.6 Hz, 1H), 4.31 – 4.14 (m, 4H), 1.23 (t, *J* = 7.1 Hz, 6H) ppm.

^{13}C NMR (101 MHz, DMSO) δ = 166.1, 163.8, 135.0, 130.6 (q, *J* = 33.4 Hz), 128.5, 127.1, 125.6 (d, *J* = 4.0 Hz), 124.4, 121.7, 119.0, 61.9, 56.6, 13.9 ppm.

^{19}F NMR (376 MHz, DMSO-d_6): δ = -61.3 ppm.

R_f = 0.6 (cyclohexane:ethyl acetate, 7:3).

HRMS (ESI+) calculated for $C_{16}H_{15}F_6NO_5$ ($[M+Na]^+$) 438.0752, found 438.0744.

Diethyl 2-(picolinamido)malonate

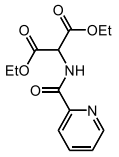

Following **GP1**, pyridine-2-carboxylic acid (1.16 g, 9.4 mmol), was used and the reaction mixture and allowed to stir at 40 °C for 3 h. The pure product was obtained as a colorless solid (2.1 g, 7.5 mmol, 79%).[13]

^{1}H NMR (400 MHz, DMSO-d_6): δ = 9.06 (d, *J* = 6.5 Hz, 1H), 8.72 (dt, *J* = 4.7, 1.3 Hz, 1H), 8.06 – 8.04 (m, 2H), 7.68 (td, *J* = 4.9, 3.8 Hz, 1H), 5.22 (d, *J* = 6.5 Hz, 1H), 4.22 (q, *J* = 7.1 Hz, 4H), 1.22 (t, *J* = 7.1 Hz, 6H) ppm.

^{13}C NMR (101 MHz, DMSO-d_6): δ = 166.5, 163.9, 149.3, 148.8, 138.6, 127.8, 122.5, 62.5, 56.9, 14.3 ppm.

R_f = 0.5 (cyclohexane:ethyl acetate, 7:3).

UPLC-MS t_R = 2.059 min, m/z = 281 $[M+H]^+$.

Diethyl 2-(2-methoxybenzamido) malonate

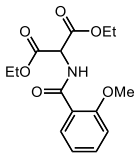

Following **GP1**, 2-methoxybenzoic acid (1.3 g, 5.2 mmol), was used and the reaction mixture and allowed to stir at 40 °C for 3 h. The pure product was obtained as a colorless solid (0.63 g, 1.5 mmol, 45%).

^{1}H NMR (400 MHz, DMSO-d_6): δ = 9.03 (d, *J* = 5.5 Hz, 1H), 7.91 (dd, *J* = 7.8, 1.9 Hz, 1H), 7.57 (ddd, *J* = 8.4, 7.3, 1.9 Hz, 1H), 7.24 (dd, *J* = 8.4, 1.0 Hz, 1H), 7.09 (td, *J* = 7.5, 1.0 Hz, 1H), 5.20 (d, *J* = 5.5 Hz, 1H), 4.31 – 4.13 (m, 4H), 1.22 (t, *J* = 7.1 Hz, 5H) ppm.

^{13}C NMR (101 MHz, DMSO-d_6): δ = 166.1, 163.8, 157.6, 133.7, 131.0, 120.9, 119.8, 112.5, 62.0, 57.2, 56.3, 13.8 ppm.

R_f = 0.5 (cyclohexane:ethyl acetate, 7:3).

HRMS (ESI+) calculated for $C_{15}H_{19}NO_6$ ($[M+Na]^+$) 322.1110, found 322.1102.

Diethyl 2-(4-methoxybenzamido)malonate

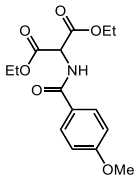

Following **GP1**, 4-methoxybenzoic acid (1.3 g, 5.2 mmol), was used and the reaction mixture and allowed to stir at 40 °C for 3 h. The pure product was obtained as a colorless solid (0.65 g, 2.1 mmol, 35%).[13]

^{1}H NMR (400 MHz, DMSO-d_6): δ = 9.16 (d, J = 7.6 Hz, 1H), 7.94 – 7.86 (m, 2H), 7.06 – 6.98 (m, 2H), 5.28 (d, J = 7.6 Hz, 1H), 4.28 – 4.11 (m, 4H), 3.82 (s, 3H), 1.22 (t, J = 7.1 Hz, 6H) ppm.

^{13}C NMR (101 MHz, DMSO-d_6): δ = 166.7, 165.8, 162.0, 129.6, 125.0, 113.6, 61.6, 56.4, 55.4, 13.9 ppm.

R_f = 0.4 (cyclohexane:ethyl acetate, 7:3).

UPLC-MS t_R = 1.93 min, m/z = 310 $[M+H]^+$.

3-Ethoxy-3-oxo-2-(4-(trifluoromethyl)benzamido) propanoic acid

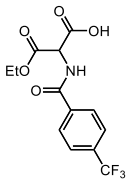

Following **GP2**, diethyl 2-[[4-(trifluoromethyl)benzoyl] amino] propanedioate (3.3 g, 9.5 mmol) was used and afforded the product as a colorless solid (2.2 g, 6.9 mmol, 72%).

^{1}H NMR (400 MHz, DMSO-*d*$_6$): δ = 13.56 (s, 1H), 9.46 (d, *J* = 7.6 Hz, 1H), 8.10 (d, *J* = 8.2 Hz, 2H), 7.88 (d, *J* = 8.2 Hz, 2H), 5.24 (d, *J* = 7.6 Hz, 1H), 4.20 (q, *J* = 1.1 Hz, 2H), 1.22 (t, *J* = 7.1 Hz, 3H) ppm.

^{13}C NMR (101 MHz, DMSO-*d*$_6$): δ = 167.4, 165.4, 136.8, 131.5 (q, *J* = 31.8 Hz), 128.6, 125.4 (m), 61.5, 56.7, 13.9 ppm.

^{19}F NMR (376 MHz, DMSO-*d*$_6$): δ = -61.3 ppm.

R_f = 0.2 (DCM:MeOH, 8:2).

HRMS (ESI+) calculated for $C_{13}H_{12}F_3NO_5$ ([M+Na]$^+$) 342.0565, found 342.0559.

2-Benzamido-3-ethoxy-3-oxopropanoic acid.

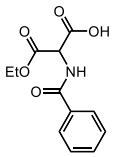

Following **GP2**, diethyl 2-benzamidomalonate (2.1 g, 7.1 mmol) was used and afforded the product as a colorless solid (0.9 g, 3.5 mmol, 44%).

^{1}H NMR (400 MHz, DMSO-*d*$_6$): δ = 13.54 (s, 1H), 9.12 (d, *J* = 7.5 Hz, 1H), 7.96 – 7.89 (m, 2H), 7.60 – 7.53 (m, 1H), 7.49 (dd, *J* = 8.2, 6.7 Hz, 2H), 5.19 (d, *J* = 7.5 Hz, 1H), 4.23 – 4.14 (m, 2H), 1.22 (t, *J* = 7.1 Hz, 3H) ppm.

^{13}C NMR (126 MHz, DMSO-*d*$_6$): δ = 166.5, 132.9, 131.9, 128.4, 127.6, 61.6, 56.5, 13.9 ppm.

R_f = 0.2 (DCM:MeOH, 8:2).

LCMS t_R = 0.275 min, m/z = 251 [M+H]$^+$.

HRMS (ESI+) calculated for $C_{12}H_{13}NO_5$ ([M+H]$^+$) 252.0872, found 252.0866.

2-(3,5-Bis(trifluoromethyl)benzamido)-3-ethoxy-3-oxopropanoic acid

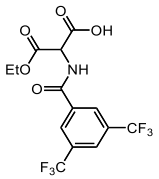

Following **GP2**, diethyl 2-(3,5-bis(trifluoromethyl)benzamido)malonate (1.1 g, 2.7 mmol) was used and afforded the product as a colorless solid (0.28 g, 0.72 mmol, 21%).[1]

^{1}H NMR (400 MHz, DMSO-d_6): δ = 13.70 (s, 1H), 9.87 (d, *J* = 7.6 Hz, 1H), 8.55 (dd, *J* = 19.4, 1.7 Hz, 2H), 8.38 (s, 1H), 5.29 (d, *J* = 7.6 Hz, 1H), 4.21 (q, *J* = 7.1 Hz, 2H), 1.23 (t, *J* = 7.1 Hz, 3H) ppm.

^{13}C NMR (101 MHz, DMSO-d_6): δ = 167.3, 166.6, 163.7, 135.1, 130.5 (m), 128.6 (m), 125.5, 61.6, 56.8, 13.9 ppm.

^{19}F NMR (376 MHz, DMSO-d_6): δ = -61.3 ppm.

R_f = 0.2 (DCM:MeOH, 8:2).

HRMS (ESI+) calculated for $C_{14}H_{11}F_6NO_5$ ($[M+Na]^+$) 410.0439, found 410.0437.

3-Ethoxy-3-oxo-2-(picolinamido) propanoic acid

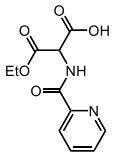

Following **GP2**, diethyl 2-(picolinamido)malonate (2.1 g, 7.1 mmol) was used and afforded the product as a colorless semiliquid (0.8 g, 3.1 mmol, 37%).[2]

^{1}H NMR (500 MHz, DMSO-d_6): δ = 13.92 (s, 1H), 8.90 (d, *J* = 6.3 Hz, 1H), 8.71 (dt, *J* = 4.7, 1.4 Hz, 1H), 8.05 (d, *J* = 1.3 Hz, 1H), 8.04 (dd, *J* = 2.5, 1.3 Hz, 1H), 7.68 (ddd, *J* = 5.8, 4.7, 3.2 Hz, 1H), 5.12 (d, *J* = 6.3 Hz, 1H), 4.21 (q, *J* = 7.1 Hz, 2H), 1.21 (t, *J* = 7.1 Hz, 3H) ppm.

^{13}C NMR (126 MHz, DMSO-d_6): δ = 167.1, 166.5, 163.2, 148.8, 148.4, 138.2, 127.3, 121.9, 61.8, 56.6, 54.9, 13.9 ppm.

---

[1] Minor Proto decarboxylation (~12%) occurs as a background process without affecting the cross-coupling reaction.

[2] Minor Proto decarboxylation (~6%) occurs as a background process without affecting the cross-coupling reaction.

R_f = 0.1 (DCM:MeOH, 8:2).

UPLC-MS t_R = 0.76-0.94 min, m/z = 253 $[M+H]^+$.

HRMS (ESI+) calculated for $C_{11}H_{12}N_2O_5$ ($[M+H]^+$) 253.0824, found 253.0818.

3-Ethoxy-2-(2-methoxybenzamido)-3-oxopropanoic acid

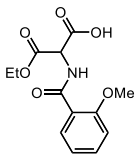

Following **GP2**, diethyl 2-(2-methoxybenzamido) malonate (0.65 g, 2.7 mmol) was used and afforded the product as a colorless solid (0.66 g, 2.3 mmol, 68%).[3]

^{1}H NMR (400 MHz, DMSO-d_6): δ = 13.80 (s, 1H), 8.99 (d, *J* = 5.4 Hz, 1H), 7.93 (dd, *J* = 7.8, 1.9 Hz, 1H), 7.57 (td, *J* = 7.3, 1.9 Hz, 1H), 7.24 (dd, *J* = 8.5, 1.0 Hz, 1H), 7.10 (td, *J* = 7.5, 1.0 Hz, 1H), 5.08 (d, *J* = 5.4 Hz, 1H), 4.20 (qd, *J* = 7.1, 0.9 Hz, 2H), 3.99 (s, 3H), 1.22 (t, *J* = 7.1 Hz, 3H) ppm.

^{13}C NMR (101 MHz, DMSO-d_6): δ = 167.6, 167.2, 164.1, 158.1, 134.1, 131.5, 121.4, 113.0, 62.09, 57.8, 56.8, 14.3 ppm.

R_f = 0.1 (DCM:MeOH, 8:2).

HRMS (ESI+) calculated for $C_{13}H_{15}NO_6$ ($[M+H]^+$) 282.0978, found 282.0971.

3-Ethoxy-2-(4-methoxybenzamido)-3-oxopropanoic acid

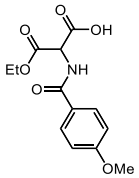

Following **GP2**, diethyl 2-(2-methoxybenzamido) malonate (0.65 g, 2.7 mmol) was used and afforded the product as a colorless solid (0.22g, 0.78 mmol, 18%).[4]

---

[3] Minor Proto decarboxylation (~10%) occurs as a background process without affecting the cross-coupling reaction.

[4] Proto decarboxylation (~50%) occurs as a background process (Note- bit challenging to synthesis, decomposes to proto-decarboxylation side product).

^{1}H NMR (400 MHz, DMSO-d_6): δ = 13.4 (s, 1H), 8.92 (d, J = 7.5 Hz, 1H), 7.94 – 7.86 (m, 3H), 7.01 (d, J = 8.6 Hz, 2H), 5.15 (d, J = 7.4 Hz, 1H), 4.17 (q, J = 7.1 Hz, 2H), 3.84 – 3.78 (m, 6H), 1.25 – 1.17 (m, 6H) ppm.

R_f = 0.1 (DCM:MeOH, 8:2).

UPLC-MS t_R = 2.42 min, m/z = 282 $[M+H]^+$, Proto-decarboxylation: t_R = 1.44 min, m/z = 238 $[M+H]^+$.

6.3 Syntheses

Ethyl 3-(4-chlorophenyl)-2-(4-(trifluoromethyl)benzamido) propanoate (6a)

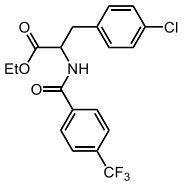

Following **GP3**, 3-ethoxy-3-oxo-2-(4-(trifluoromethyl)benzamido) propanoic acid (96 mg, 0.3 mmol, 1 equiv) and 1-chloro-4-(chloromethyl)benzene (90 µL, 0.69 mmol, 2.3 equiv) were used. The pure product as an off-white solid (50 mg, 0.12 mmol, 37%).

^{1}H NMR (400 MHz, DMSO-d_6): δ = 9.11 (d, J = 7.8 Hz, 1H), 7.98 (d, 2H), 7.86 (d, 2H), 7.37 – 7.28 (m, 4H), 4.66 (ddd, J = 10.0, 7.8, 5.5 Hz, 1H), 4.15 – 4.05 (m, 2H), 3.20 – 3.05 (m, 1H), 1.18 – 1.10 (m, 4H) ppm.

^{13}C NMR (101 MHz, DMSO-d_6): δ = 171.7, 165.7, 137.8, 137.0, 131.6, 131.4, 128.6 (d, J = 7.0 Hz), 125.9 (d, J = 3.8 Hz), 61.2, 54.6, 35.9, 14.4 ppm.

^{19}F NMR (376 MHz, DMSO-d_6): δ = -61.3 ppm.

R_f = 0.6 (cyclohexane:ethyl acetate, 7:3).

HRMS (ESI+) calculated for $C_{19}H_{17}ClF_3NO_3$ ($[M+H]^+$) 400.0927, found 400.0922.

Ethyl 2-benzamido-3-(4-chlorophenyl) propanoate (6b)

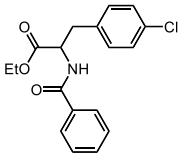

Following **GP3**, 2-benzamido-3-ethoxy-3-oxopropanoic acid (76 mg, 0.3 mmol, 1 equiv), and 1-chloro-4-(chloromethyl)benzene (90 µL, 0.69 mmol, 2.3 equiv) were used. The pure product as an off-white solid (34 mg, 0.1 mmol, 34%).

^{1}H NMR (400 MHz, DMSO-d_6): δ = 8.83 (d, J = 7.8 Hz, 1H), 7.81 – 7.76 (m, 2H), 7.56 – 7.51 (m, 1H), 7.49 – 7.43 (m, 2H), 7.33 (s, 4H), 4.68 – 4.59 (m, 1H), 4.10 (q, J = 7.1 Hz, 2H), 3.19 – 3.04 (m, 2H), 1.14 (t, J = 7.1 Hz, 3H) ppm.

^{13}C NMR (126 MHz, DMSO-d_6): δ = 171.5, 166.4, 136.7, 133.6, 131.5, 131.1, 131.0, 128.3, 128.1, 127.3, 60.6, 54.1, 35.5, 14.0 ppm.

R_f = 0.5 (cyclohexane:ethyl acetate, 7:3).

HRMS (ESI+) calculated for $C_{18}H_{18}ClNO_3$ ([M+Na]$^+$) 354.0873, found 354.0865.

Ethyl 2-(3,5-bis(trifluoromethyl)benzamido)-3-(4-chlorophenyl)propanoate (6c)

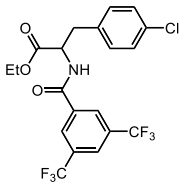

Following **GP3**, 2-(3,5-bis(trifluoromethyl)benzamido)-3-ethoxy-3-oxopropanoic acid (116 mg, 0.29 mmol, 1 equiv), and 1-chloro-4-(chloromethyl)benzene (90 µL, 0.69 mmol, 2.3 equiv) were used. The pure product as an off-white solid (62.5 mg, 0.13 mmol, 45%).

^{1}H NMR (400 MHz, DMSO-*d*$_6$): δ = 9.39 (d, *J* = 7.7 Hz, 1H), 8.47 – 8.39 (m, 2H), 8.35 (s, 1H), 7.37 – 7.29 (m, 4H), 4.72 (ddd, *J* = 9.6, 7.7, 5.9 Hz, 1H), 4.10 (q, *J* = 7.1 Hz, 2H), 3.24 – 3.04 (m, 2H), 1.13 (t, *J* = 7.1 Hz, 3H) ppm.

^{13}C NMR (101 MHz, DMSO-*d*$_6$): δ = 171.4, 163.9, 136.7, 136.1, 131.7, 131.4, 131.2, 130.8, 128.6, 61.3, 54.7, 36.0, 14.4 ppm.

^{19}F NMR (376 MHz, DMSO-*d*$_6$): δ = -61.3 ppm.

R_f = 0.5 (cyclohexane:ethyl acetate, 7:3).

HRMS (ESI+) calculated for $C_{20}H_{16}ClF_6NO_3$ ([M+Na]$^+$) 490.0621, found 490.0613.

Ethyl (4-(trifluoromethyl) benzoyl) phenylalaninate (6d)

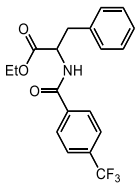

Following **GP3**, 3-ethoxy-3-oxo-2-(4-(trifluoromethyl)benzamido)propanoic acid (96 mg, 0.3 mmol, 1 equiv), and chloromethyl benzene (79 µl, 0.69 mmol, 2.3 equiv), were used. The pure product as an off-white solid (45 mg, 0.12 mmol, 41%).

^{1}H NMR (400 MHz, DMSO-*d*$_6$): δ = 9.11 (d, *J* = 7.7 Hz, 1H), 7.99 (d, 2H), 7.86 (d, 2H), 7.32 – 7.24 (m, 4H), 7.23 – 7.16 (m, 1H), 4.66 (ddd, *J* = 9.9, 7.7, 5.6 Hz, 1H), 4.09 (q, *J* = 7.1 Hz, 2H), 3.21 – 3.06 (m, 2H), 1.13 (t, *J* = 7.1 Hz, 3H) ppm.

^{13}C NMR (101 MHz, DMSO-d_6): δ = 71.9, 165.8, 137.9, 129.5, 128.7 (d, *J* = 1.0 Hz), 127.0, 125.8 (d, *J* = 3.8 Hz), 61.1, 54.9, 36.7, 14.4 ppm.

^{19}F NMR (376 MHz, DMSO-d_6): δ = -58.5 ppm.

R_f = 0.5 (cyclohexane:ethyl acetate, 1:1).

HRMS (ESI+) calculated for $C_{19}H_{18}F_3NO_3$ ([M+Na]$^+$) 388.1136, found 388.1129.

Ethyl 3-(4-fluorophenyl)-2-(4-(trifluoromethyl)benzamido)propanoate (6e)

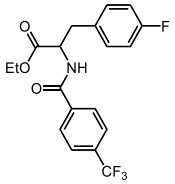

Following **GP3**, 3-ethoxy-3-oxo-2-(4-(trifluoromethyl)benzamido)propanoic acid (96 mg, 0.3 mmol, 1 equiv), and 1-(chloromethyl)-4-fluorobenzene (83 µl, 0.69 mmol, 2.3 equiv), were used. The pure product as an off-white solid (48 mg, 0.12 mmol, 42%).

^{1}H NMR (400 MHz, DMSO-d_6): δ = 9.09 (d, *J* = 7.8 Hz, 1H), 7.98 (d, *J* = 8.2 Hz, 2H), 7.86 (d, *J* = 8.2 Hz, 2H), 7.36 – 7.30 (m, 2H), 7.13 – 7.06 (m, 2H), 4.65 (ddd, *J* = 9.9, 7.7, 5.6 Hz, 1H), 4.10 (q, *J* = 7.1 Hz, 2H), 3.20 – 3.04 (m, 2H), 1.14 (t, *J* = 7.1 Hz, 3H) ppm.

^{13}C NMR (101 MHz DMSO-d_6): δ = 171.3, 165.3, 162.2, 159.8, 137.3, 133.6 (d, *J* = 3.2 Hz), 130.9 (d, *J* = 8.1 Hz), 128.2, 125.41(d, *J* = 3.7 Hz), 115.0, 114.8, 60.6, 54.4, 35.3, 14.0 ppm.

^{19}F NMR (376 MHz, DMSO-d_6): δ = -61.3, -116.5 ppm.

R_f = 0.4 (cyclohexane:ethyl acetate, 7:3).

HRMS (ESI+) calculated for $C_{19}H_{17}F_4NO_3$ ([M+Na]$^+$) 406.1042, found 406.1035.

Ethyl 3-(4-bromophenyl)-2-(4-(trifluoromethyl)benzamido)propanoate (6f)

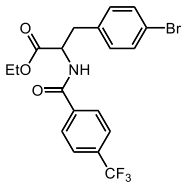

Following **GP3**, 3-ethoxy-3-oxo-2-(4-(trifluoromethyl)benzamido)propanoic acid (96 mg, 0.3 mmol, 1 equiv), and 1-bromo-4-(chloromethyl) benzene (142 mg, 0.69 mmol, 2.3 equiv), were used. The pure product as an off-white solid (56 mg, 0.12 mmol, 42%).

^{1}H NMR (500 MHz, DMSO-d_6): δ = 9.10 (d, J = 7.8 Hz, 1H), 7.98 (d, J = 8.1 Hz, 1H), 7.86 (d, J = 8.0 Hz, 1H), 7.47 (d, J = 8.4 Hz, 1H), 7.26 (d, J = 8.4 Hz, 2H), 4.66 (ddd, J = 10.1, 7.8, 5.4 Hz, 1H), 4.10 (q, J = 7.1 Hz, 2H), 3.18 – 3.03 (m, 2H), 1.14 (t, J = 7.1 Hz, 3H) ppm.

^{13}C NMR (126 MHz, DMSO-d_6): δ = 171.2, 165.3, 137.3, 137.0, 131.5, 131.4, 131.2, 131.1, 128.2, 125.45 (q, J = 3.7 Hz), 119.7, 60.7, 54.1, 35.5, 14.0 ppm.

^{19}F NMR (470 MHz, DMSO-d_6): δ = -61.3 ppm.

R_f = 0.5 (cyclohexane:ethyl acetate, 1:1).

HRMS (ESI+) calculated for $C_{19}H_{17}BrF_3NO_3$ ($[M+Na]^+$) 466.0242, found 466.0234.

Ethyl 2-(4-(trifluoromethyl) benzamido)-3-(4-(trifluoromethyl) phenyl) propanoate (6g)

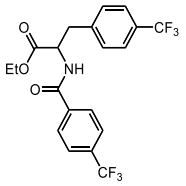

Following **GP3**, 3-ethoxy-3-oxo-2-(4-(trifluoromethyl)benzamido)propanoic acid (96 mg, 0.3 mmol, 1 equiv), and 1-(chloromethyl)-4-(trifluoromethyl) benzene (103 µL, 0.69 mmol, 2.3 equiv), were used. The pure product as an off-white solid (50 mg, 0.11 mmol, 37%).

^{1}H NMR (400 MHz, DMSO-d_6): δ = 9.15 (d, J = 7.7 Hz, 1H), 7.98 (d, 2H), 7.86 (d, J = 8.3 Hz, 2H), 7.65 (d, J = 8.0 Hz, 2H), 7.53 (d, J = 7.9 Hz, 2H), 4.72 (ddd, J = 9.9, 7.8, 5.6 Hz, 1H), 4.10 (q, J = 7.1 Hz, 2H), 3.31 – 3.16 (m, 2H), 1.13 (t, J = 7.1 Hz, 3H) ppm.

^{13}C NMR (101 MHz, DMSO-d_6): δ = 171.7, 165.7, 137.8, 137.0, 131.6, 131.4, 128.6 (d, J = 7.0 Hz), 125.9 (d, J = 3.8 Hz), 61.2, 54.6, 35.9, 14.4 ppm.

^{19}F NMR (376 MHz, DMSO-d_6): = -57.9, -58.5 ppm.

R_f = 0.5 (cyclohexane:ethyl acetate, 1:1).

HRMS (ESI+) calculated for $C_{20}H_{17}F_6NO_3$ ($[M+Na]^+$) 456.1010, found 456.1005.

Ethyl 3-(4-isopropylphenyl)-2-(4-(trifluoromethyl) benzamido) propanoate (6h)

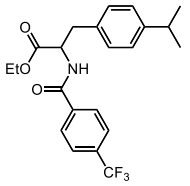

Following **GP3**, 3-ethoxy-3-oxo-2-(4-(trifluoromethyl)benzamido)propanoic acid (96 mg, 0.3 mmol, 1 equiv), and 1-(chloromethyl)-4-propan-2-ylbenzene (78 µl, 0.69 mmol, 2.3 equiv), were used. The pure product as an off-white solid (33 mg, 0.08 mmol, 27%).

^{1}H NMR (400 MHz, DMSO-d_6): δ = 9.09 (d, *J* = 7.6 Hz, 1H), 8.00 (d, *J* = 8.1 Hz, 2H), 7.86 (d, *J* = 8.2 Hz, 2H), 7.24 – 7.11 (m, 4H), 4.66 – 4.56 (m, 1H), 4.14 – 4.02 (m, 2H), 3.17 – 3.02 (m, 2H), 2.82 (h, *J* = 6.9 Hz, 1H), 1.15 (d, *J* = 6.9 Hz, 6H), 1.11 (t, *J* = 7.1 Hz, 3H) ppm.

^{13}C NMR (101 MHz, DMSO-d_6): δ = 171.5, 165.3, 146.5, 134.7, 128.9, 128.2, 126.1, 125.3 (d, *J* = 3.8 Hz), 60.5, 54.6, 35.8, 33.0, 23.8 (d, *J* = 5.6 Hz), 13.9 ppm.

^{19}F NMR (376 MHz, DMSO-d_6): δ = -61.3 ppm.

R_f = 0.5 (cyclohexane:ethyl acetate, 1:1).

HRMS (ESI+) calculated for $C_{22}H_{24}F_3NO_3$ ($[M+Na]^+$) 430.1606, found 430.1602.

Ethyl 3-(2-chlorophenyl)-2-(4-(trifluoromethyl)benzamido)propanoate (6i)

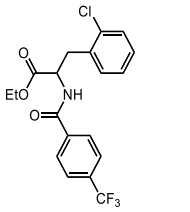

Following **GP3**, 3-ethoxy-3-oxo-2-(4-(trifluoromethyl)benzamido)propanoic acid (96 mg, 0.3 mmol, 1 equiv), and 1-chloro-2-(chloromethyl)benzene (86 µl, 0.69 mmol, 2.3 equiv), were used. The pure product as an off-white solid (50 mg, 0.12 mmol, 42%).

^{1}H NMR (500 MHz, DMSO-d_6): δ = 9.17 (d, *J* = 7.9 Hz, 1H), 7.99 (d, *J* = 8.0 Hz, 1H), 7.86 (d, *J* = 8.2 Hz, 2H), 7.45 – 7.39 (m, 2H), 7.28 – 7.22 (m, 2H), 4.77 (ddd, *J* = 10.0, 7.9, 5.5 Hz, 1H), 4.10

(q, *J* = 7.1 Hz, 2H), 3.37 (dd, *J* = 13.8, 5.6 Hz, 1H), 3.18 (dd, *J* = 13.8, 10.0 Hz, 1H), 1.13 (t, *J* = 7.1 Hz, 3H) ppm.

^{13}C NMR (126 MHz, DMSO-d_6): δ = 171.1, 165.3, 137.3, 134.9, 133.3, 131.9, 131.3 (m), 129.3, 128.7, 128.2, 127.0, 125.4 (q), 60.8, 52.3, 34.2 ppm.

^{19}F NMR (470 MHz, DMSO-d_6): δ = -61.3 ppm.

R_f = 0.5 (cyclohexane:ethyl acetate, 1:1).

HRMS (ESI+) calculated for $C_{19}H_{17}ClF_3NO_3$ ([M+Na]$^+$) 422.0747, found 422.0741.

Ethyl 4-oxo-4-phenyl-2-(4-(trifluoromethyl)benzamido)butanoate (6j)

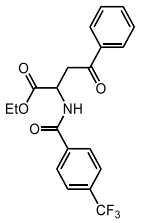

Following **GP3**, 3-ethoxy-3-oxo-2-(4-(trifluoromethyl)benzamido)propanoic acid (96 mg, 0.3 mmol, 1 equiv), and 2-chloro-1-phenylethan-1-one (107 mg, 0.69 mmol, 2.3 equiv), were used. The pure product as yellow solid (48 mg, 0.12 mmol, 40%)

^{1}H NMR (400 MHz, $CDCl_3$): δ = 7.98 – 7.94 (m, 2H), 7.92 (d, *J* = 8.0 Hz, 2H), 7.70 (d, *J* = 8.1 Hz, 2H), 7.63 – 7.57 (m, 1H), 7.52 – 7.45 (m, 2H), 7.38 (d, *J* = 7.9 Hz, 1H), 5.18 – 5.12 (m, 1H), 4.26 (q, *J* = 7.1 Hz, 2H), 3.89 (dd, *J* = 18.3, 4.0 Hz, 1H), 3.71 (dd, *J* = 18.3, 4.0 Hz, 1H), 1.26 (t, *J* = 7.1 Hz, 3H) ppm.

^{13}C NMR (101 MHz, $CDCl_3$): δ = 198.2, 171.0, 165.8, 137.2, 136.0, 134.1, 128.9, 128.3, 127.7, 125.3 (q), 62.2, 49.1, 40.5, 14.2 ppm.

^{19}F NMR (376 MHz, $CDCl_3$): δ = -62.9 ppm.

R_f = 0.4 (cyclohexane:ethyl acetate, 1:1).

HRMS (ESI+) calculated for $C_{20}H_{18}ClF_3NO_4$ ([M+Na]$^+$) 416.1086, found 416.1080.

Ethyl 4-(4-chlorophenyl)-4-oxo-2-(4-(trifluoromethyl)benzamido)butanoate (6k)

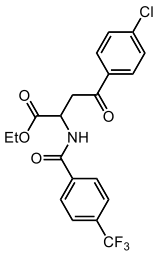

Following **GP3**, 3-ethoxy-3-oxo-2-(4-(trifluoromethyl)benzamido)propanoic acid (96 mg, 0.3 mmol, 1 equiv), and 2-chloro-1-(4-chlorophenyl)ethan-1-one (131 mg, 0.69 mmol, 2.3 equiv), were used. The pure product as yellow solid (44 mg, 0.1 mmol, 34%).

^{1}H NMR (400 MHz, $CDCl_3$): δ = 7.98 – 7.94 (m, 2H), 7.92 (d, *J* = 8.0 Hz, 2H), 7.70 (d, *J* = 8.1 Hz, 2H), 7.63 – 7.57 (m, 1H), 7.52 – 7.45 (m, 2H), 7.38 (d, *J* = 7.9 Hz, 1H), 5.18 – 5.12 (m, 1H), 4.26 (q, *J* = 7.1 Hz, 2H), 3.89 (dd, *J* = 18.3, 4.0 Hz, 1H), 3.71 (dd, *J* = 18.3, 4.0 Hz, 1H), 1.26 (t, *J* = 7.1 Hz, 3H) ppm.

^{13}C NMR (101 MHz, $CDCl_3$): δ = 196.9, 170.9, 165.8, 140.6, 134.3, 129.7, 129.3, 127.7, 125.8 (q), 62.2, 49.1, 40.4, 14.2 ppm.

^{19}F NMR (376 MHz, $CDCl_3$): δ = -63.0 ppm.

R_f = 0.4 (cyclohexane:ethyl acetate, 1:1).

HRMS (ESI+) calculated for $C_{20}H_{17}ClF_3NO_4$ ($[M+Na]^+$) 450.0696, found 450.0692.

Ethyl 4-oxo-2-(4-(trifluoromethyl) benzamido) pentanoate (6l)

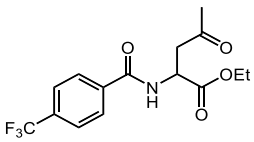

Following **GP3**, 3-ethoxy-3-oxo-2-(4-(trifluoromethyl)benzamido)propanoic acid (96 mg, 0.3 mmol, 1 equiv), and 1-chloropropan-2-one (60 µl, 0.69 mmol, 2.3 equiv), were used. The pure product as an off-white solid (38 mg, 0.11 mmol, 38%).

^{1}H NMR (400 MHz, DMSO-*d*$_6$): δ = 8.98 (d, *J* = 7.3 Hz, 1H), 8.02 (d, *J* = 8.1 Hz, 2H), 7.88 (d, *J* = 8.2 Hz, 2H), 4.83 – 4.75 (m, 1H), 4.10 (q, *J* = 7.1 Hz, 2H), 3.13 – 2.92 (m, 2H), 2.15 (s, 3H), 1.17 (t, *J* = 7.1 Hz, 3H) ppm.

^{13}C NMR (126 MHz, DMSO-*d*$_6$): δ = 204.9, 171.1, 165.1, 137.4, 131.3 (m), 128.2, 125.4 (q, *J* = 3.7 Hz), 60.8, 48.6, 43.6, 29.8, 14.0 ppm.

^{19}F NMR (470 MHz, DMSO-*d*$_6$): δ = -61.3 ppm.

R_f = 0.3 (cyclohexane:ethyl acetate, 1:1).

HRMS (ESI+) calculated for $C_{15}H_{16}F_3NO_4$ ($[M+Na]^+$) 354.0929, found 354.0922.

6.4 NMR Spectra

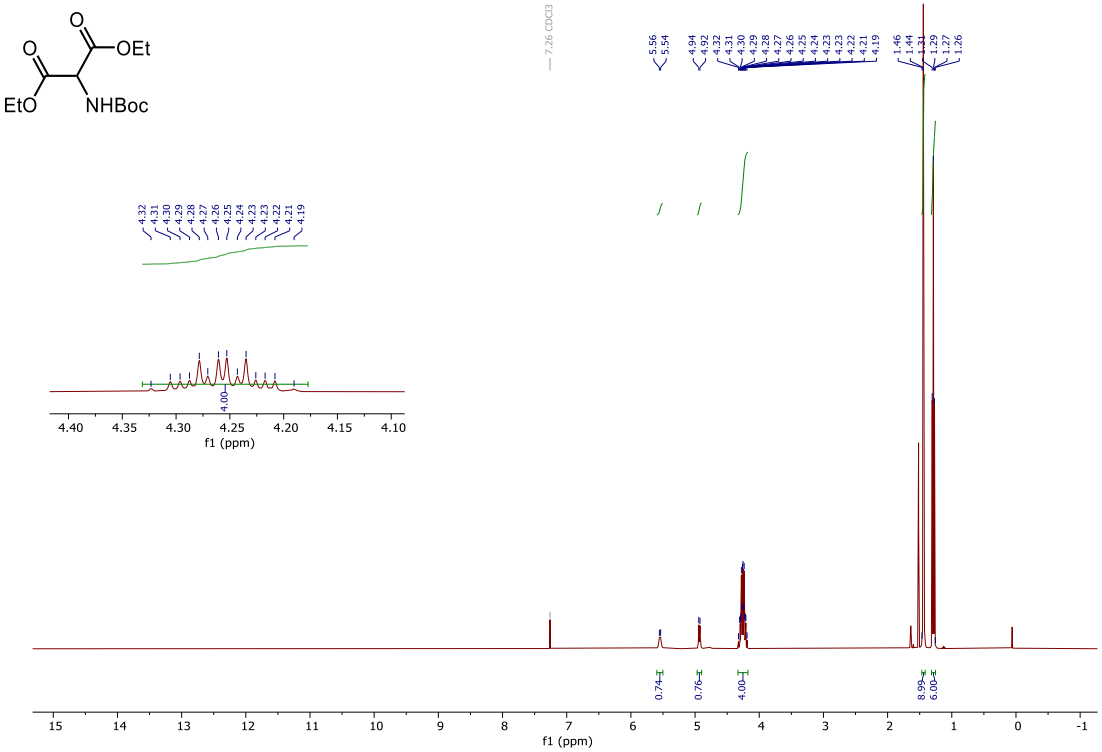

Figure S17: ^{1}H NMR spectra of **S2a** (400 MHz, $CDCl_3$).

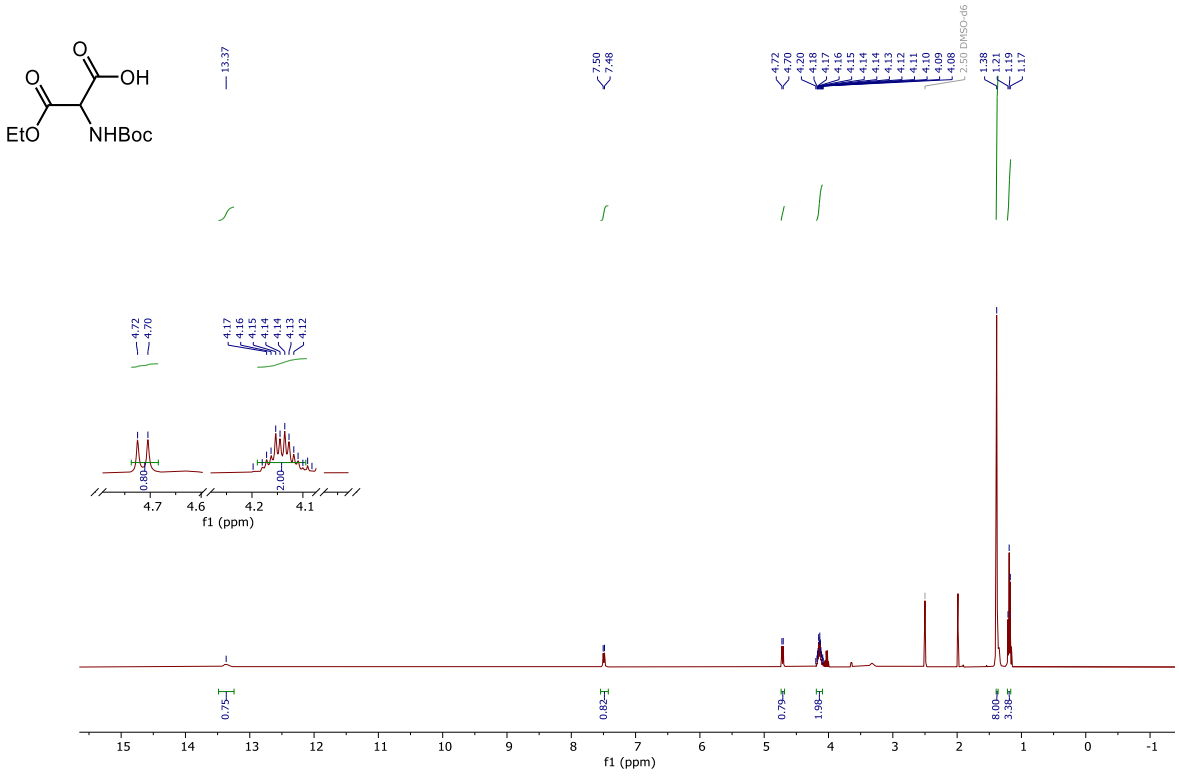

Figure S18: ^{1}H NMR spectra of **2a** (400 MHz, DMSO-d_6).

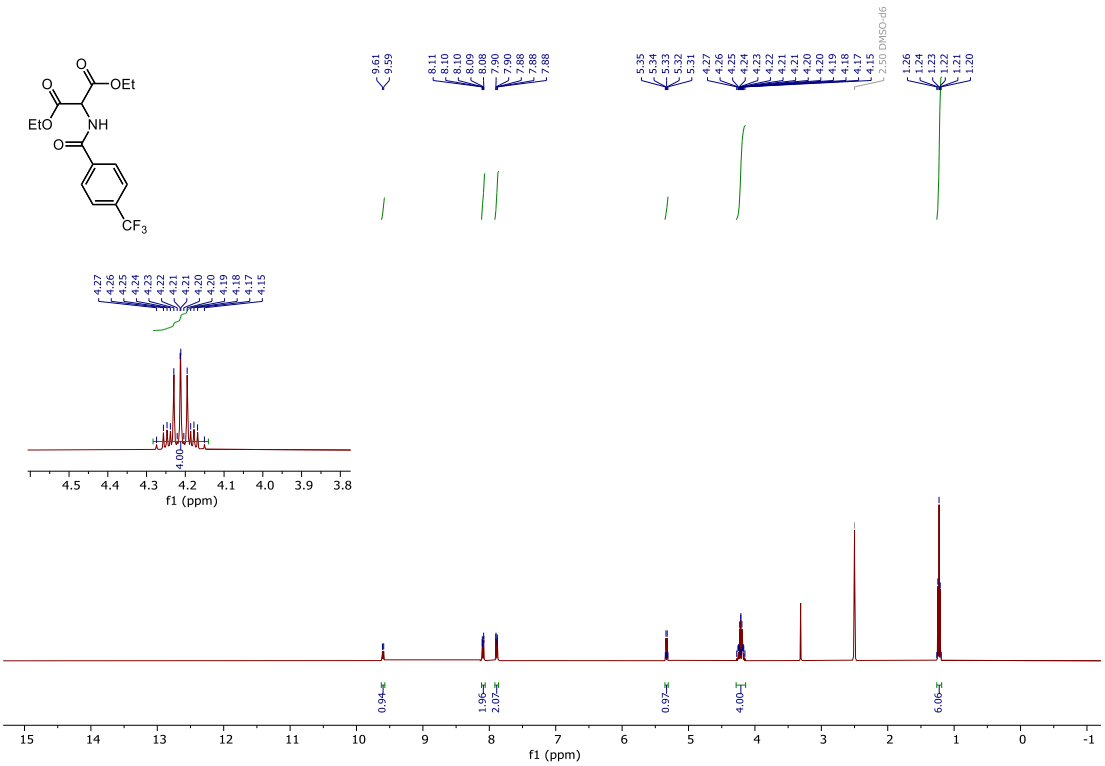

Figure S19: ^{1}H NMR spectra of **S2d** (400 MHz, DMSO-d_6)**.**

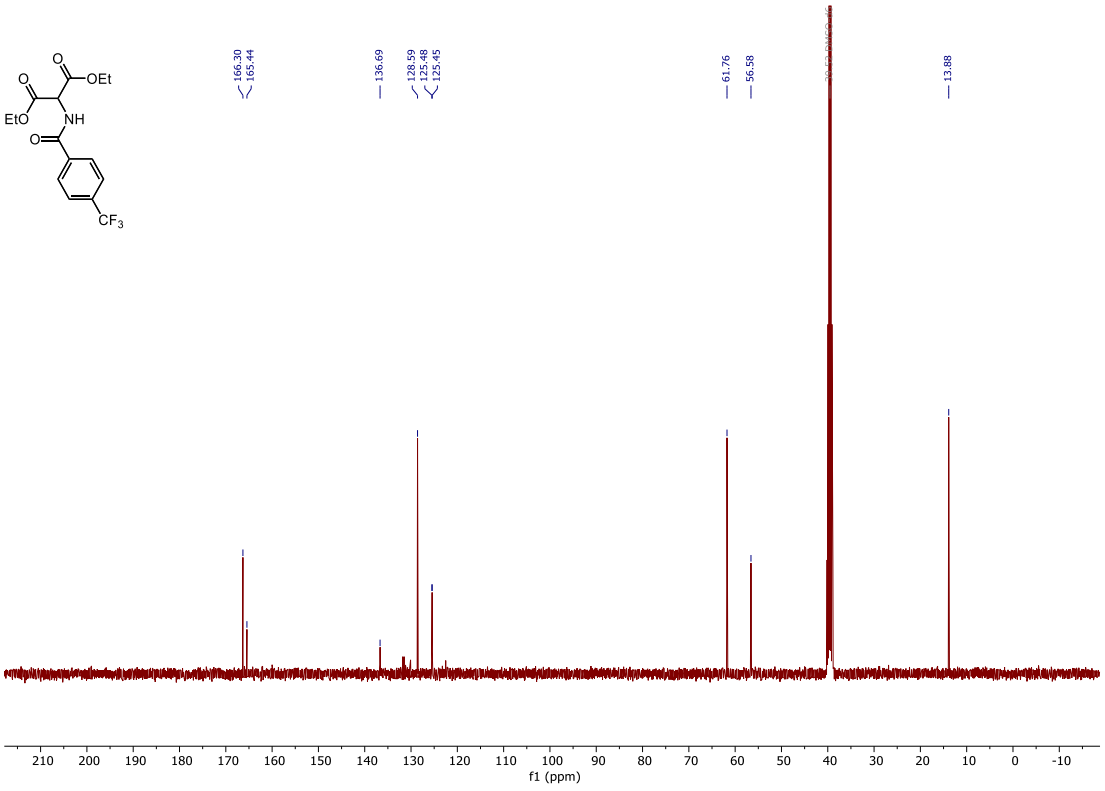

Figure S20: ^{13}C NMR spectra of **S2d** (101 MHz, DMSO-d_6)**.**

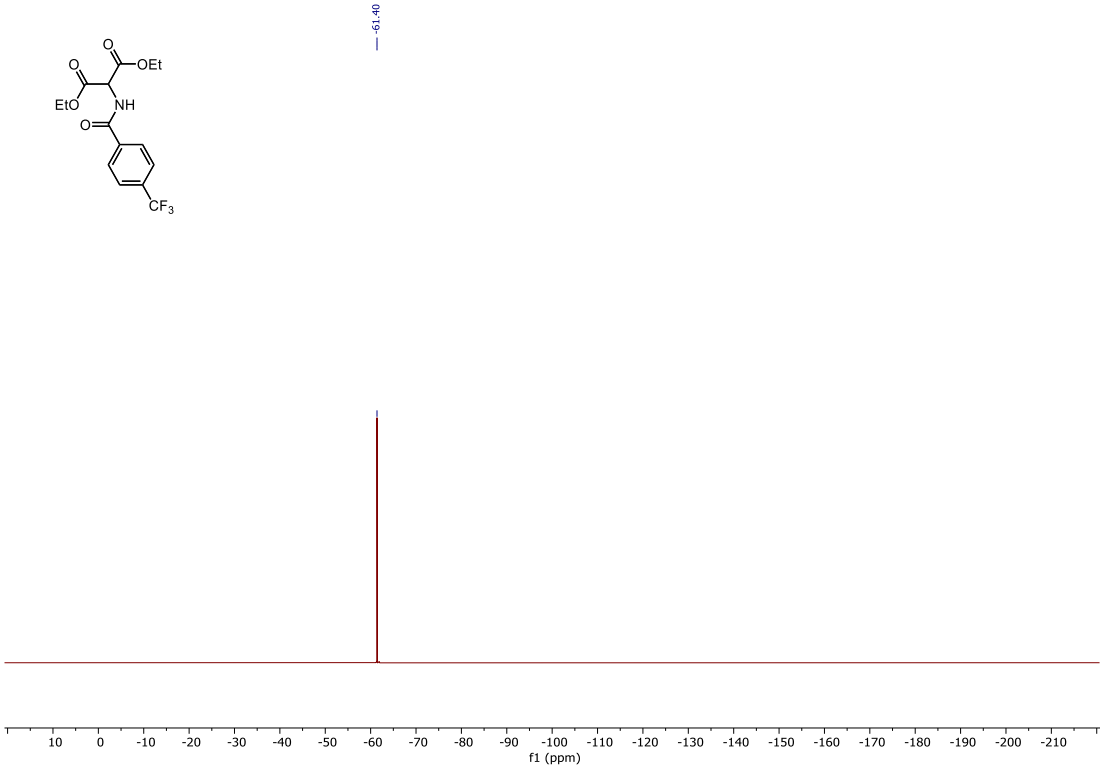

Figure S21: ^{19}F NMR spectra of **S2d** (376 MHz, DMSO-d_6)**.**

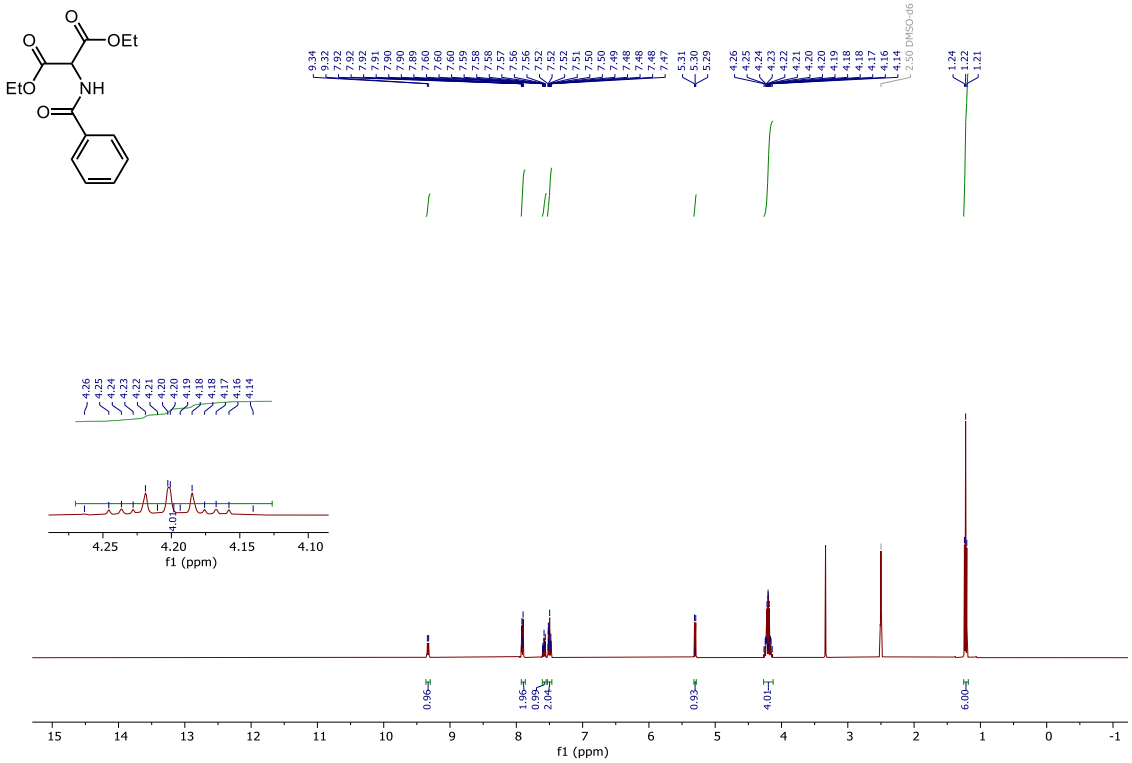

Figure S22: ^{1}H NMR spectra of **S2b** (400 MHz, DMSO-d_6).

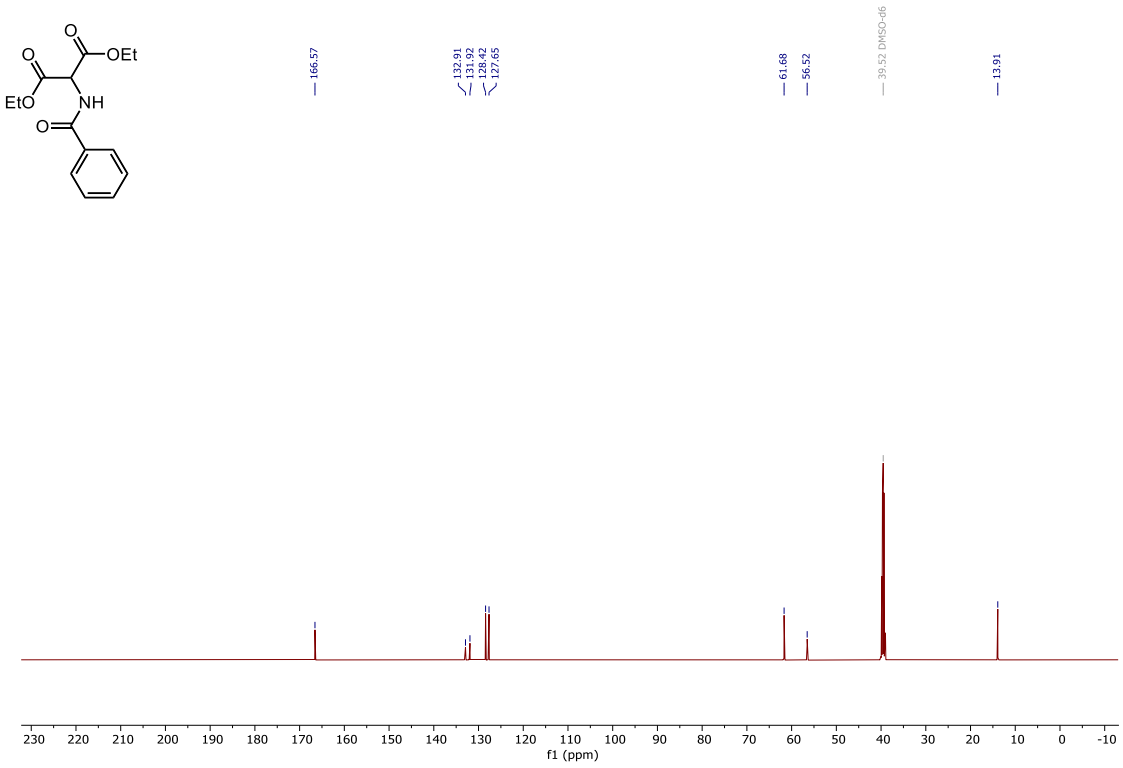

Figure S23: ^{13}C NMR spectra of **S2b** (126 MHz, DMSO-d_6)**.**

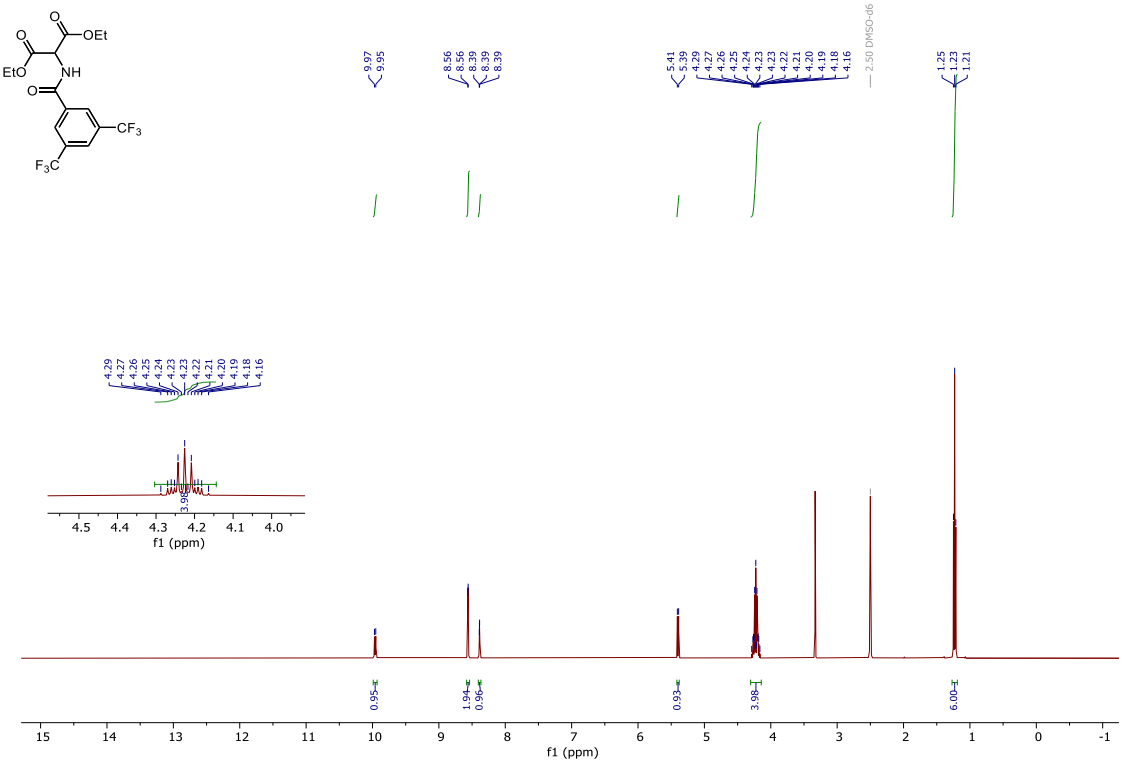

Figure S24: ^{1}H NMR spectra of **S2e** (400 MHz, DMSO-d_6)**.**

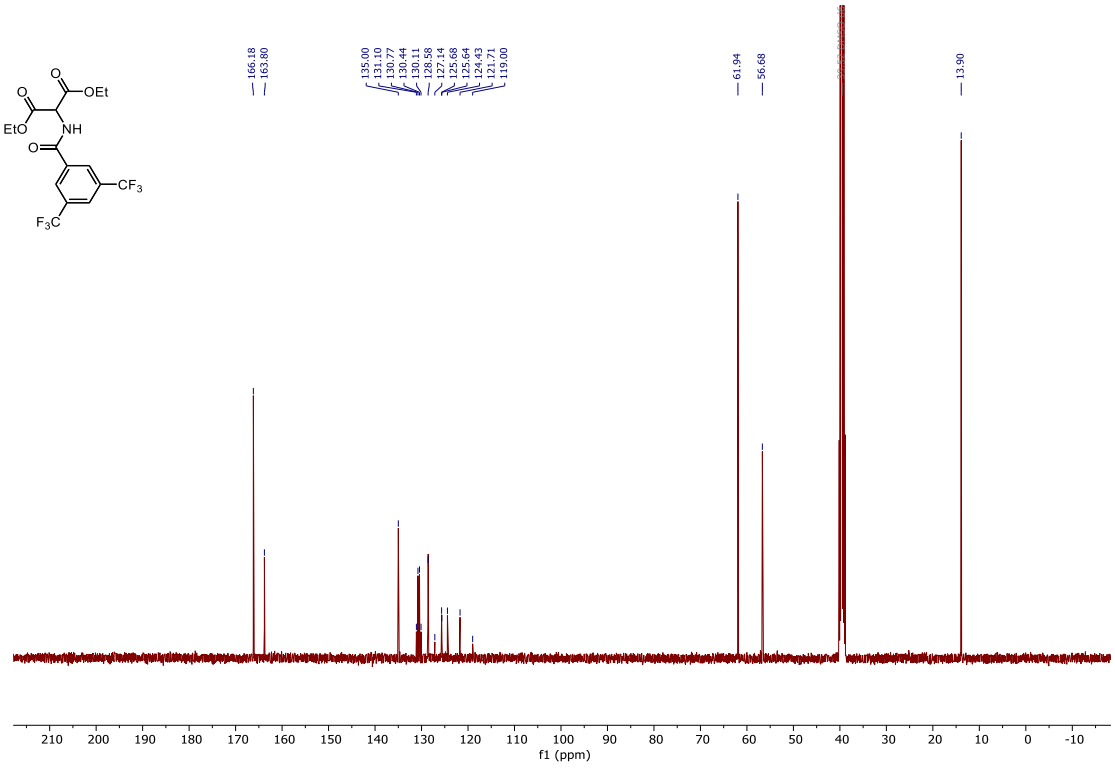

Figure S25: ^{13}C NMR spectra of **S2e** (101 MHz, DMSO-d_6)**.**

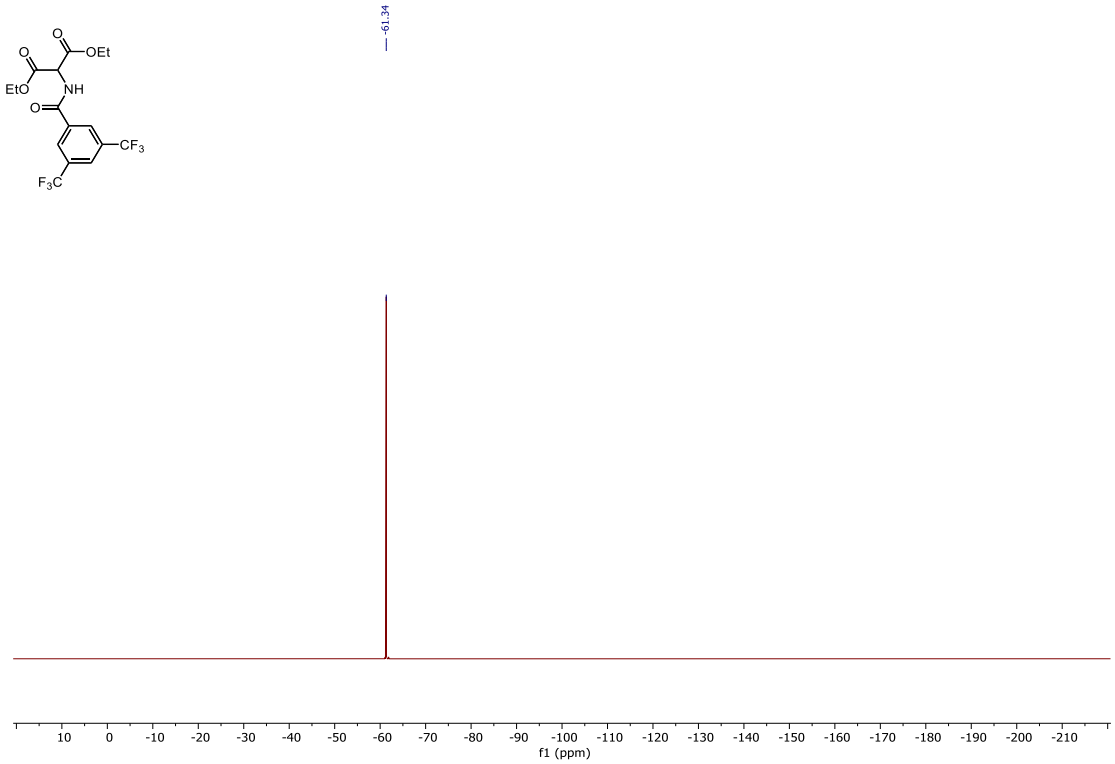

Figure S26: ^{19}F NMR spectra of **S2e** (376 MHz, DMSO-d_6)**.**

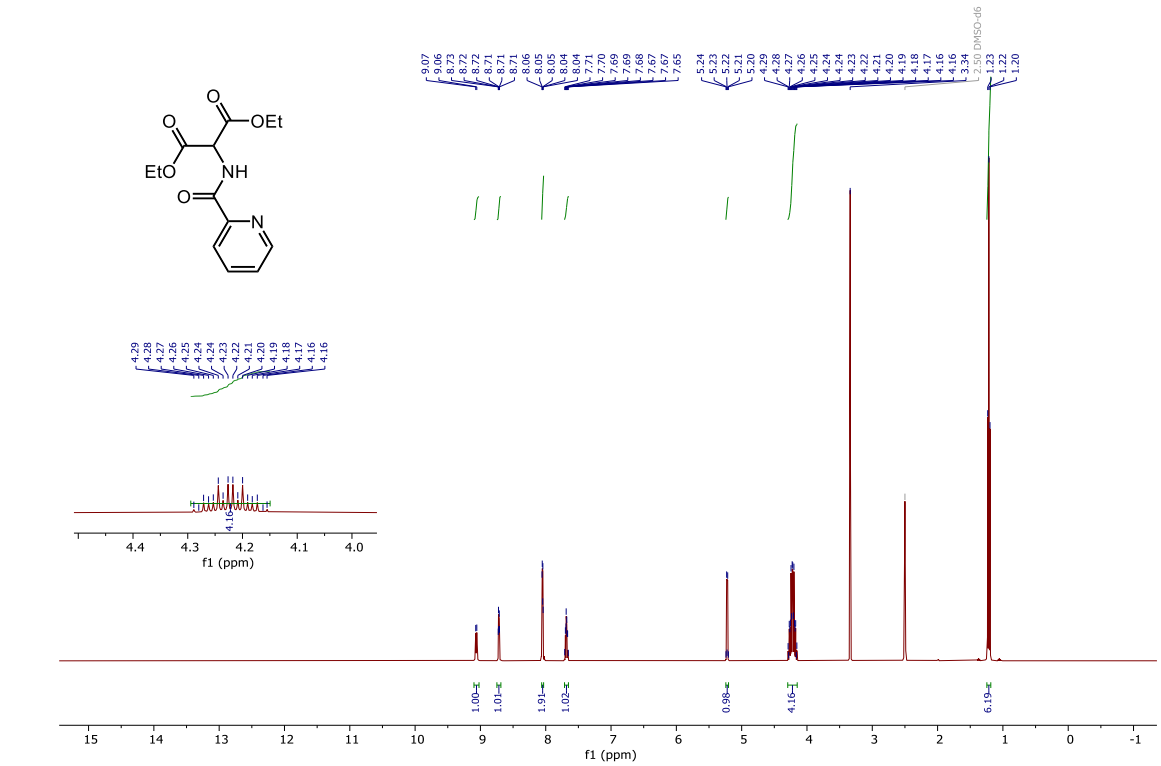

Figure S27: ^{1}H NMR spectra of diethyl 2-(picolinamido) malonate (400 MHz, DMSO-d_6)**.**

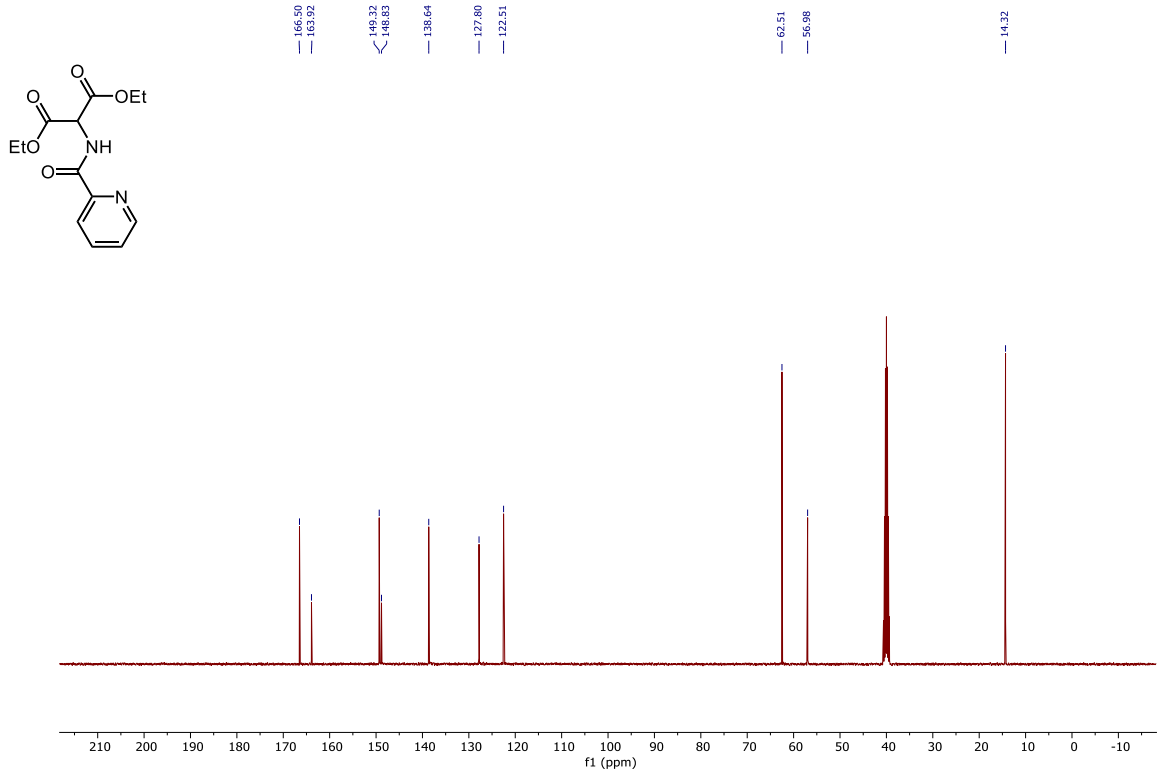

Figure S28: ^{13}C NMR spectra of diethyl 2-(picolinamido) malonate (101 MHz, DMSO-d_6)**.**

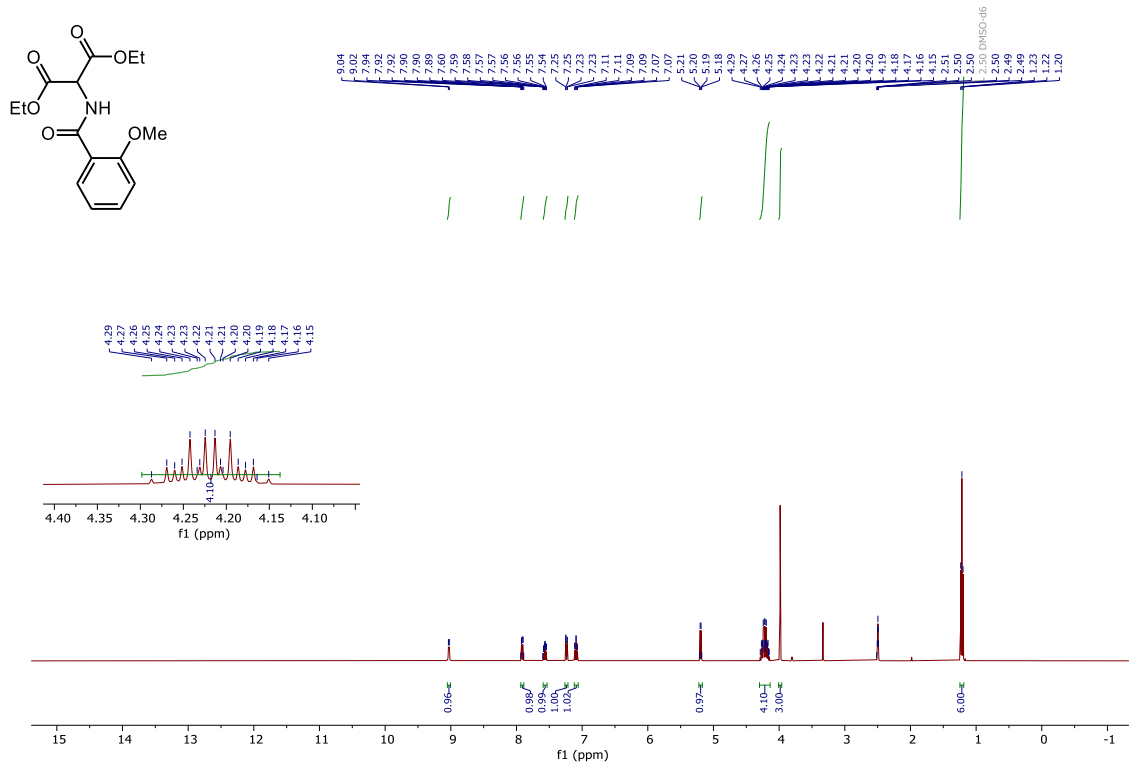

Figure S29: ^{1}H NMR spectra of **S2c** (400 MHz, DMSO-d_6)**.**

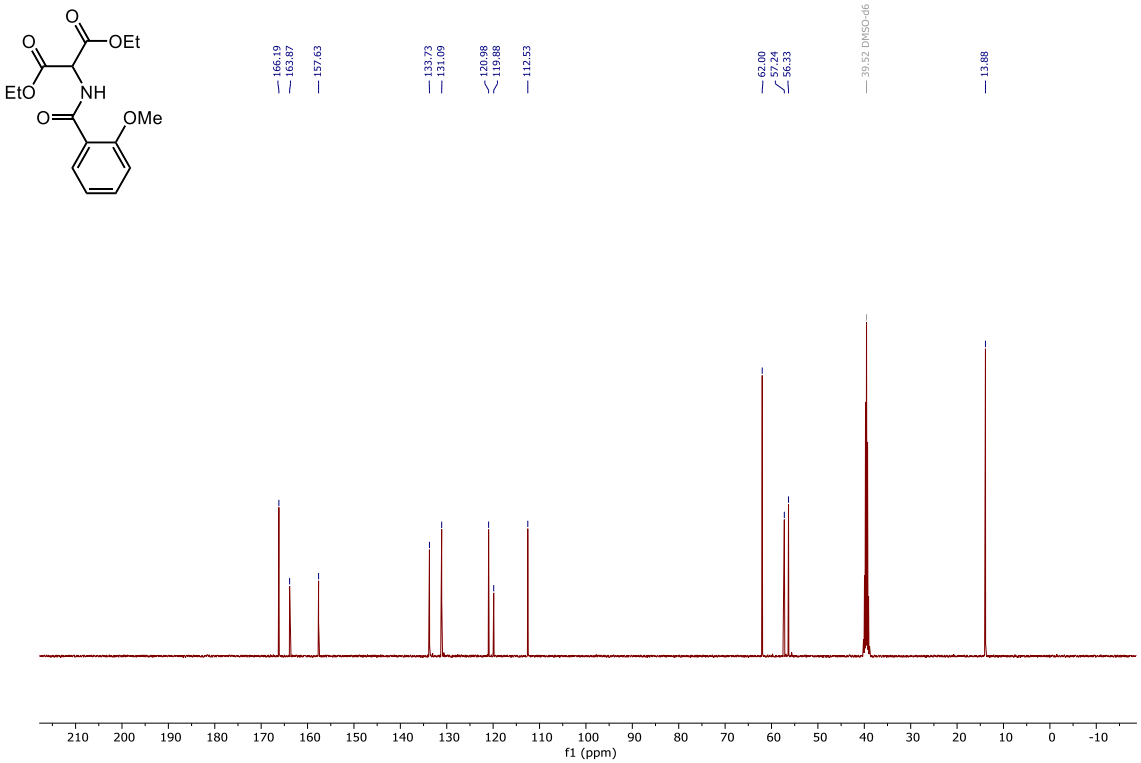

Figure S30: ^{13}C NMR spectra of **S2c** (101 MHz, DMSO-d_6)**.**

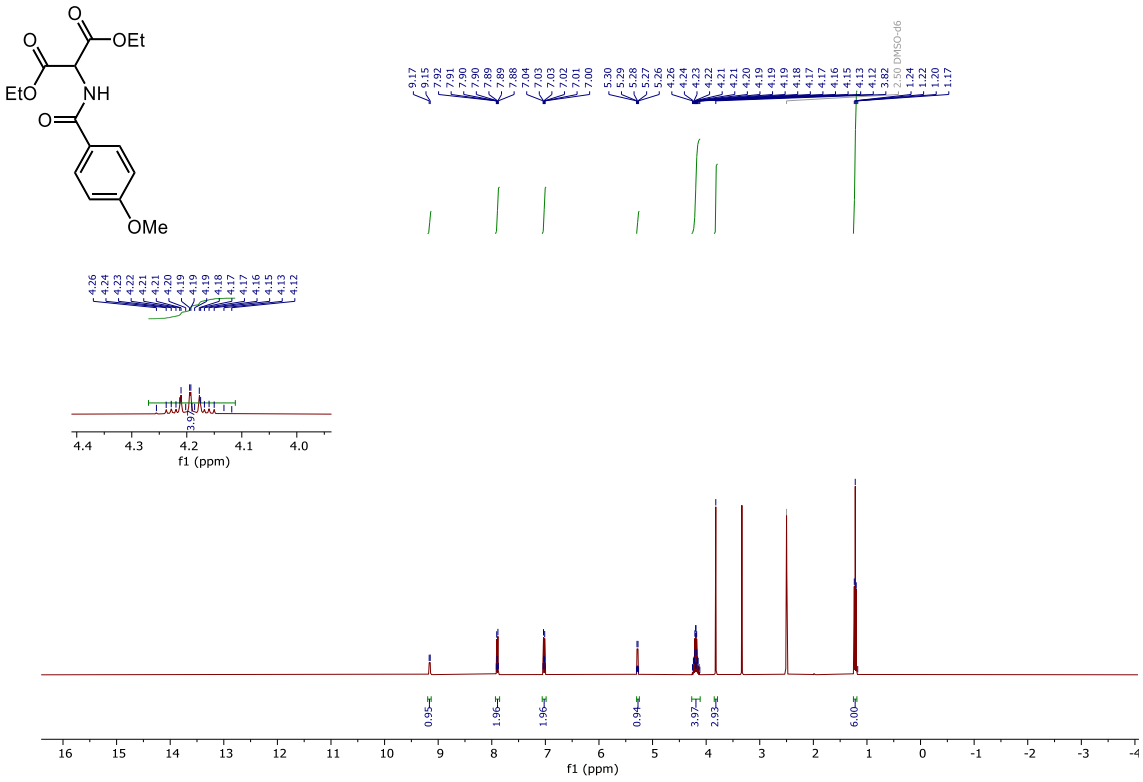

Figure S31: ^{1}H NMR spectra of diethyl 2-(4-methoxybenzamido)malonate (400 MHz, DMSO-d_6)**.**

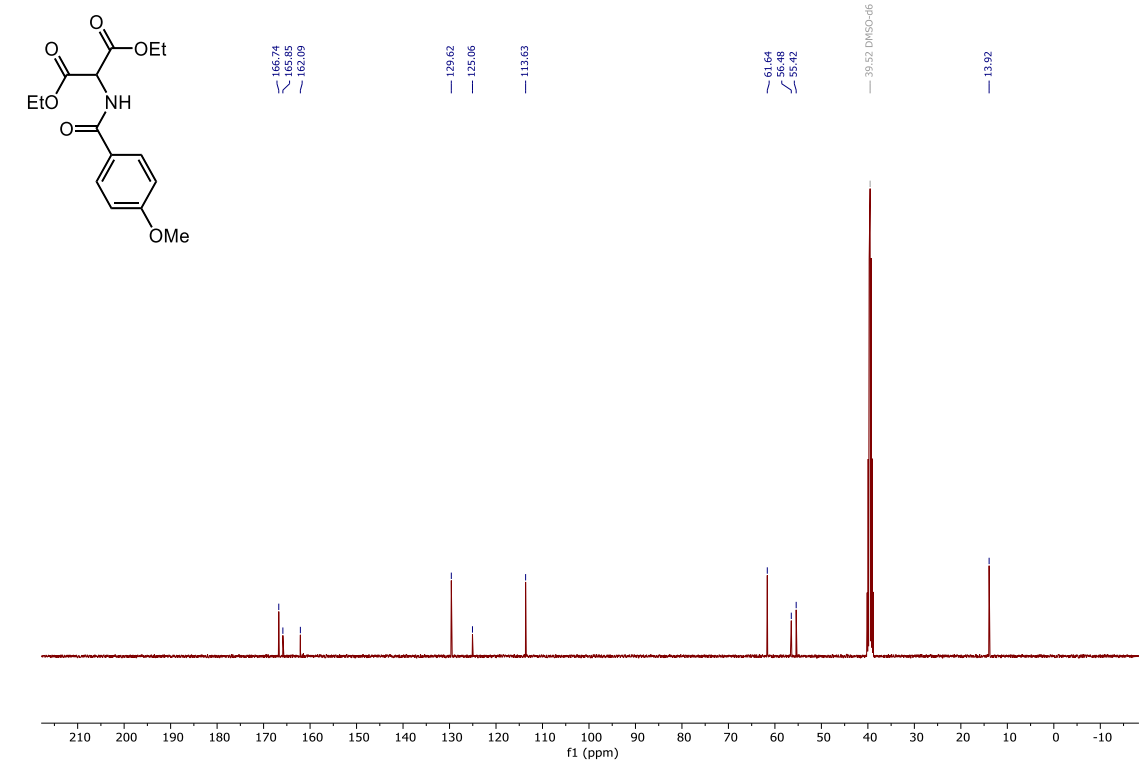

Figure S32: ^{13}C NMR spectra of diethyl 2-(4-methoxybenzamido)malonate (101 MHz, DMSO-d_6)**.**

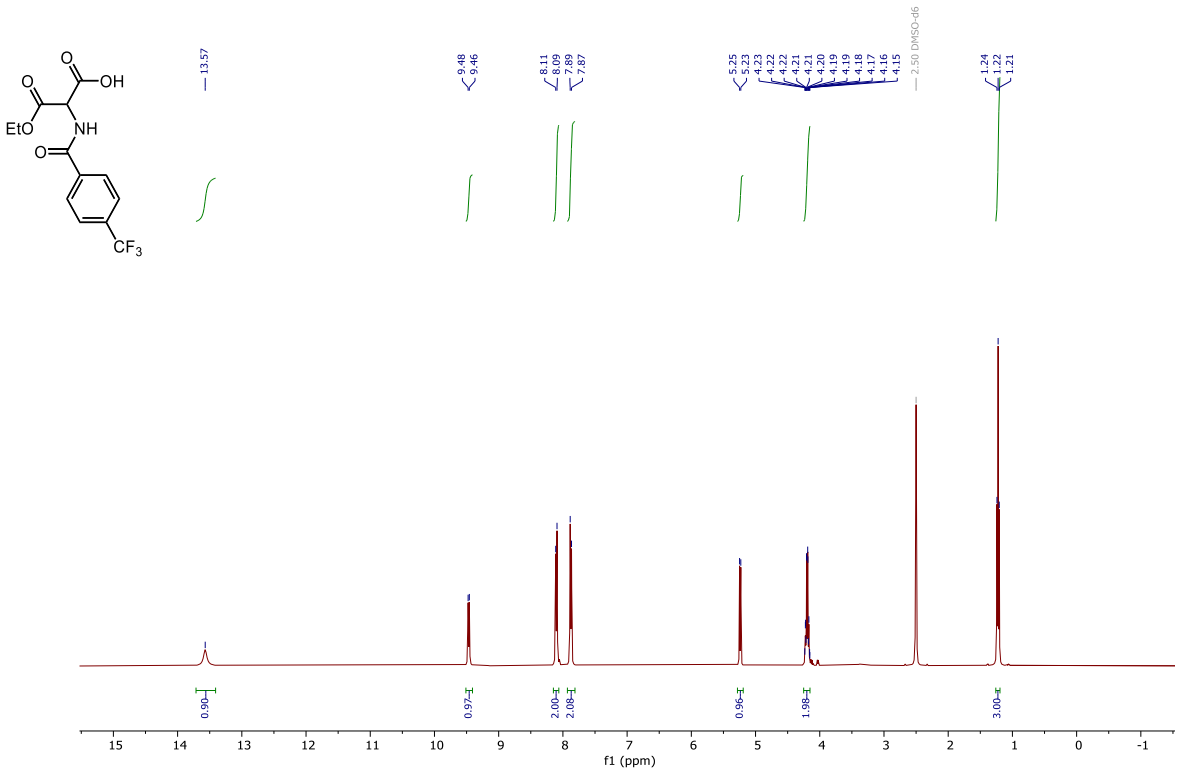

Figure S33: ^{1}H NMR spectra of **2d** (400 MHz, DMSO-*d*$_6$)**.**

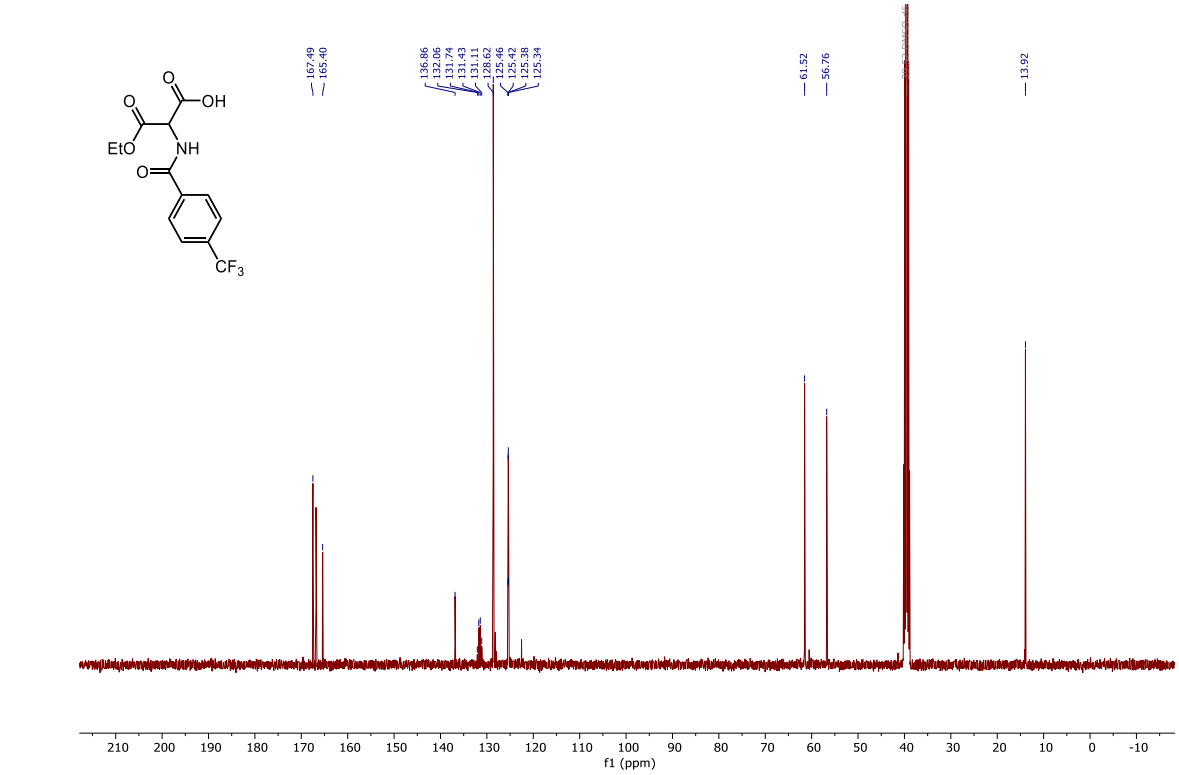

Figure S34: ^{13}C NMR spectra of **2d** (101 MHz, DMSO-*d*$_6$)**.**

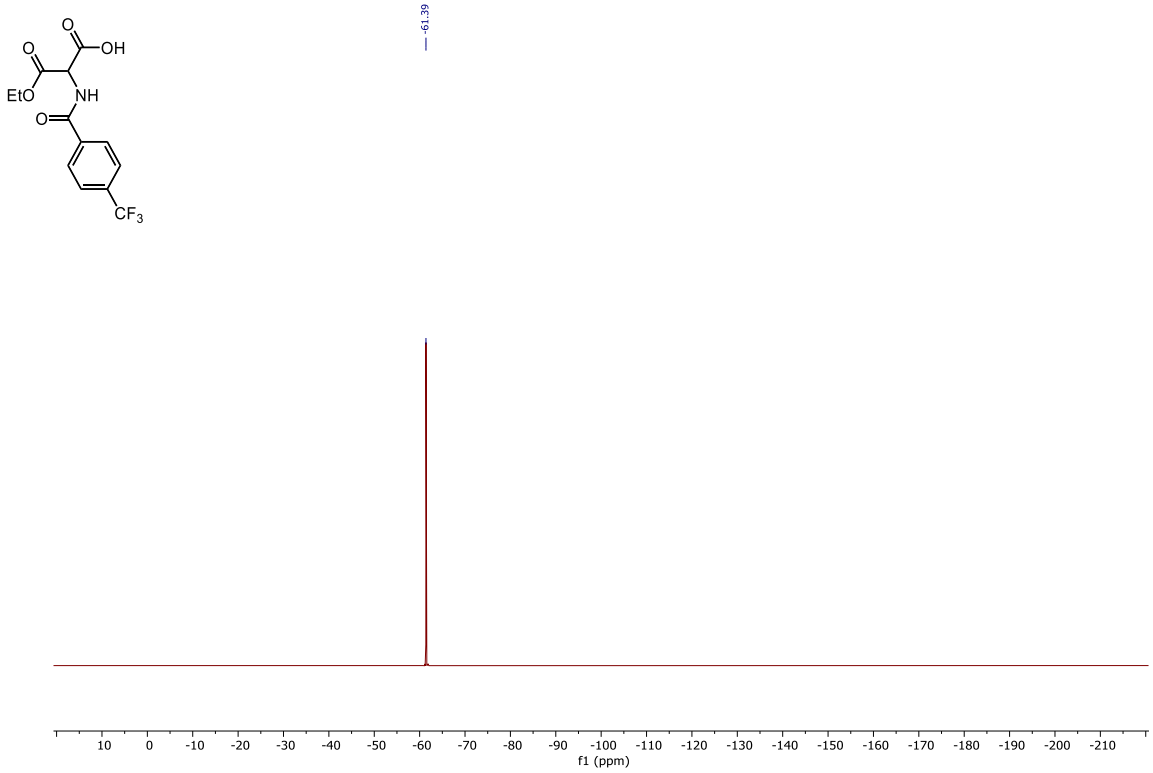

Figure S35: ^{19}F NMR spectra of **2d** (376 MHz, DMSO-*d*$_6$)**.**

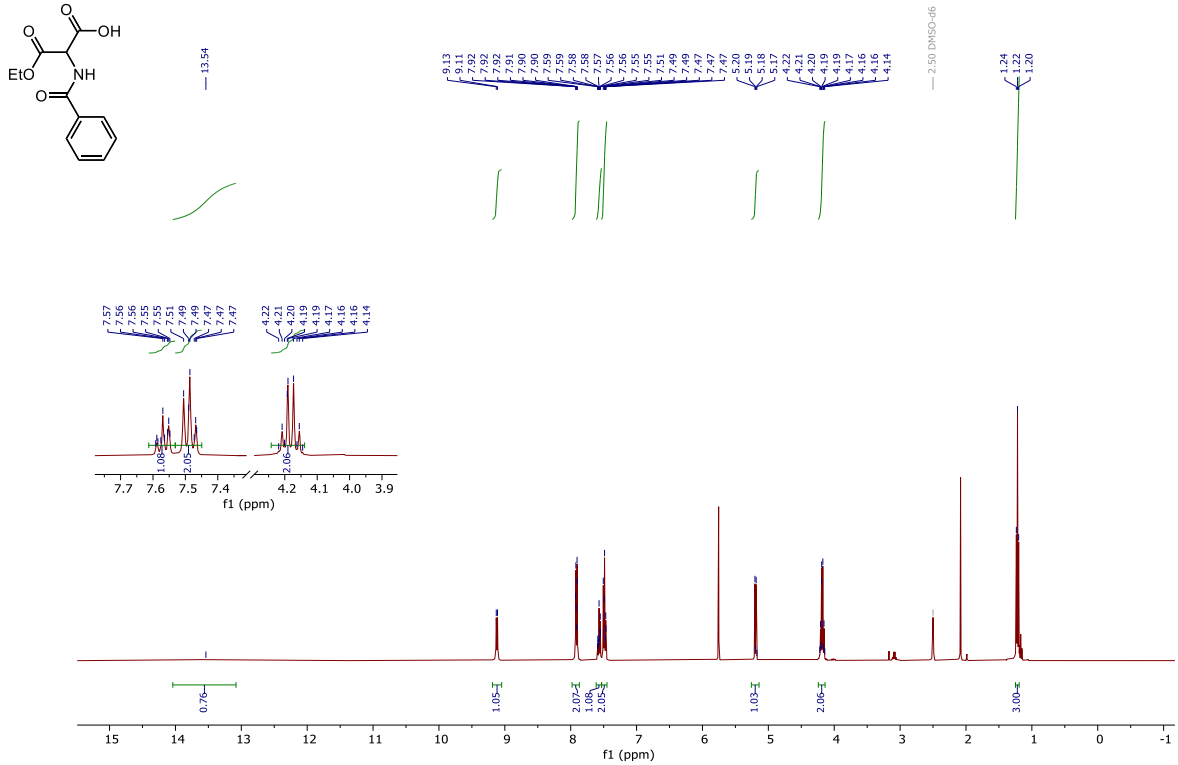

Figure S36: ^{1}H NMR spectra of **2b** (400 MHz, DMSO-*d*$_6$)**.**

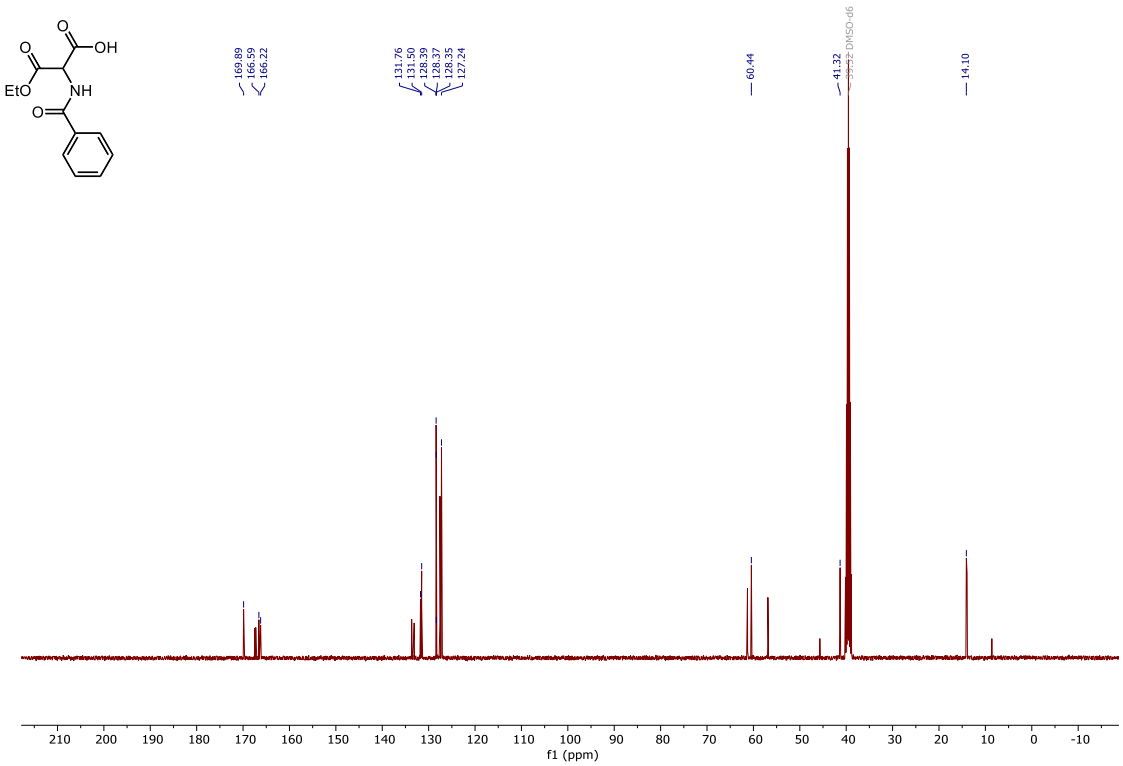

Figure S37: ^{13}C NMR spectra of **2b** (101 MHz, DMSO-*d*$_6$)**.**

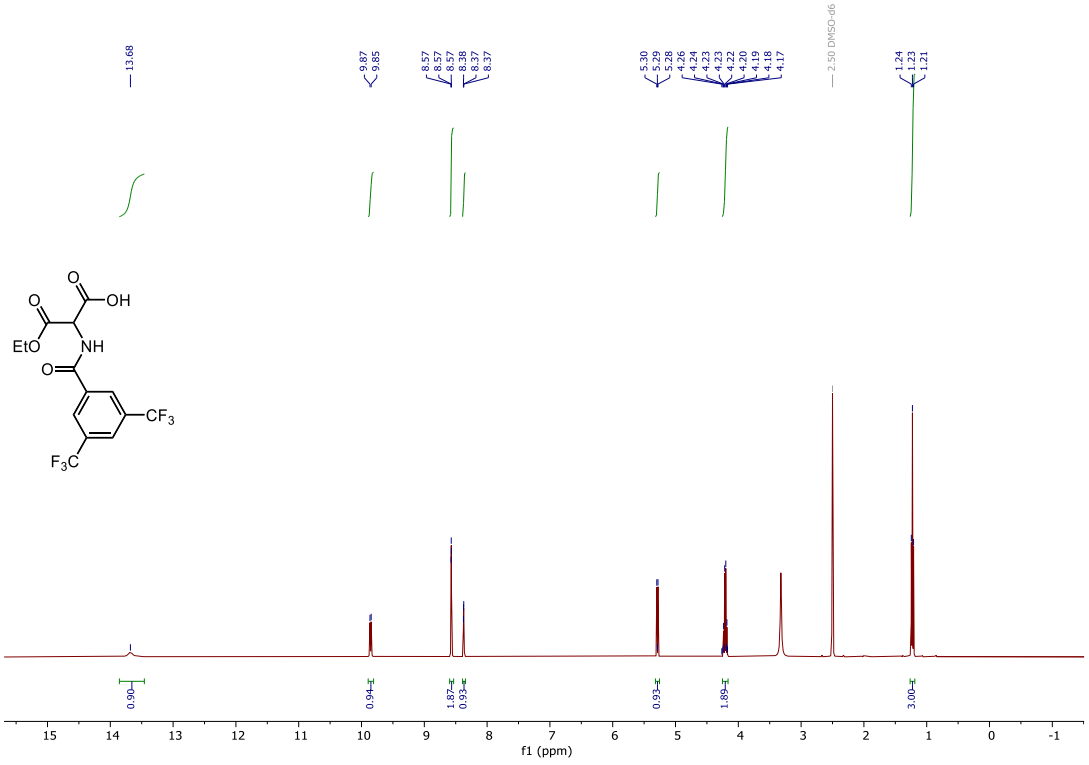

Figure S38: ^{1}H NMR spectra of **2e** (400 MHz, DMSO-*d*$_6$)**.**

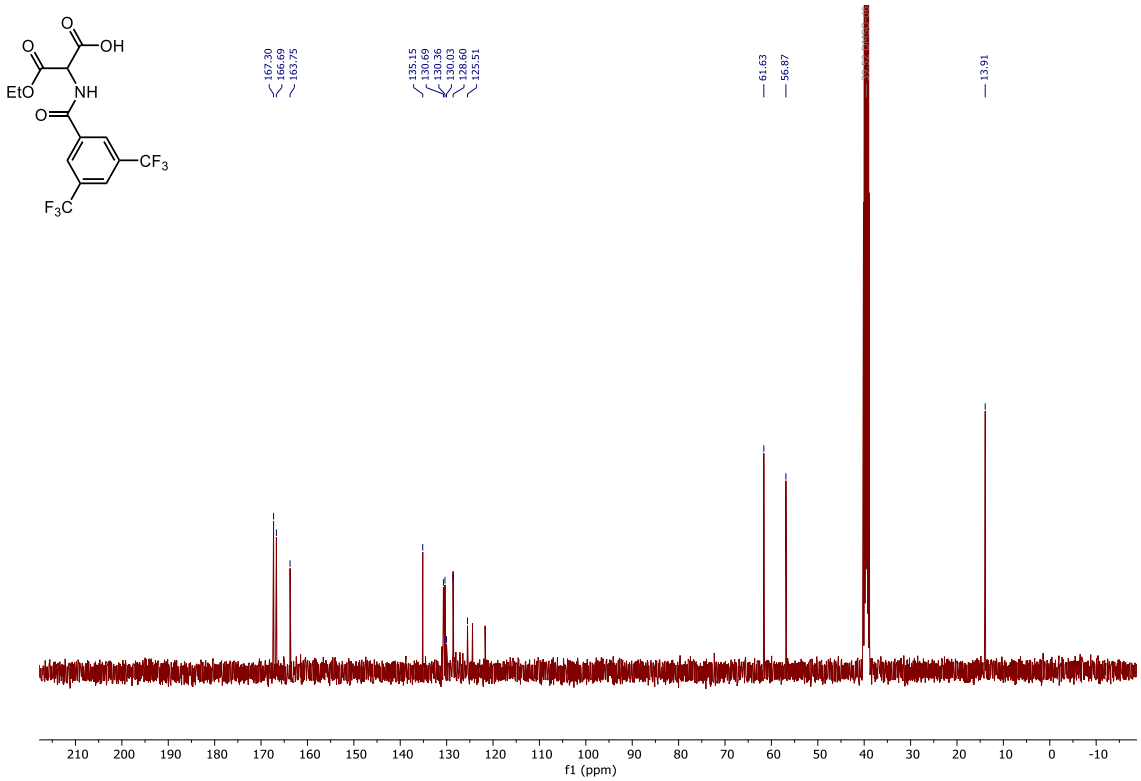

Figure S39: ^{13}C NMR spectra of **2e** (101 MHz, DMSO-d_6)**.**

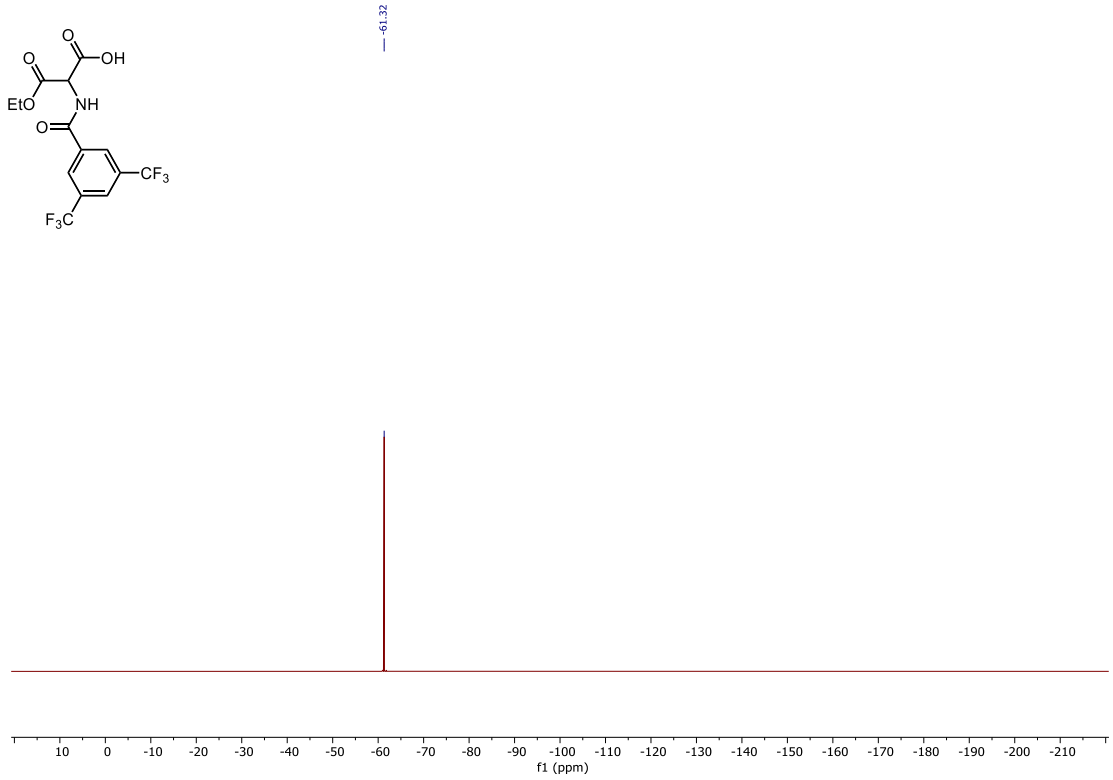

Figure S40: ^{19}F NMR spectra of **2e** (376 MHz, DMSO-d_6)**.**

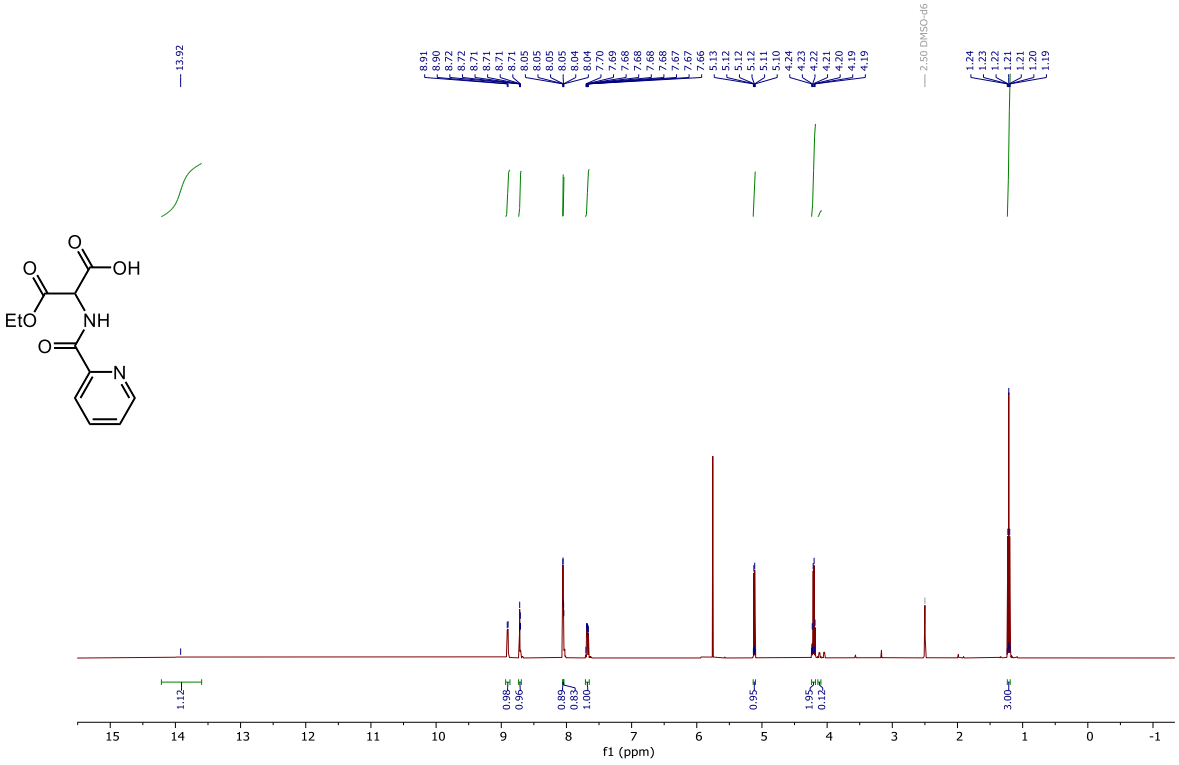

Figure S41: ^{1}H NMR spectra of 3-ethoxy-3-oxo-2-(picolinamido) propanoic acid (400 MHz, DMSO-d_6)**.**

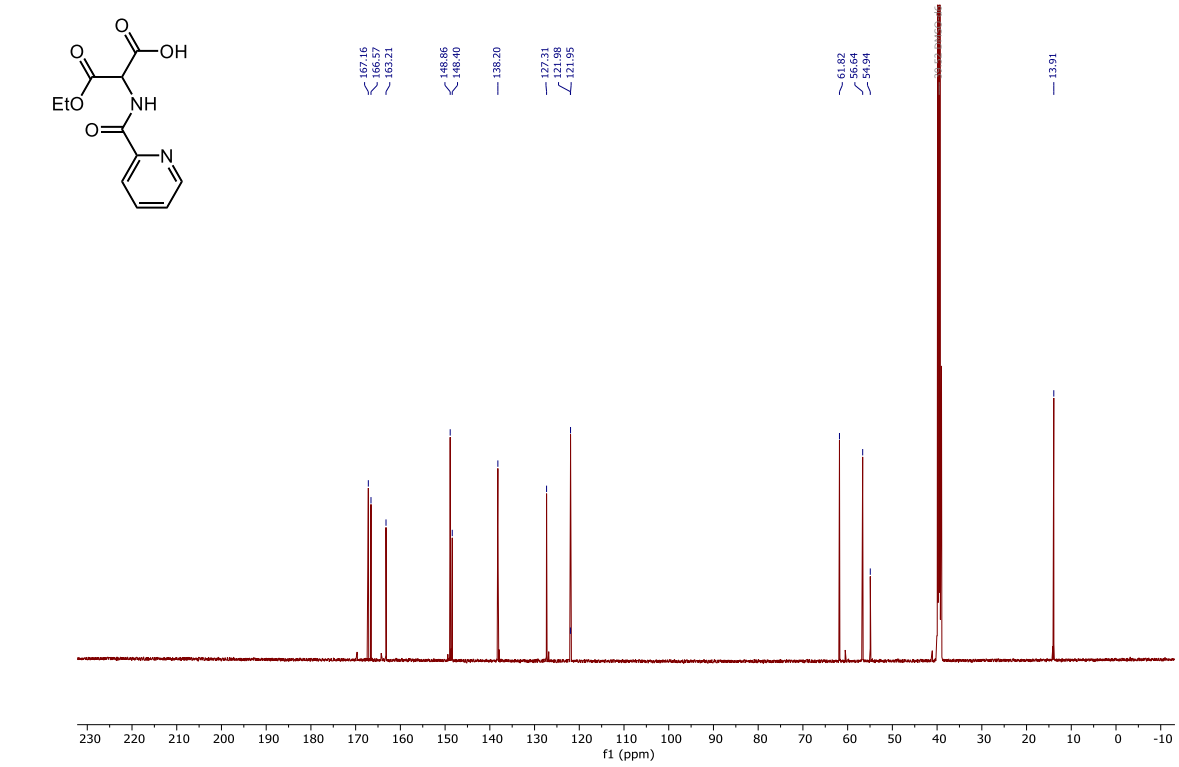

Figure S42: ^{13}C NMR spectra of 3-ethoxy-3-oxo-2-(picolinamido) propanoic acid (126 MHz, DMSO-d_6)**.**

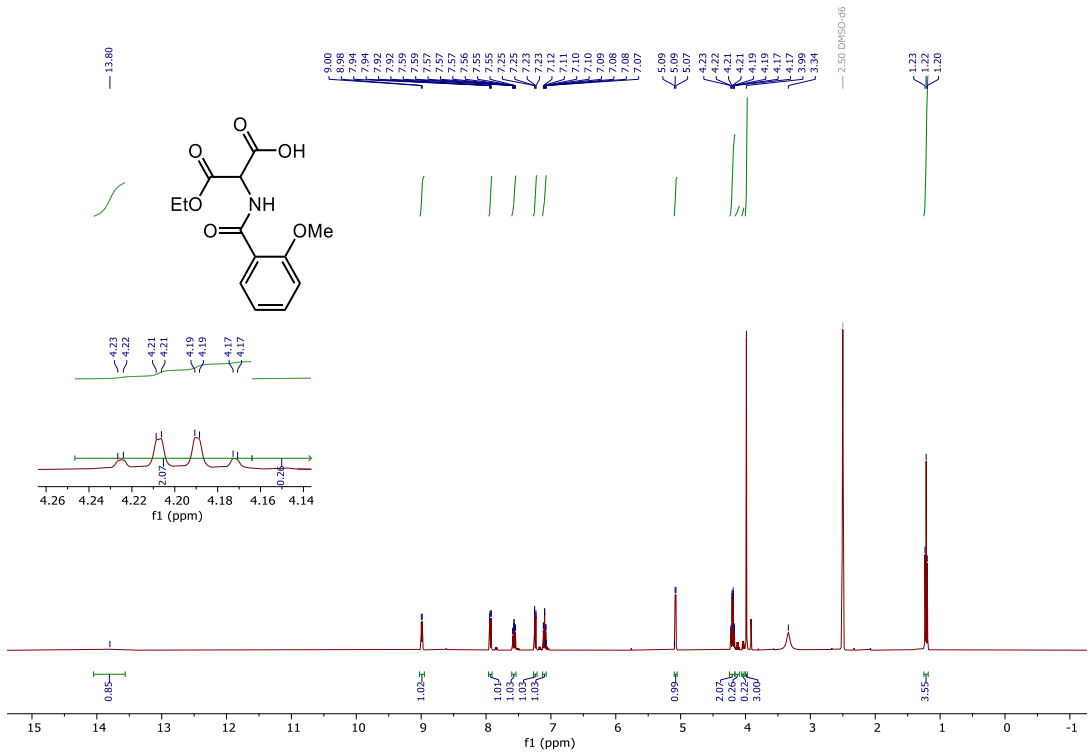

Figure S43: ^{1}H NMR spectra of **2c** (400 MHz, DMSO-d_6)**.**

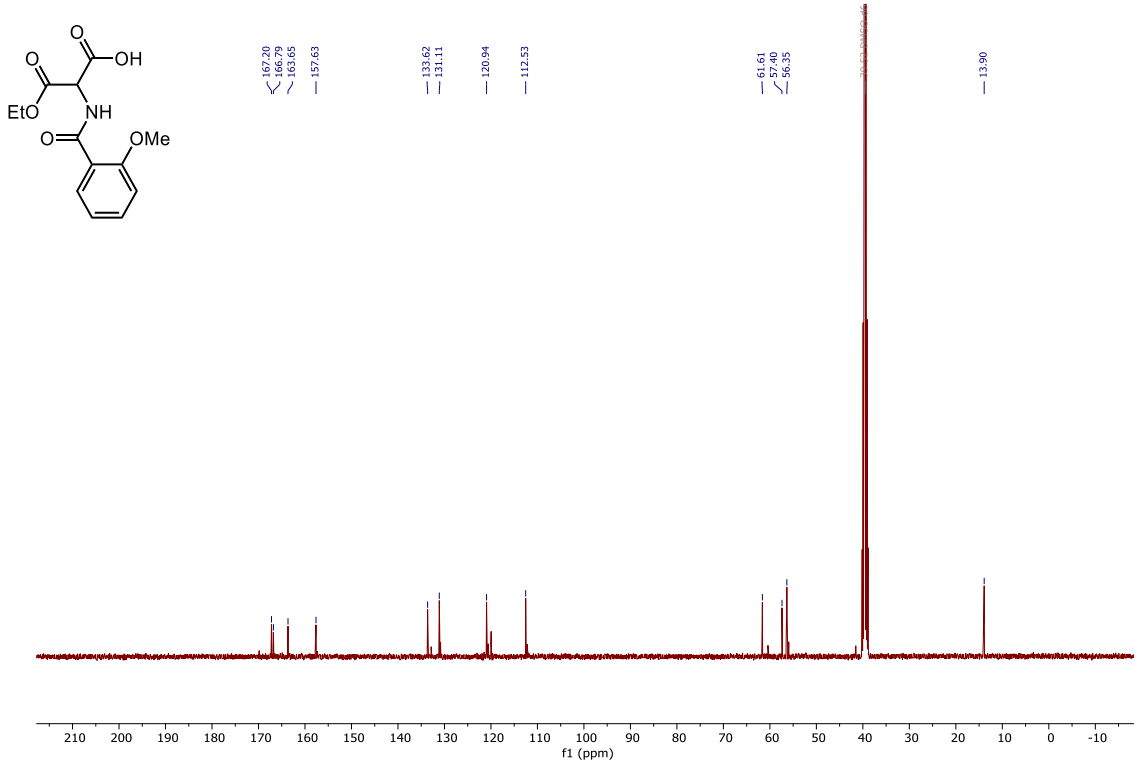

Figure S44: ^{13}C NMR spectra of **2c** (101 MHz, DMSO-d_6)**.**

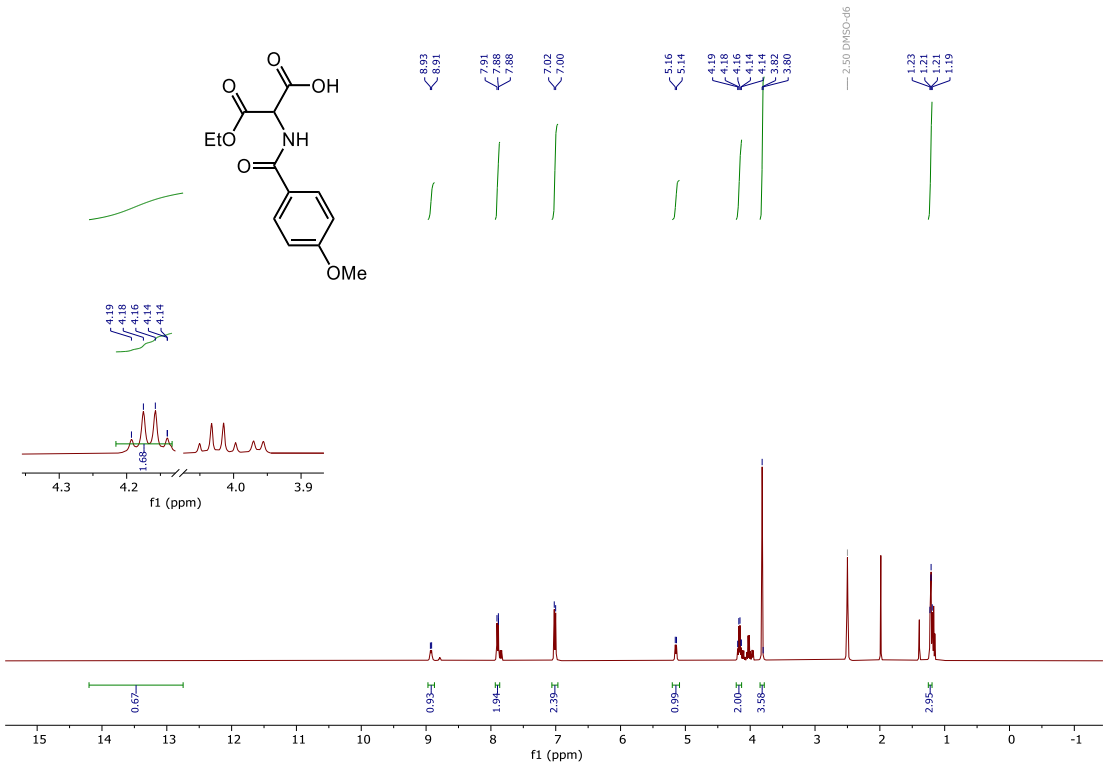

Figure S45: ^{1}H NMR spectra of 3-ethoxy-2-(4-methoxybenzamido)-3-oxopropanoic acid (400 MHz, DMSO-d6)**.**

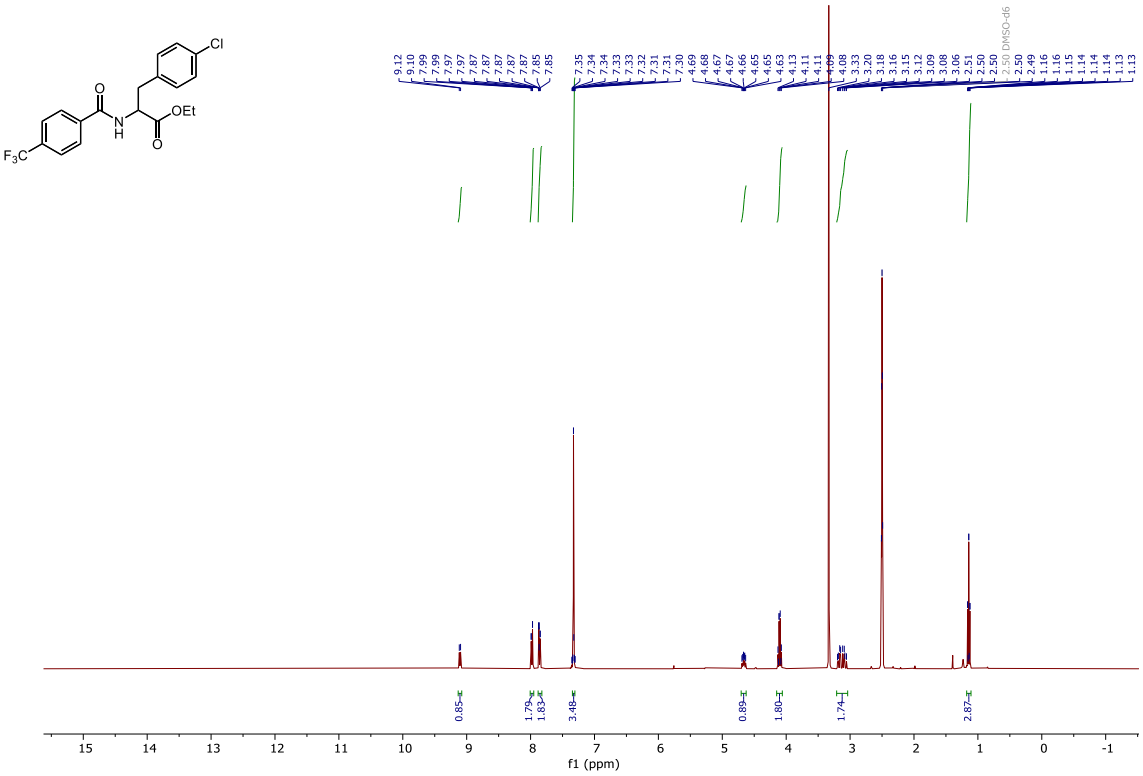

Figure S46: ^{1}H NMR spectra of **6a** (400 MHz, DMSO-d_6)**.**

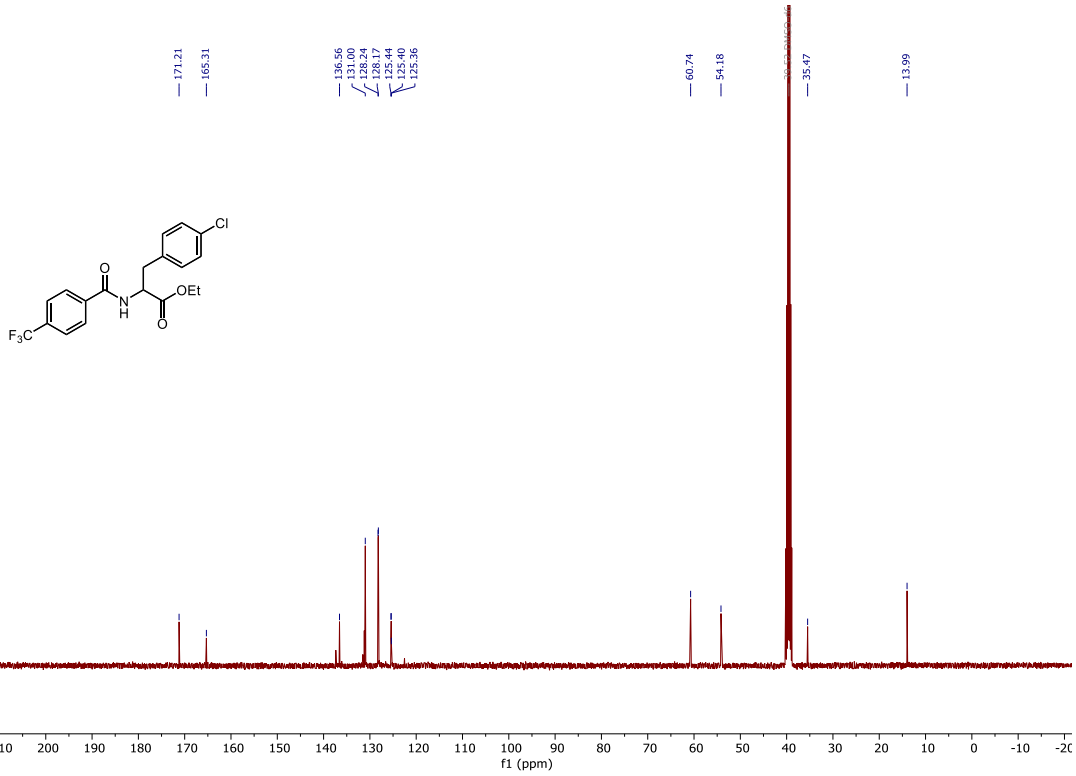

Figure S47: ^{13}C NMR spectra of **6a** (101 MHz, DMSO-d_6)**.**

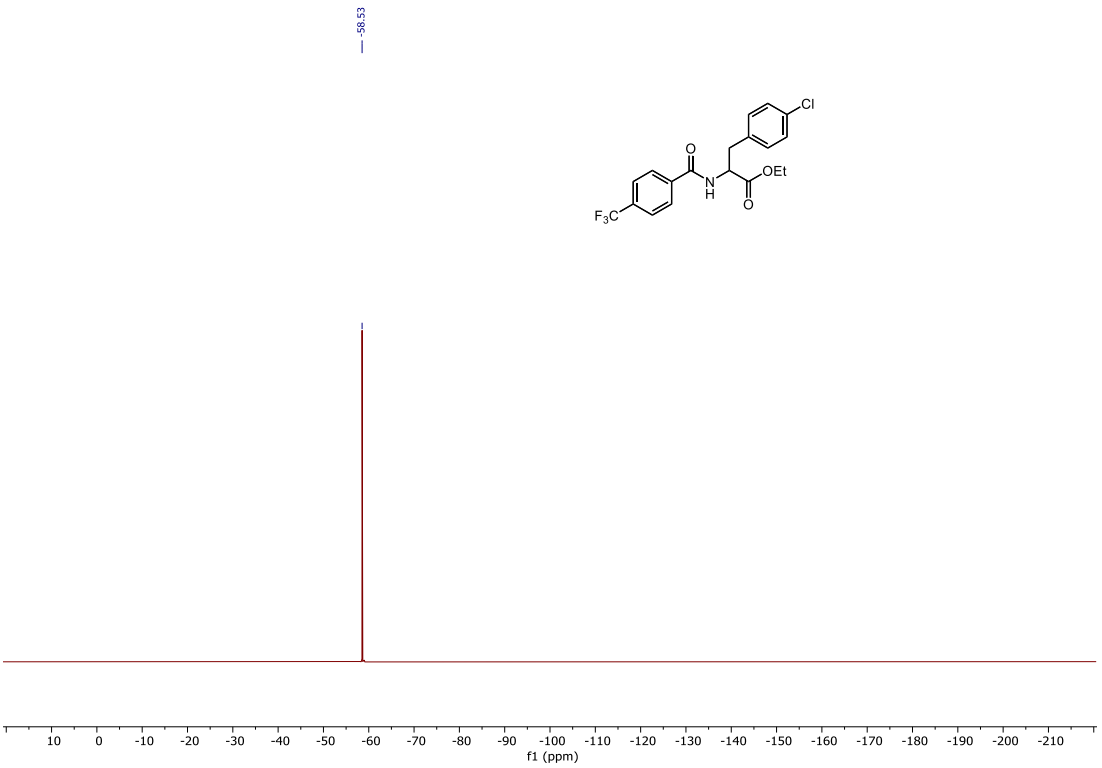

Figure S48: ^{19}F NMR spectra of **6a** (376 MHz, DMSO-d_6)**.**

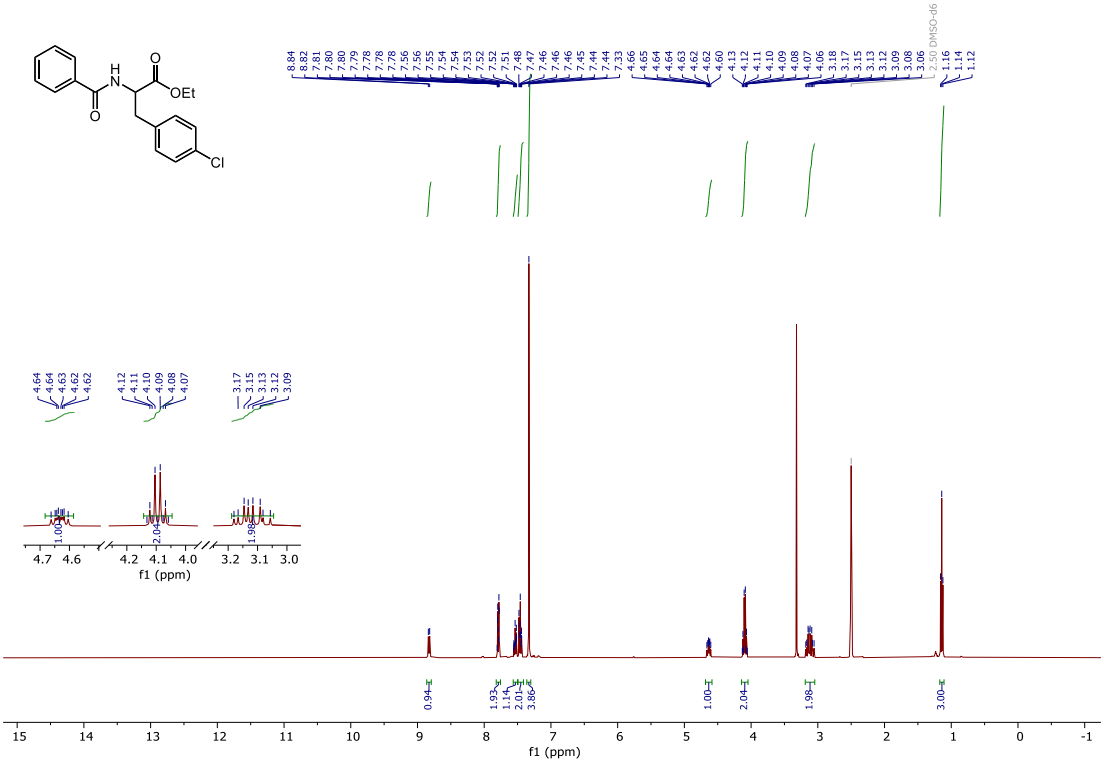

Figure S49: ^{1}H NMR spectra of **6b** (400 MHz, DMSO-d_6)**.**

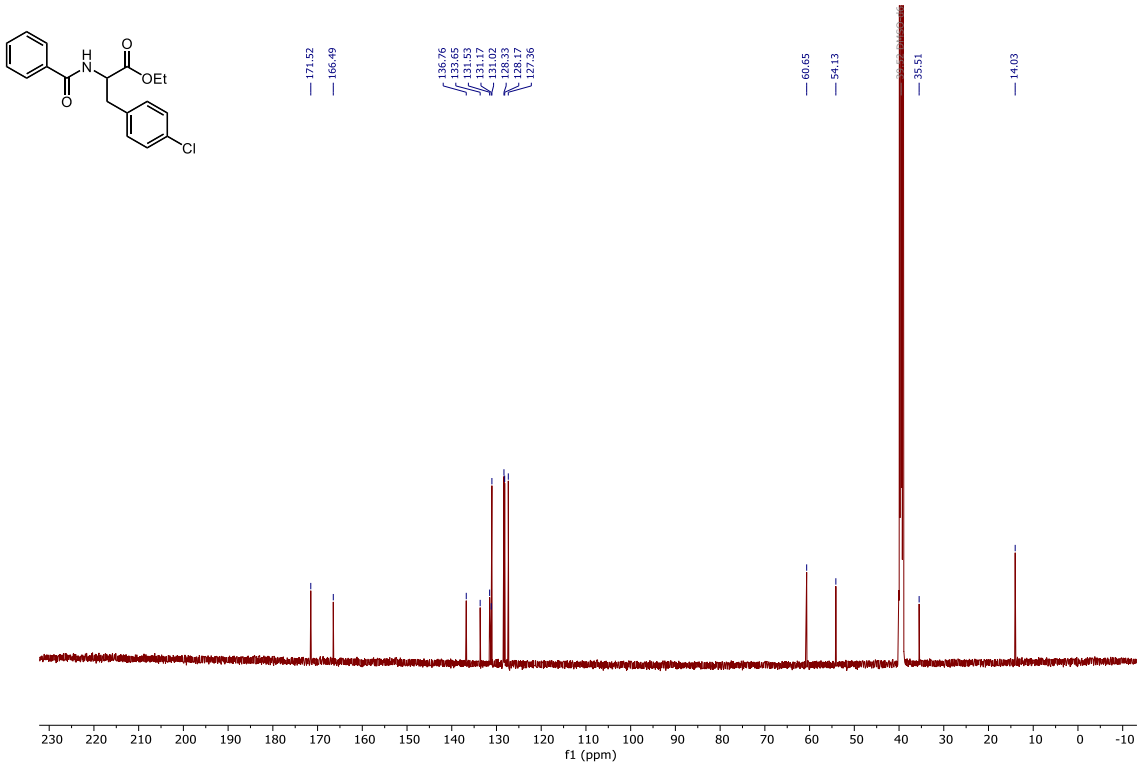

Figure S50: ^{13}C NMR spectra of **6b** (126 MHz, DMSO-d_6)**.**

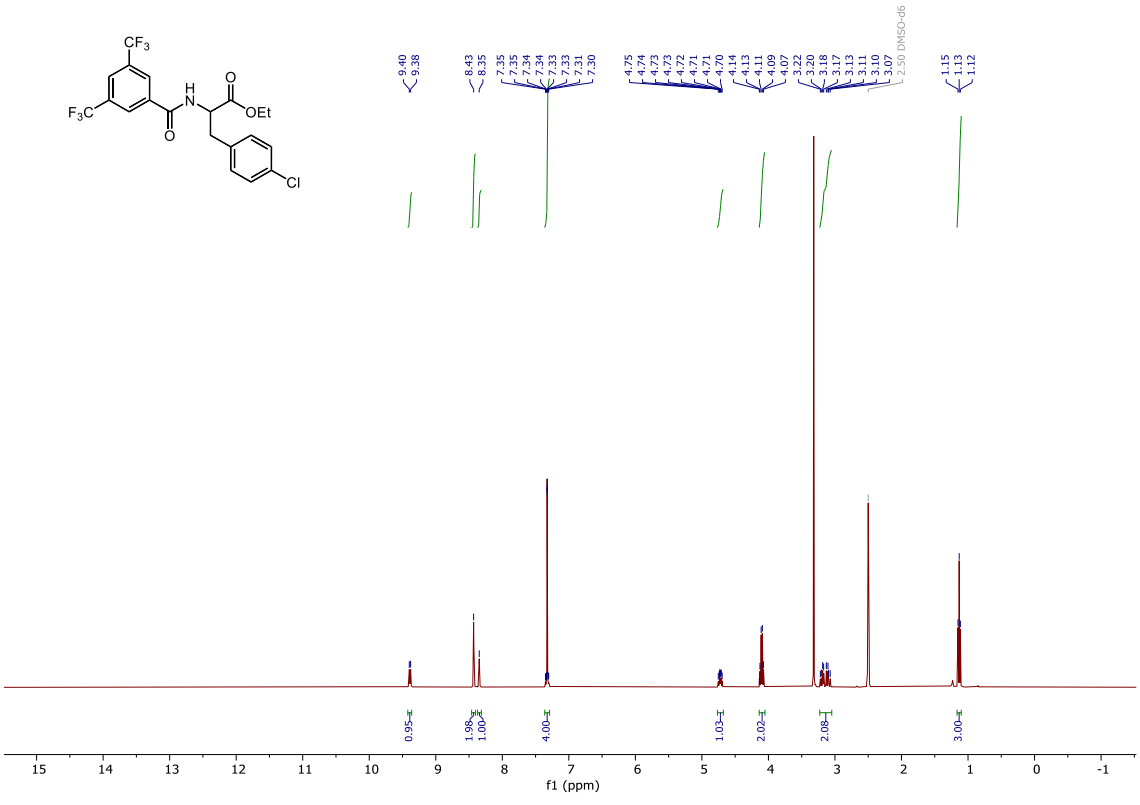

Figure S51: ^{1}H NMR spectra of **6c** (400 MHz, DMSO-d_6)**.**

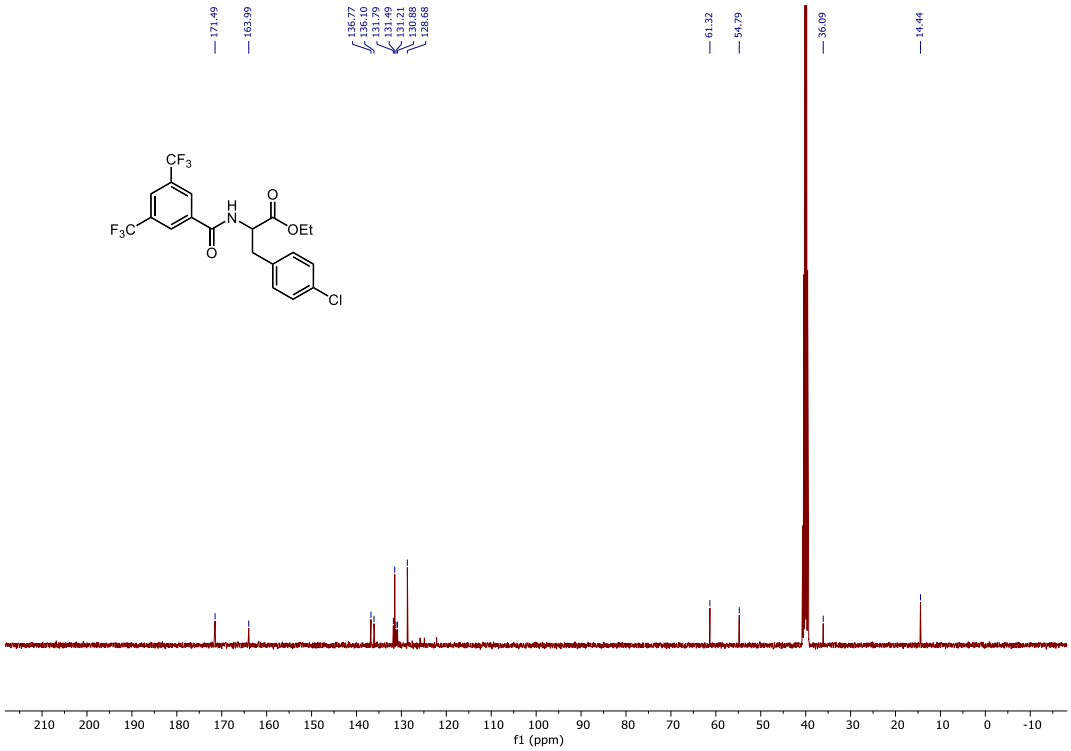

Figure S52: ^{13}C NMR spectra of **6c** (101 MHz, DMSO-d_6).

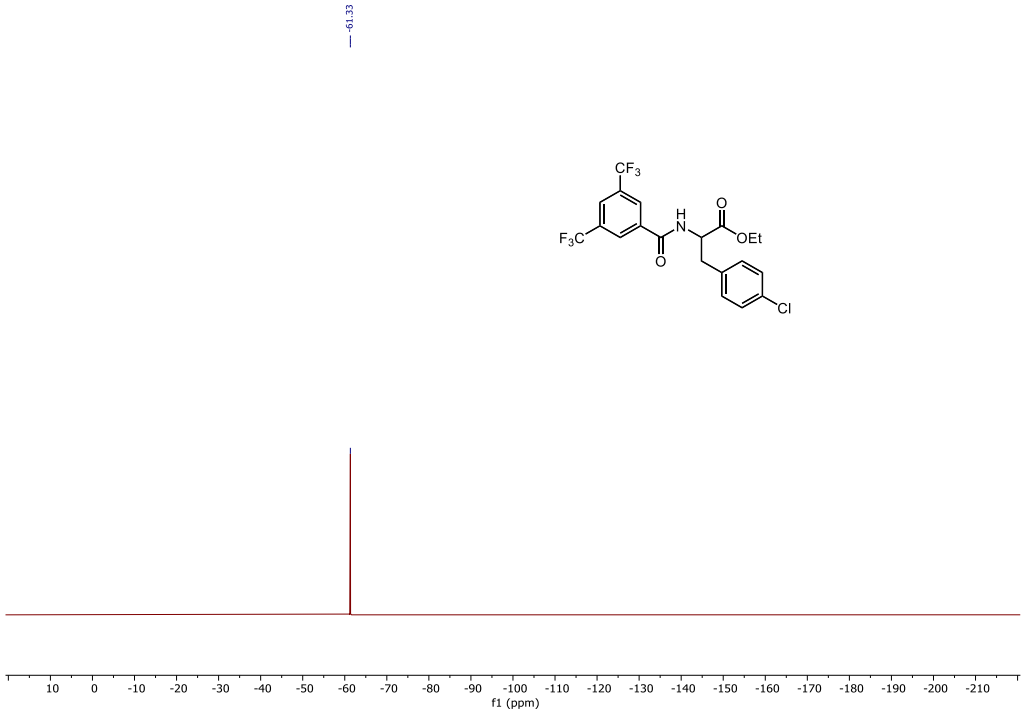

Figure S53: ^{19}F NMR spectra of **6c** (376 MHz, DMSO-d_6).

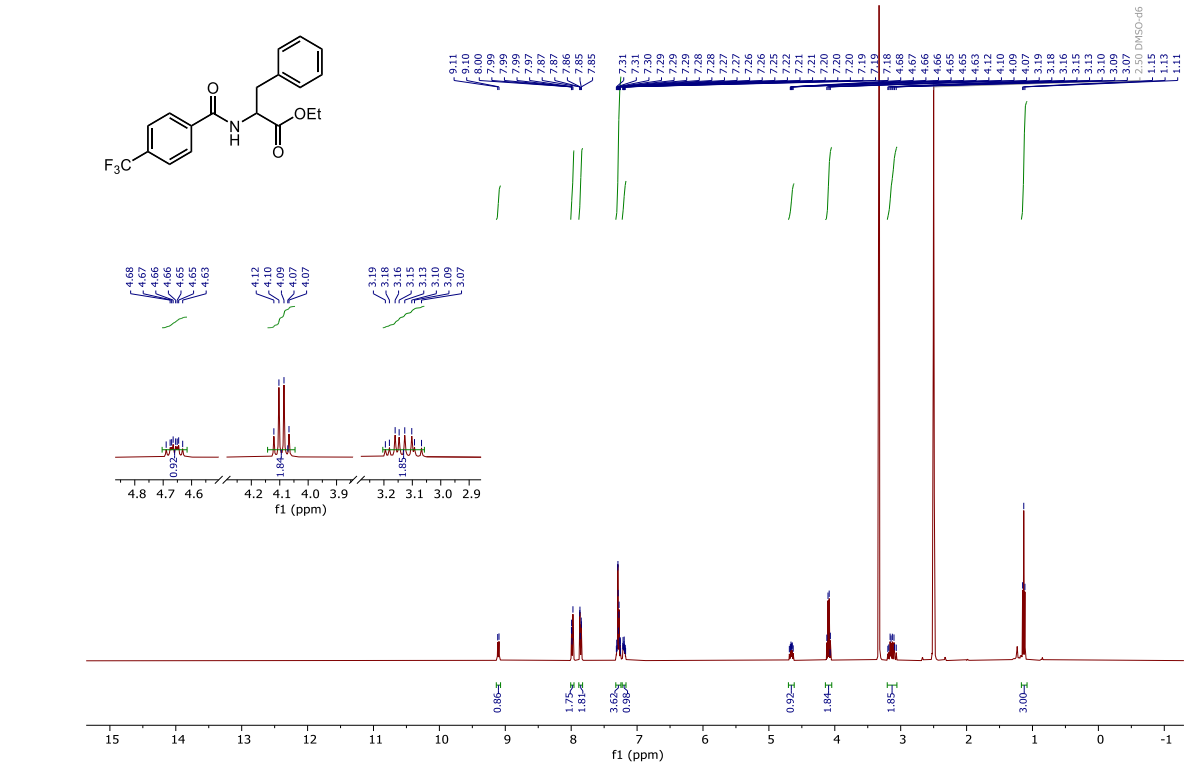

Figure S54: ^{1}H NMR spectra of **6d** (400 MHz, DMSO-d_6).

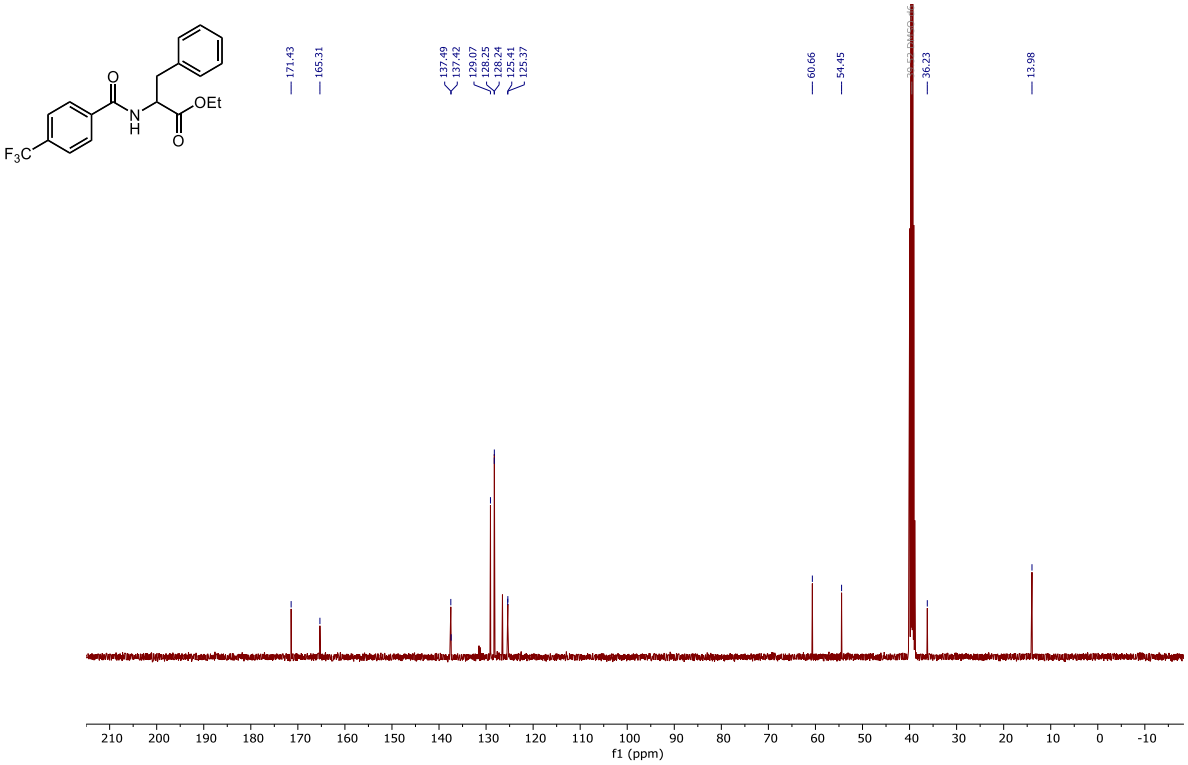

Figure S55: ^{13}C NMR spectra of **6d** (101 MHz, DMSO-d_6)**.**

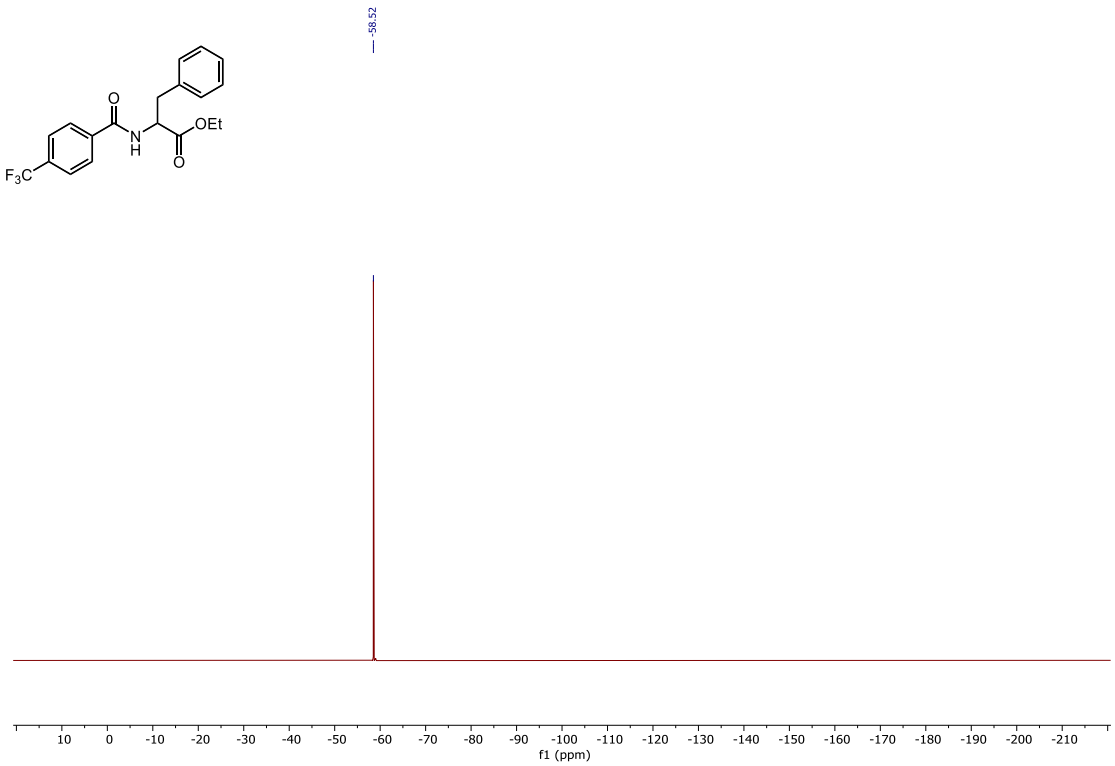

Figure S56: ^{19}F NMR spectra of **6d** (376 MHz, DMSO-d_6)**.**

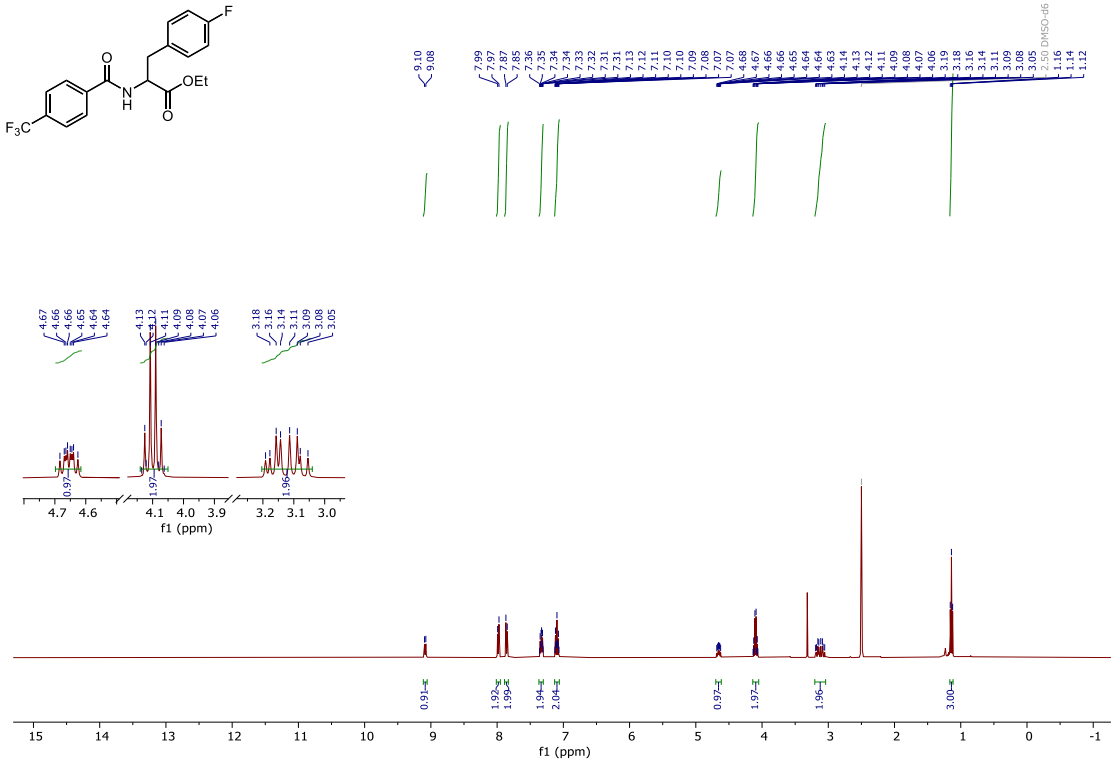

Figure S57: ^{1}H NMR spectra of **6e** (400 MHz, DMSO-d_6)**.**

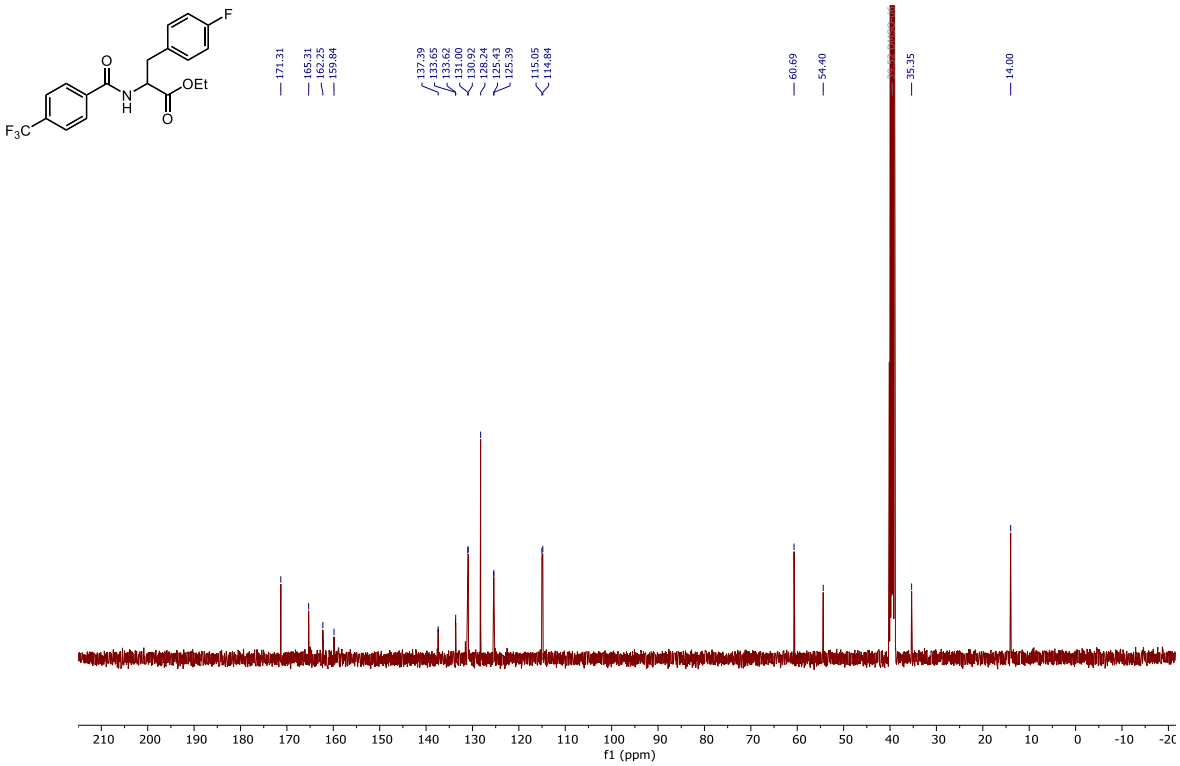

Figure S58: ^{13}C NMR spectra of **6e** (101 MHz, DMSO-d_6)**.**

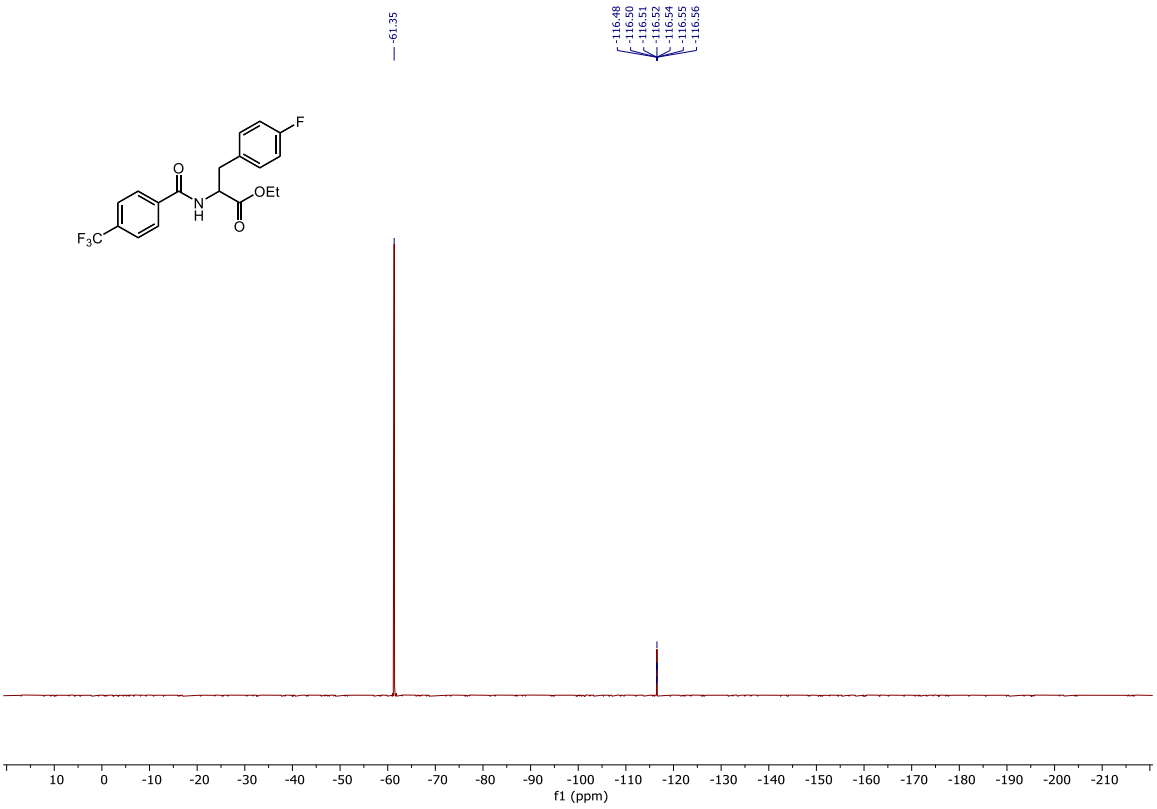

Figure S59: ^{19}F NMR spectra of **6e** (376 MHz, DMSO-d_6)**.**

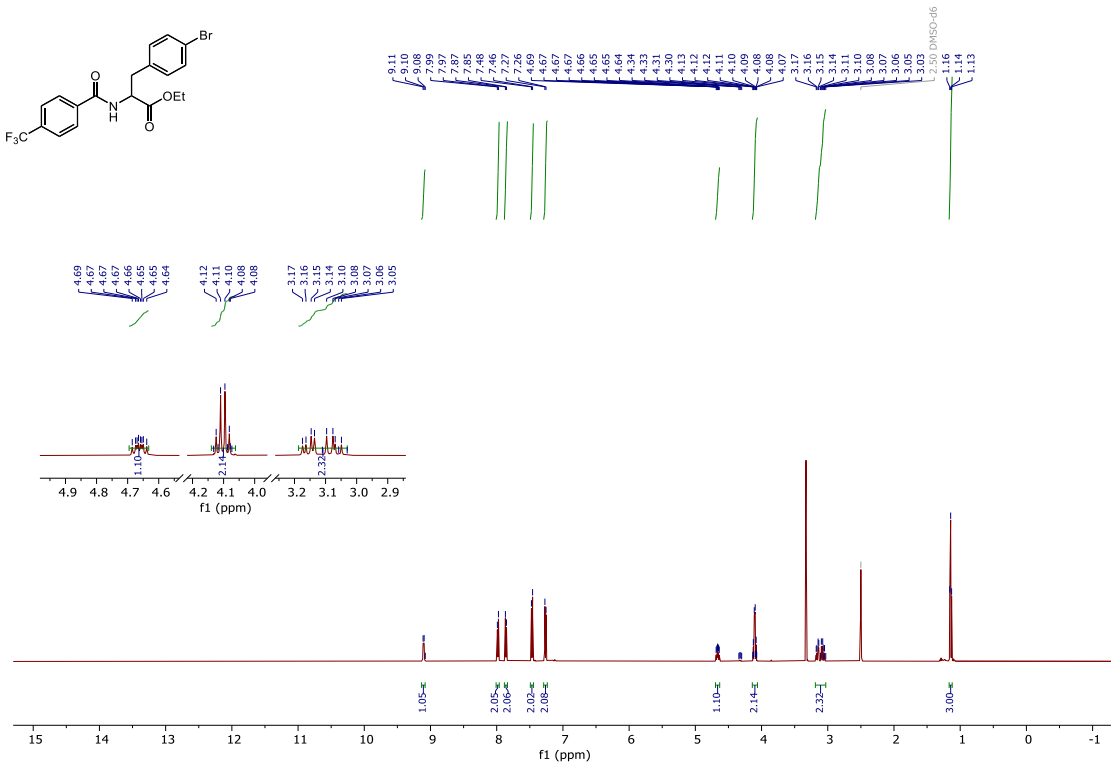

Figure S60: ^{1}H NMR spectra of **6f** (400 MHz, DMSO-d_6).

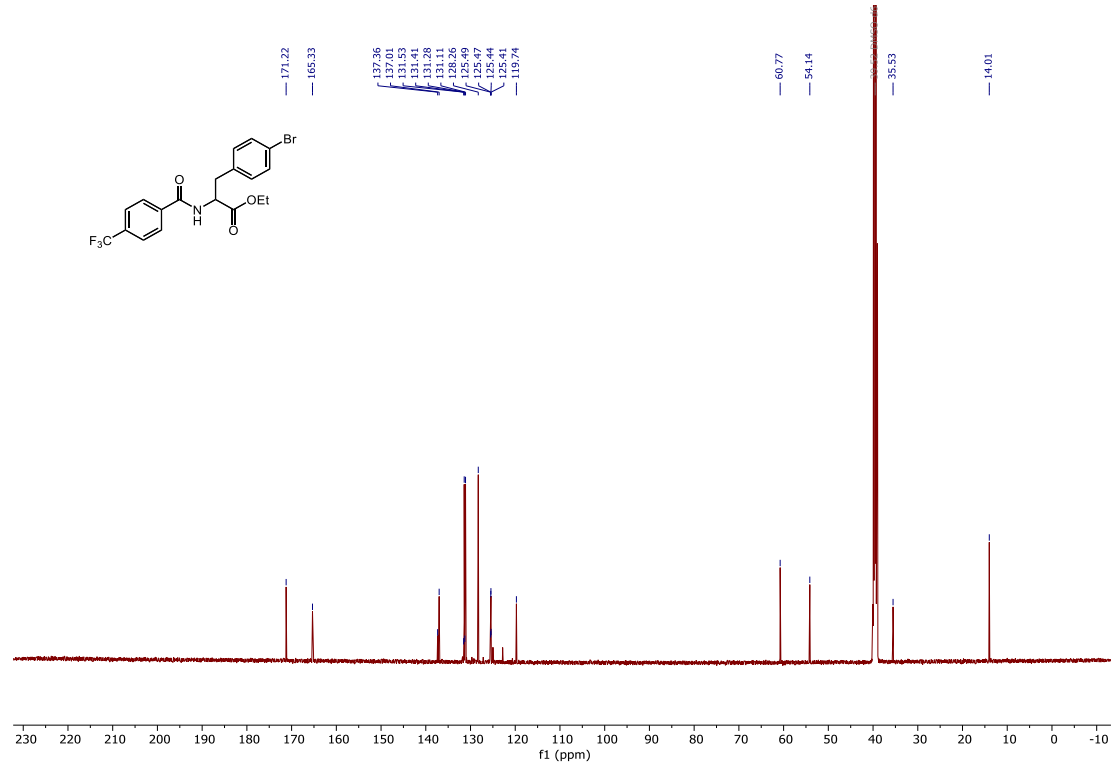

Figure S61: ^{13}C NMR spectra of **6f** (126 MHz, DMSO-d_6)**.**

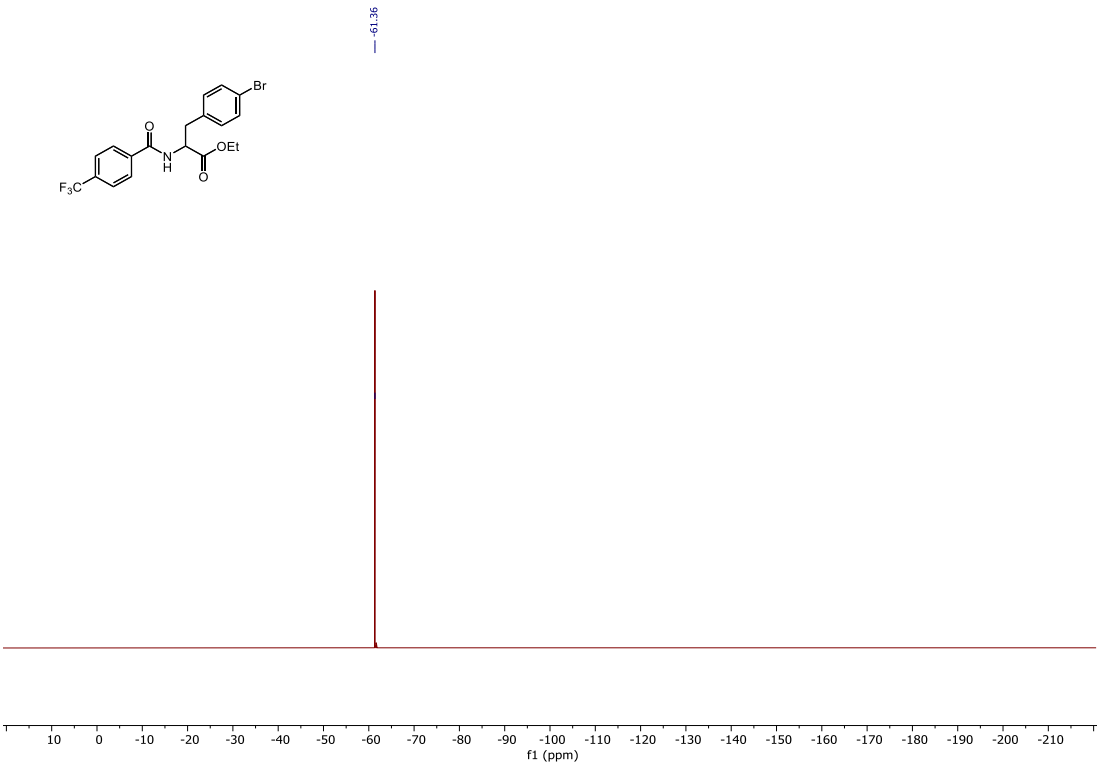

Figure S62: ^{19}F NMR spectra of **6f** (470 MHz, DMSO-d_6)**.**

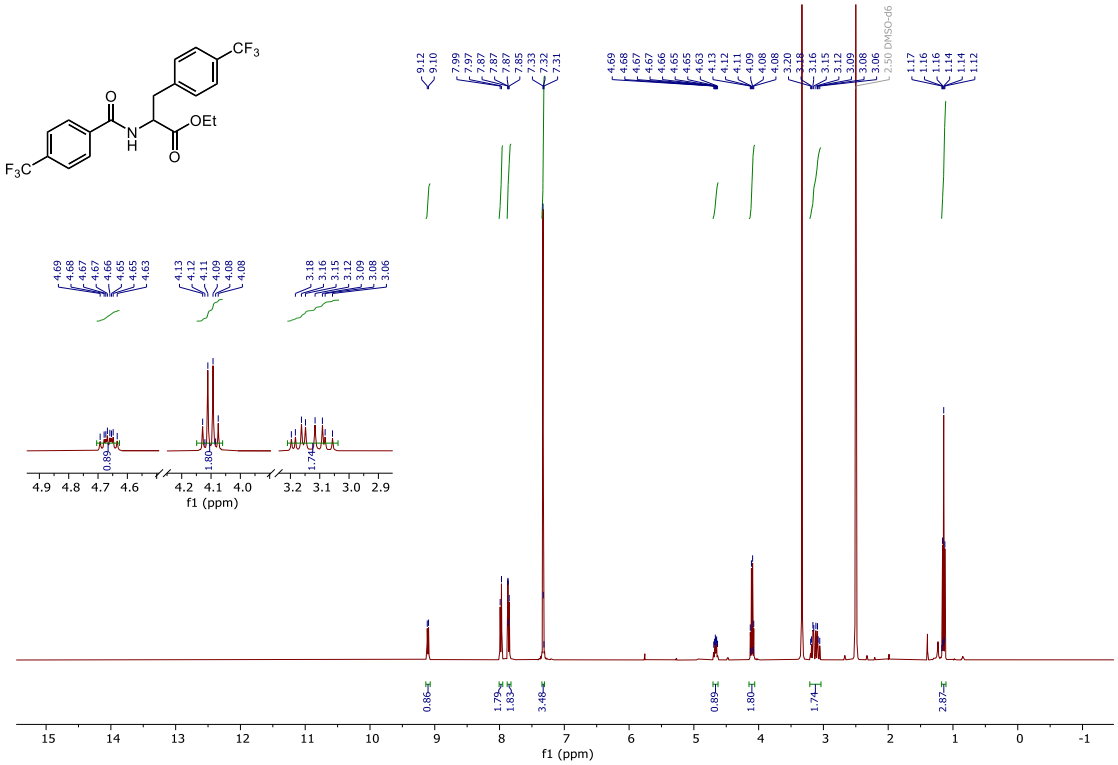

Figure S63: ^{1}H NMR spectra of **6g** (400 MHz, DMSO-d_6)**.**

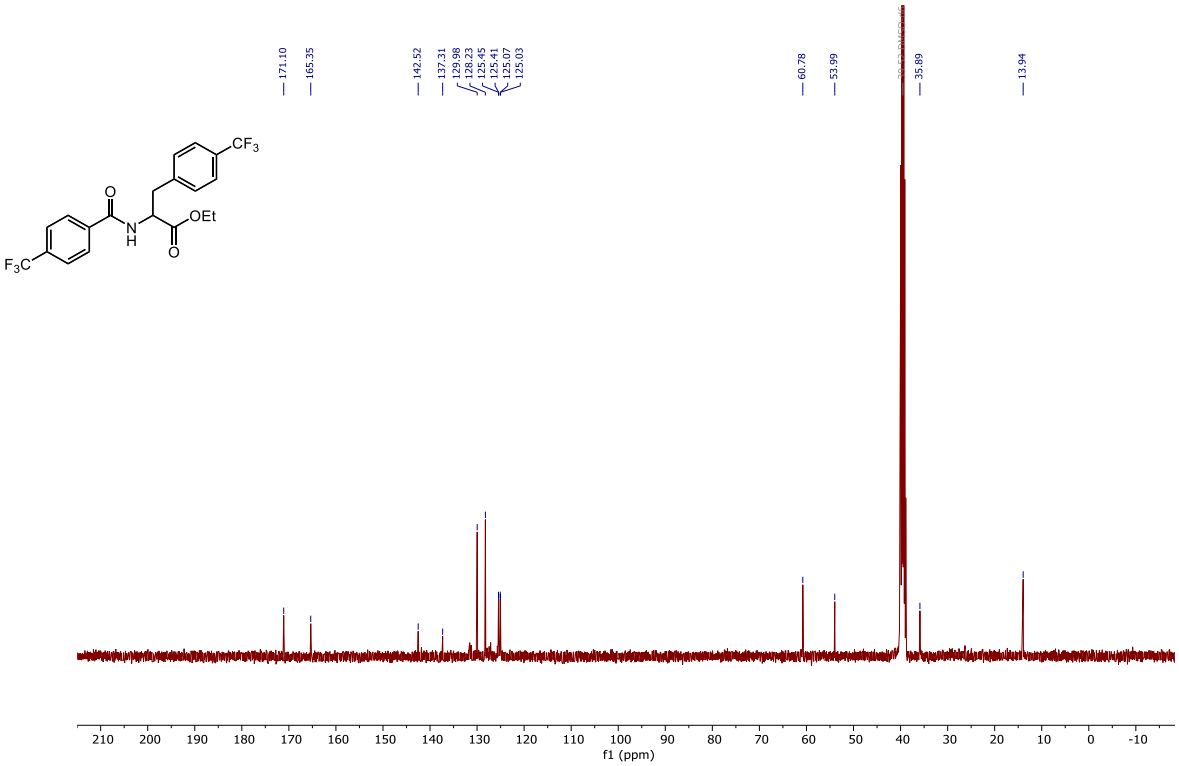

Figure S64: ^{13}C NMR spectra of **6g** (101 MHz, DMSO-d_6)**.**

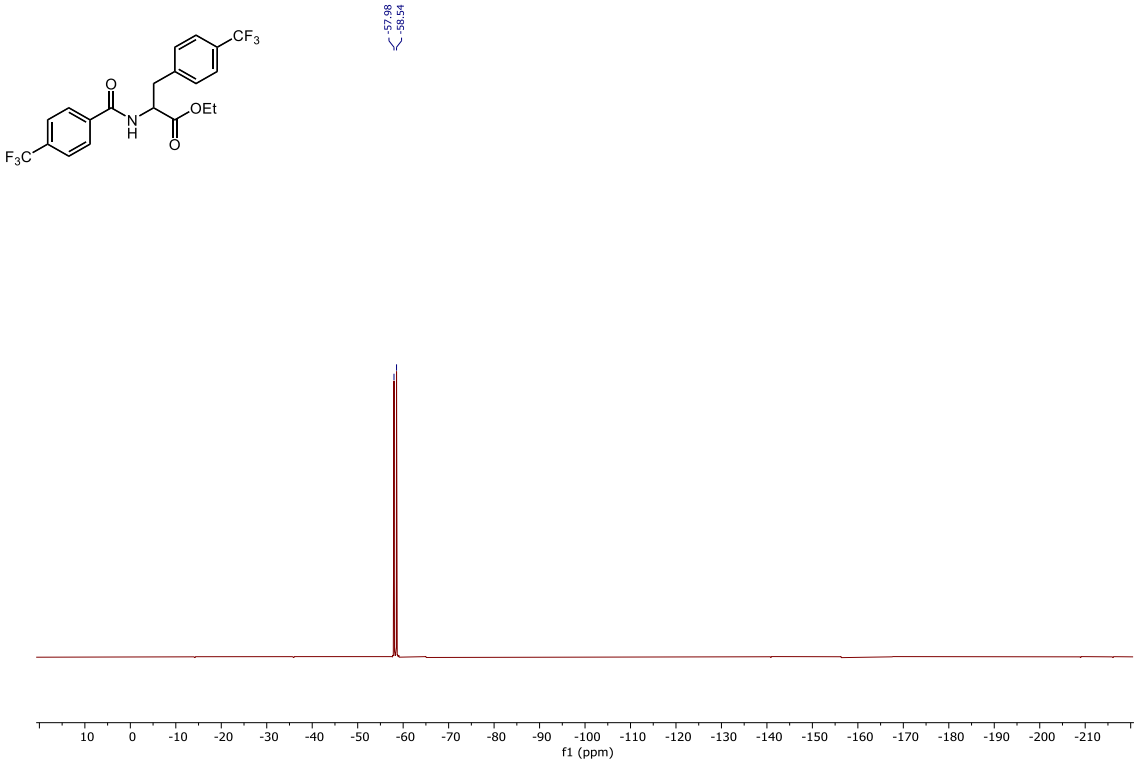

Figure S65: ^{19}F NMR spectra of **6g** (376 MHz, DMSO-d_6)**.**

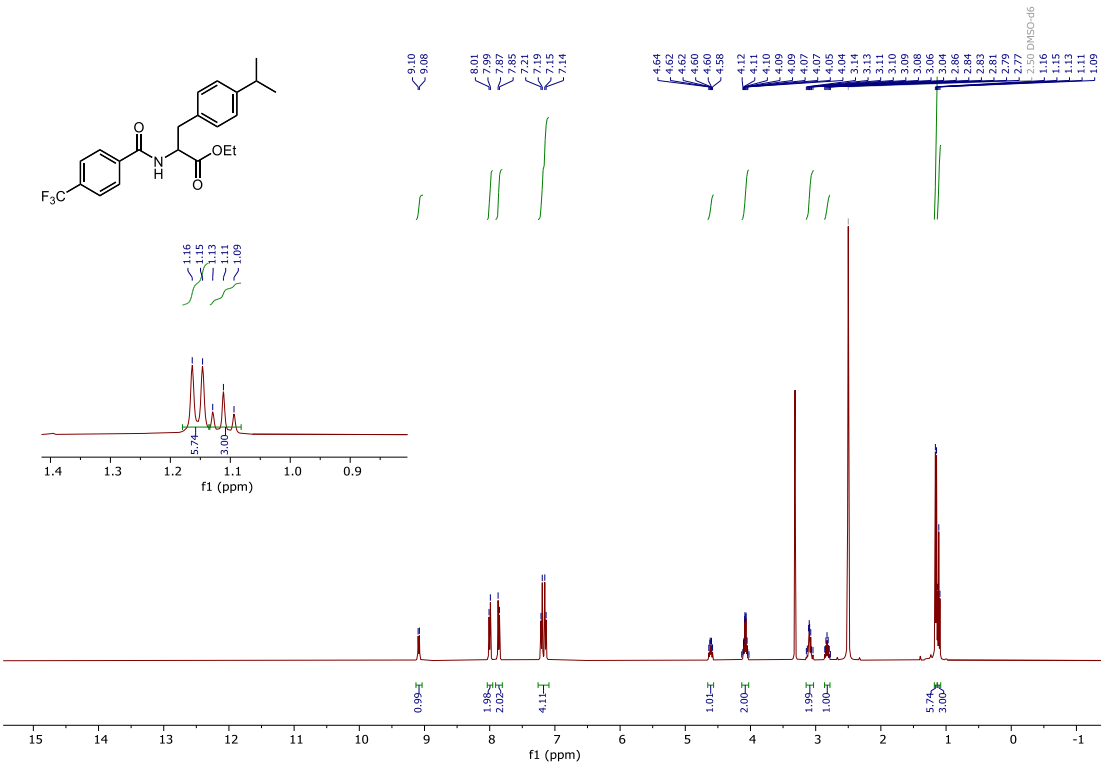

Figure S66: ^{1}H NMR spectra of **6h** (400 MHz, DMSO-d_6)**.**

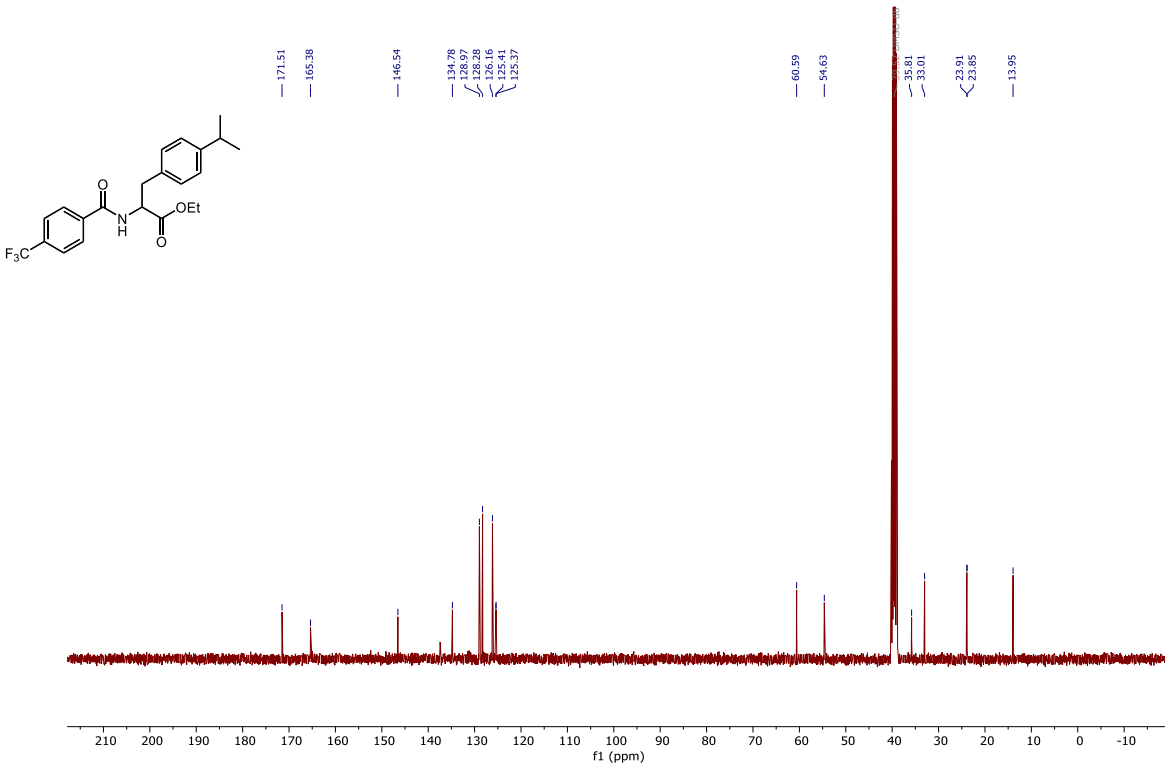

Figure S67: ^{13}C NMR spectra of **6h** (101 MHz, DMSO-d_6)**.**

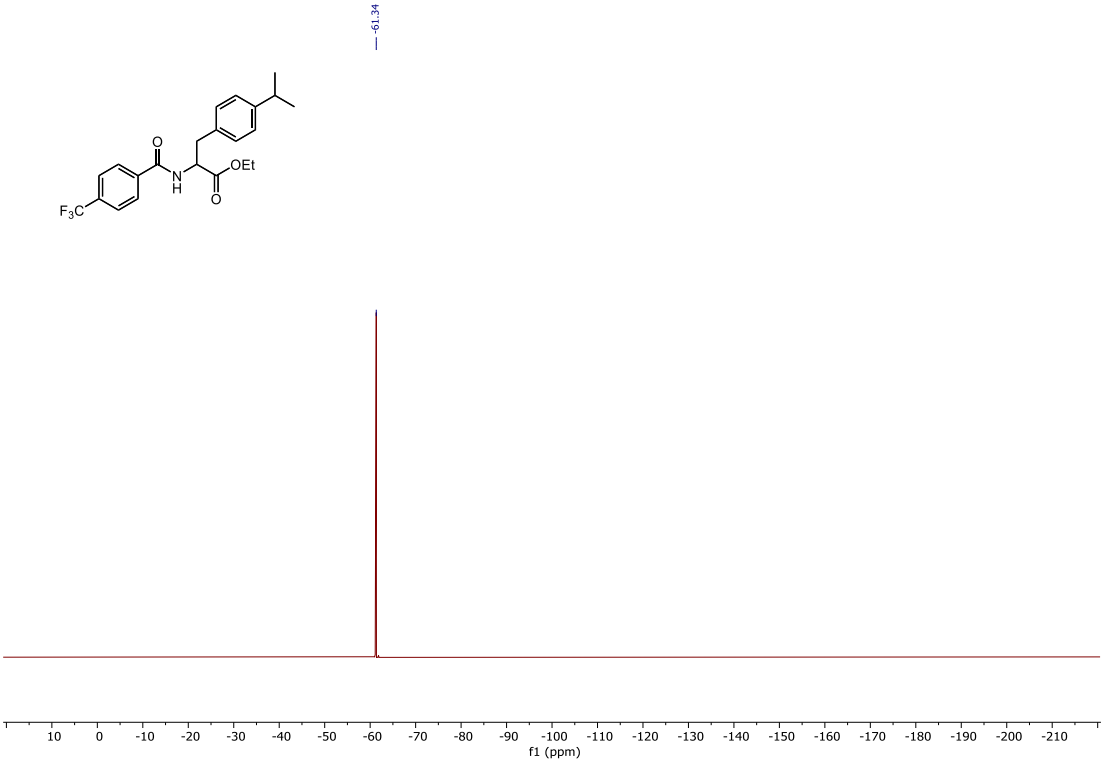

Figure S68: ^{19}F NMR spectra of **6h** (376 MHz, DMSO-d_6)**.**

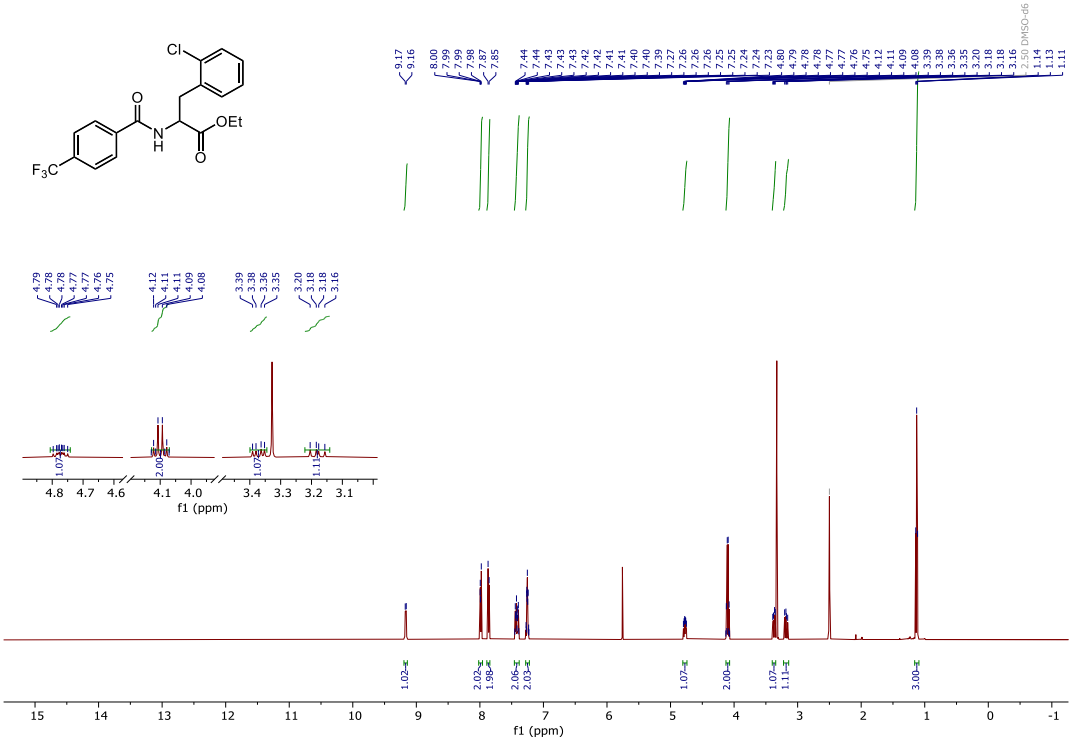

Figure S69: ^{1}H NMR spectra of **6i** (400 MHz, DMSO-d_6)**.**

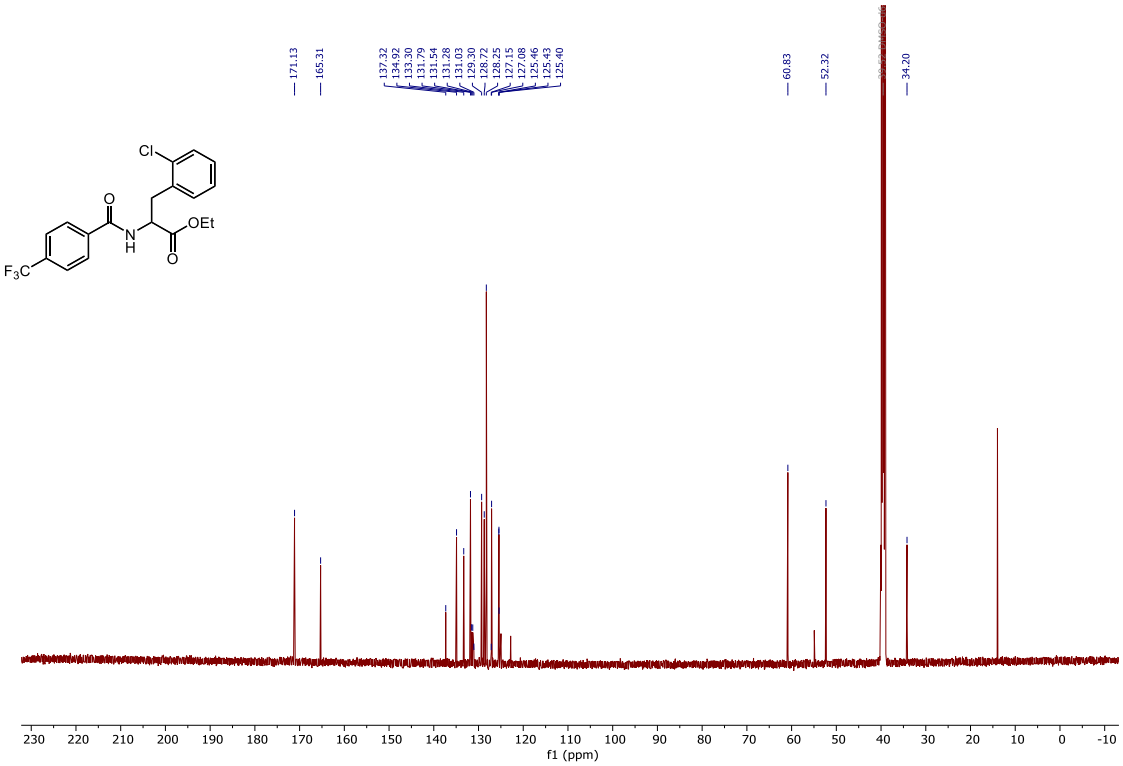

Figure S70: ^{13}C NMR spectra of **6i** (126 MHz, DMSO-d_6)**.**

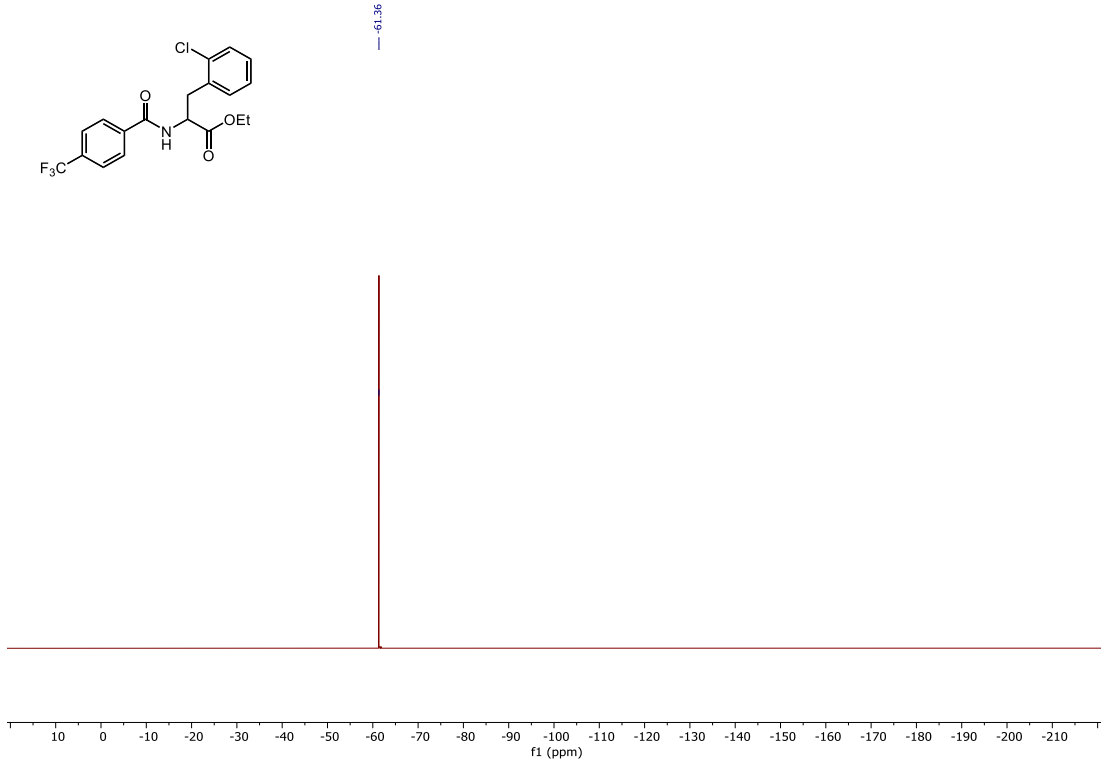

Figure S71: ^{19}F NMR spectra of **6i** (470 MHz, DMSO-d_6)**.**

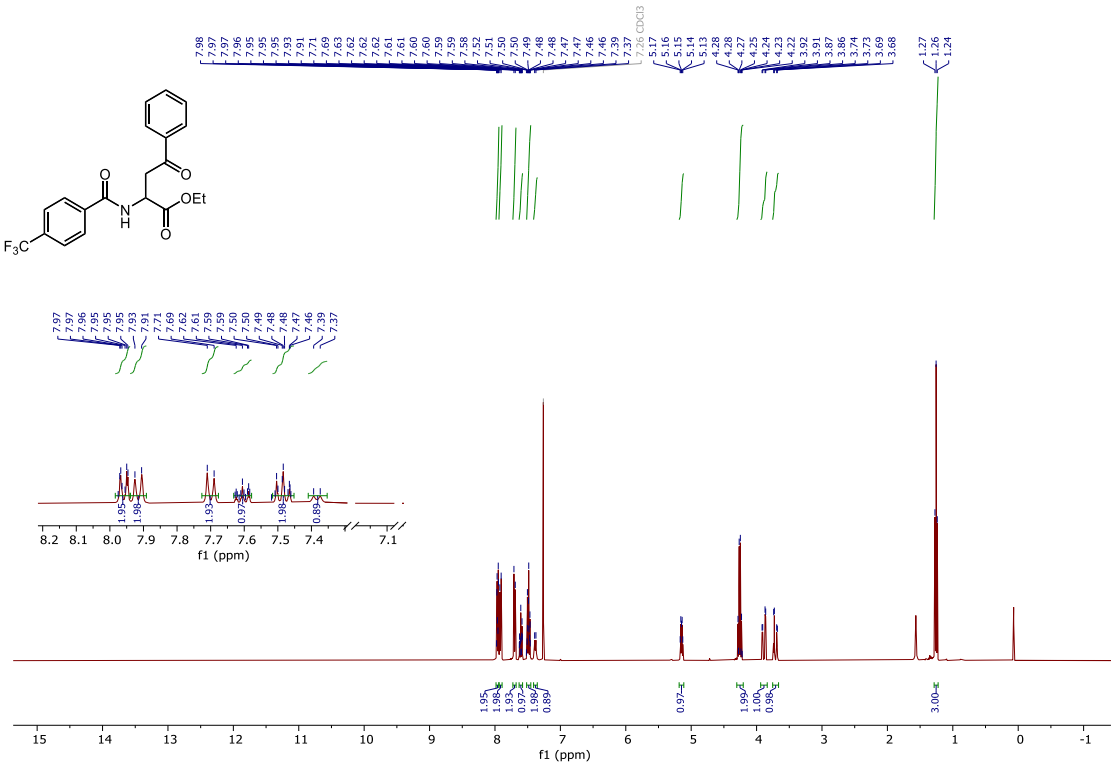

Figure S72: ^{1}H NMR spectra of **6j** (400 MHz, $CDCl_3$).

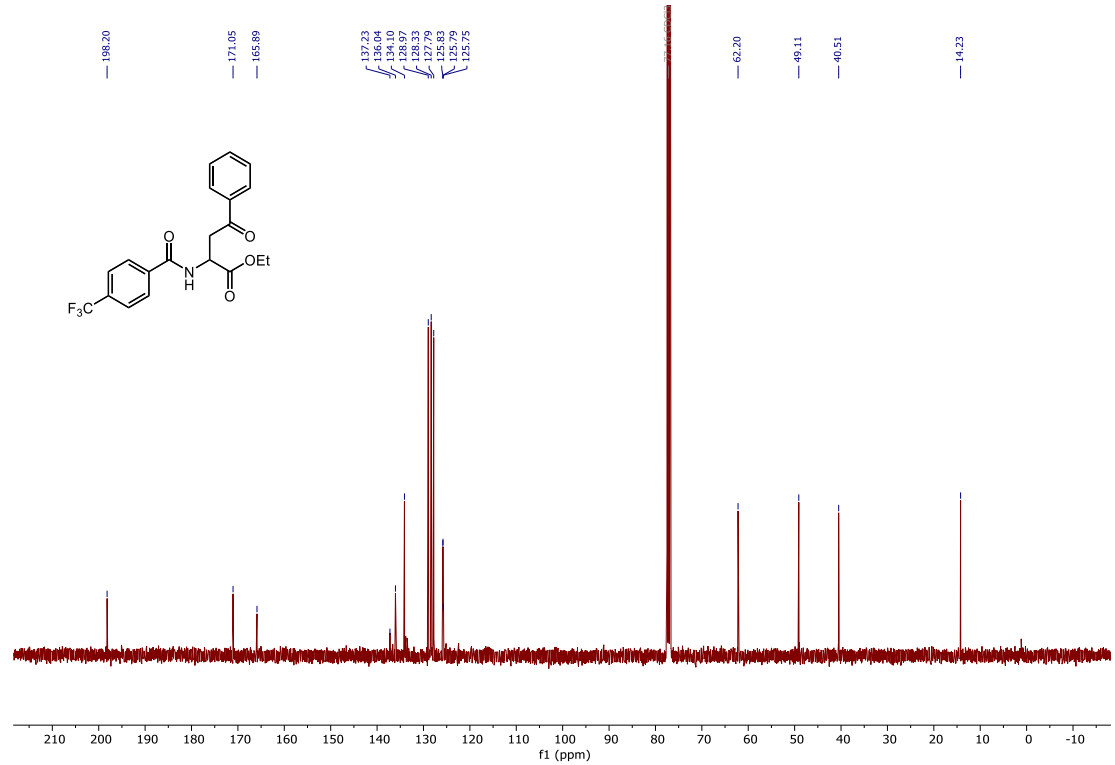

Figure S73: ^{13}C NMR spectra of **6j** (101 MHz, $CDCl_3$)**.**

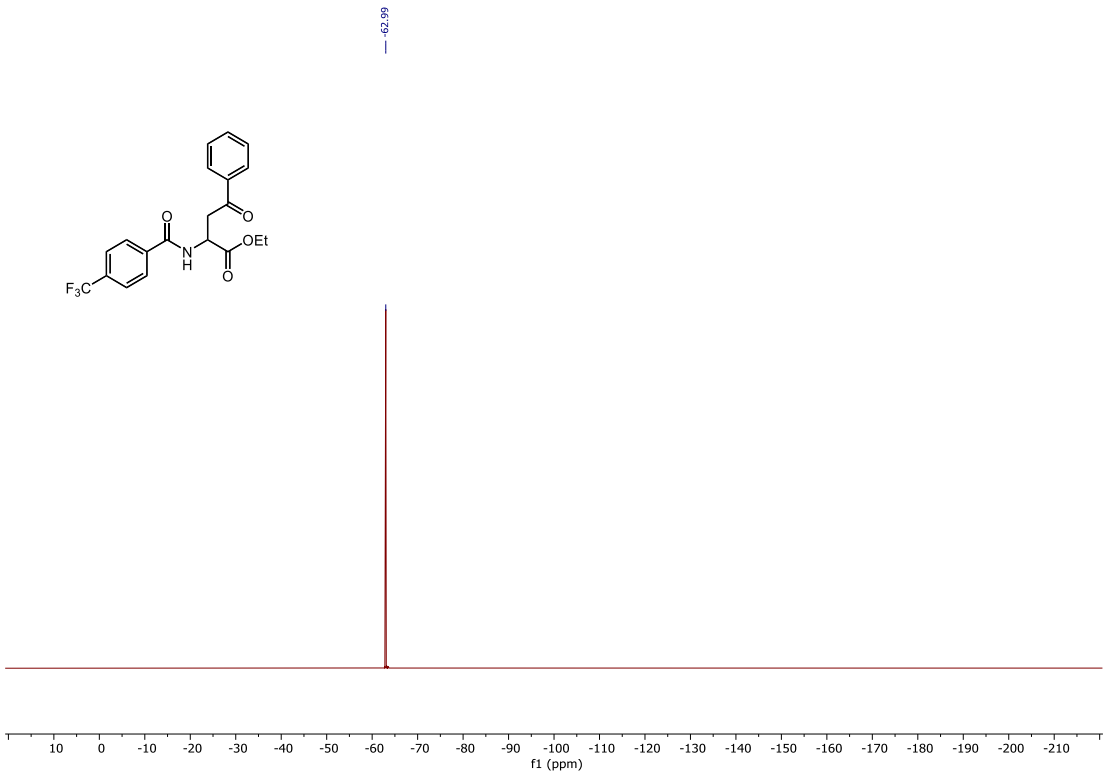

Figure S74: ^{19}F NMR spectra of **6j** (376 MHz, $CDCl_3$)**.**

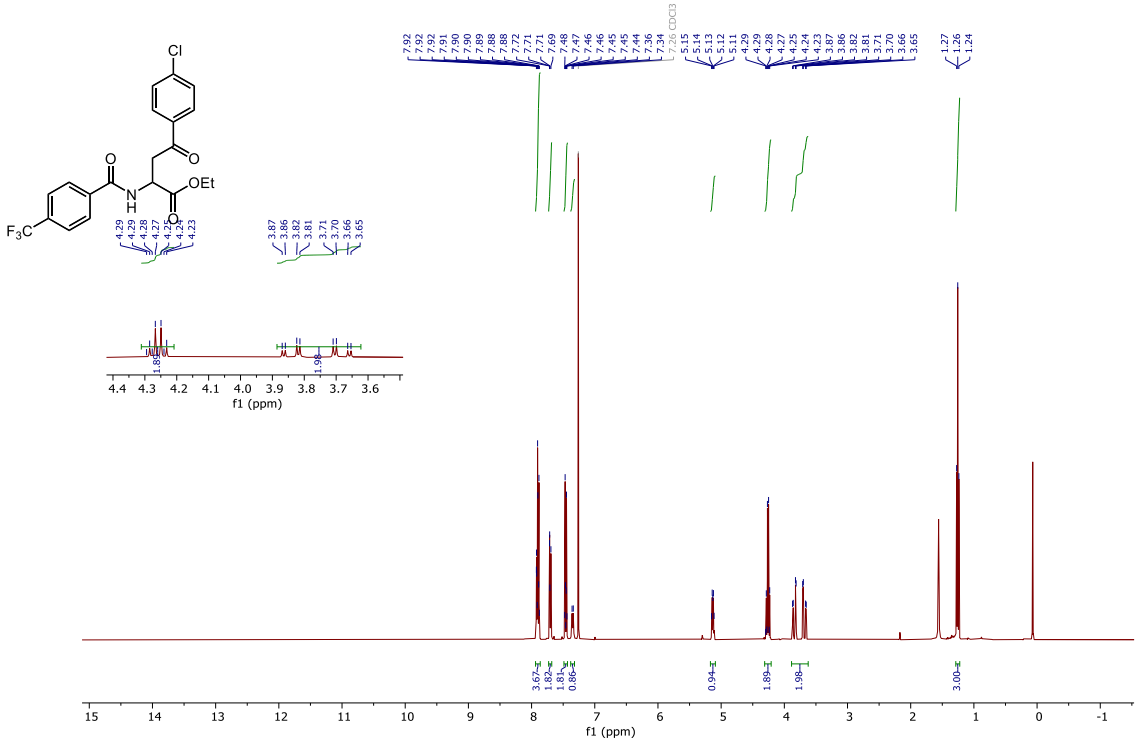

Figure S75: ^{1}H NMR spectra of **6k** (400 MHz, $CDCl_3$)**.**

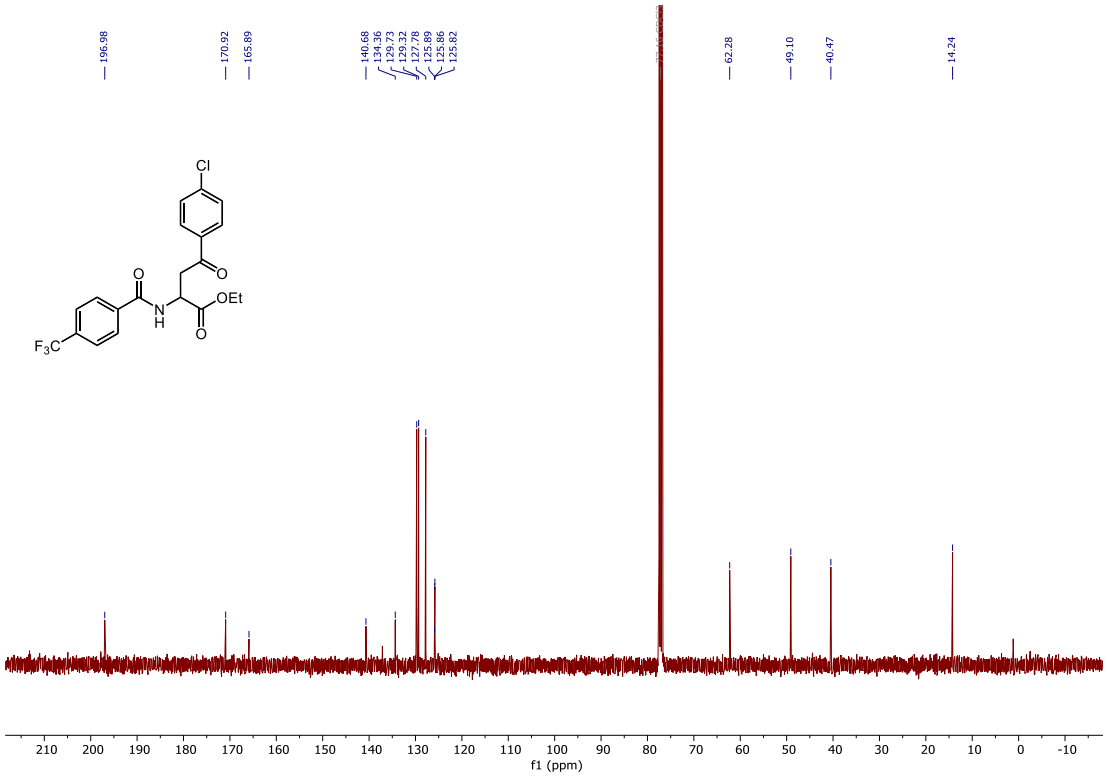

Figure S76: ^{13}C NMR spectra of **6k** (101 MHz, $CDCl_3$).

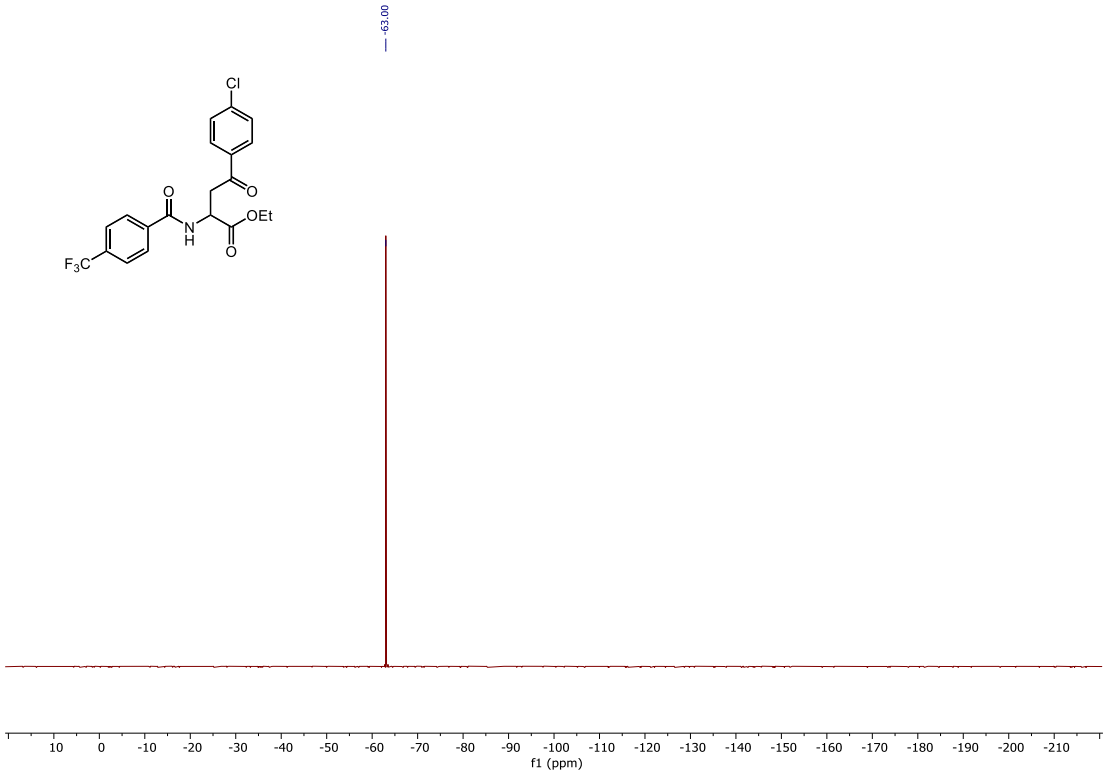

Figure S77: ^{19}F NMR spectra of **6k** (376 MHz, $CDCl_3$).

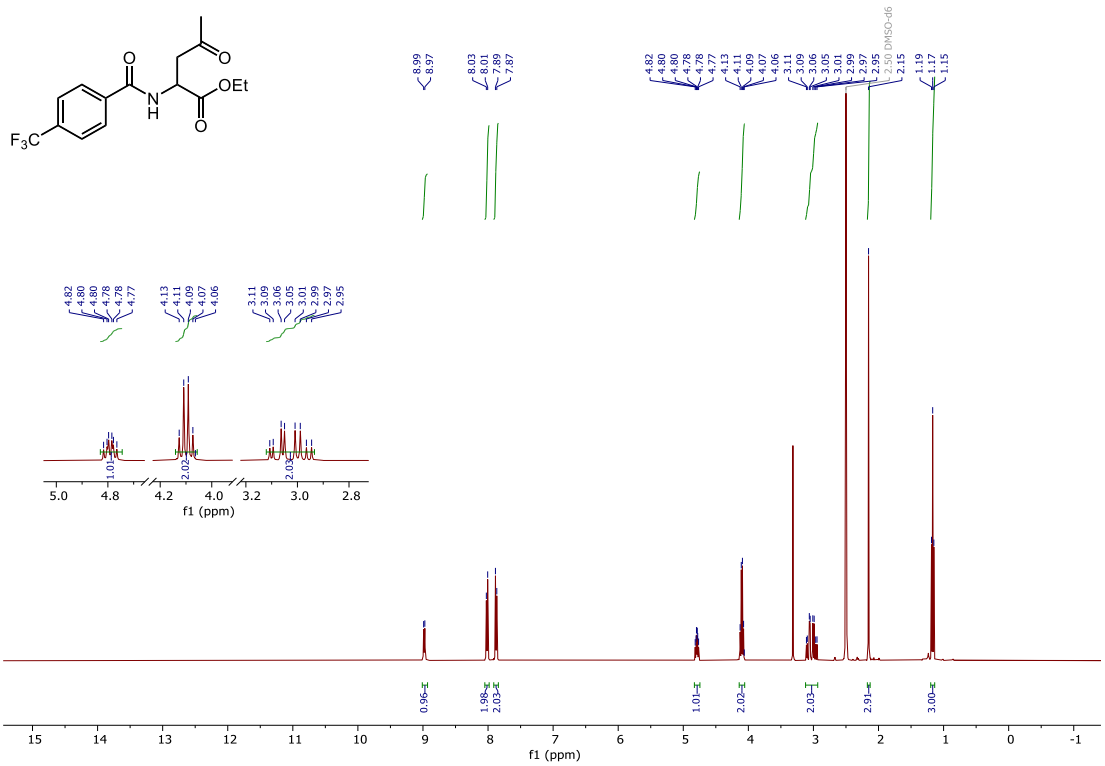

Figure S78: ^{1}H NMR spectra of **6l** (400 MHz, DMSO-*d*$_6$)**.**

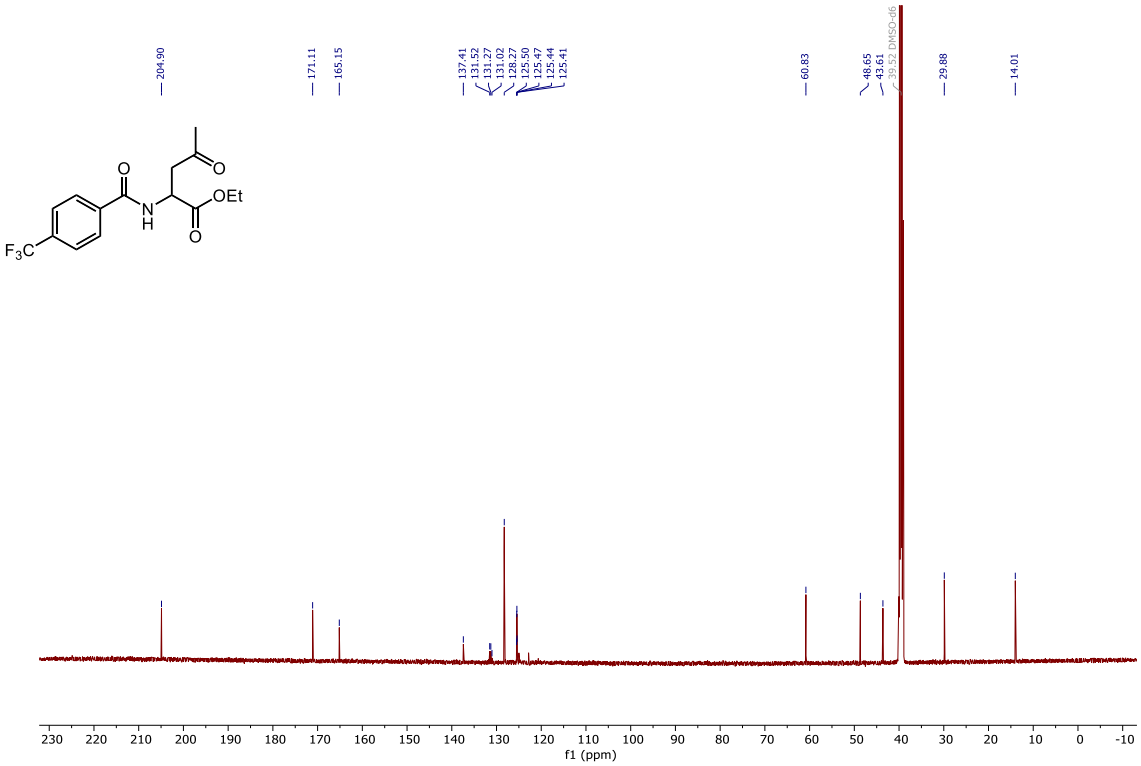

Figure S79: ^{13}C NMR spectra of **6l** (126 MHz, DMSO-*d*$_6$)**.**

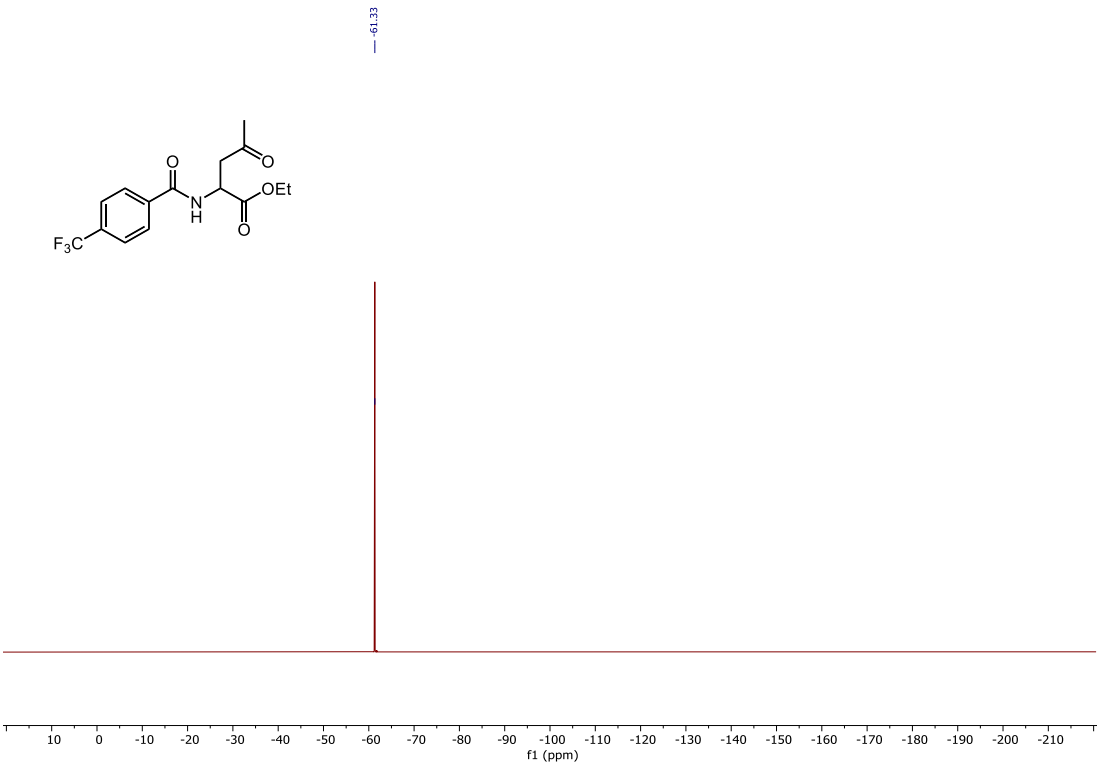

Figure S80: ^{19}F NMR spectra of **6l** (470 MHz, DMSO-d_6)**.**

9. Reference

1. E. E. Stache, A. B. Ertel, R. Tomislav and A. G. Doyle, *ACS Catal.*, 2018, **8**, 11134.
2. A. H. Mai, S. Pawar and W. M. De Borggraeve, *Tetrahedron Lett.*, 2014, **55**, 4664.
3. S. Tshepelevitsh, A. Kütt, M. Lõkov, I. Kaljurand, J. Saame, A. Heering, P. G. Plieger, R. Vianello and I. Leito, *Eur. J. Org. Chem.*, 2019, **40**, 6735.
4. F. De Vleeschouwer, V. Van Speybroeck, M. Waroquier, P. Geerlings and F. De Proft, *Org. Lett.*, 2007, **9**, 2721.
5. F. Neese, *Wiley Interdiscip. Rev. Comput. Mol. Sci.*, 2012, **2**, 73.
6. J. L. Mateo, P. Bosch and A. E. Lozano, *Macromolecules*, 1994, **27**, 7794.
7. J. J. Garwood, A. D. Chen and D. A. Nagib, *J. Am. Chem. Soc.*, 2024, **146**, 28034.
8. D. Leifert and A. Studer, *Angew. Chem. Int. Ed.*, 2020, **59**, 74.
9. K. C. Cartwright, S. B. Lang and J. A. Tunge, *J. Org. Chem.*, 2019, **84**, 2933.
10. M. Kudisch, R. X. Hooper, L. K. Valloli, J. D. Earley, A. Zieleniewska, J. Yu, S. DiLuzio, R. W. Smaha, H. Sayre, X. Zhang, M. J. Bird, A. A. Cordones, G. Rumbles and O. G. Reid, *Nat. Commun.*, 2025, **16**, 5530.
11. L. Delfau, E. Mauro, J. Pecaut, D. Martin and E. Tomás-Mendivil, *ACS Catal.*, 2024, **14**, 7149.
12. A. Gennaro, A. A. Isse and F. Maran, *J. Electroanal. Chem.*, 2001, **507**, 124.
13. Z. Zeng, A. Feceu, N. Sivendran and L. J. Gooßen, *Adv. Synth. Catal.*, 2021, **363**, 2678.
14. A. Oberheide and H.-D. Arndt, *Adv. Synth. Catal.*, 2021, **363**, 1132.